Numerical modelling and geomechanical analyses of soil slope stability evaluation in seasonal cold regions

積雪寒冷地における斜面安定性の数値モデル化と地盤力学的解析

by

Srikrishnan Siva Subramanian

A thesis submitted in partial fulfilment of the requirements for the degree of

Doctor of Philosophy in Engineering

under the guidance and supervision of

Professor Tatsuya Ishikawa

Examined by the Doctoral Committee

Professor Tatsuya Ishikawa

Professor Yoshiaki Fujii

Professor (Associate) Satoshi Nishimura

September 2017

English Engineering Education Program (e^3)

Laboratory of Analytical Geomechanics

Division of Field Engineering for the Environment

Graduate School of Engineering

Hokkaido University

Sapporo, Hokkaido, Japan

ABSTRACT

Soil slope instabilities occur frequently in snowy cold regions like Hokkaido, Japan. Stability assessment and predictions of soil slope failures in cold regions have always been highly multifaceted. The research focused on investigating the key influencing factors of soil slope failures in snowy cold regions for the mitigation of such disasters. As a result, a stability assessment approach based on two-dimensional finite element numerical modelling incorporating non-isothermal seepage flow and pseudo coupled mechanical analyses is recommended which considers the water content changes of the soil induced by the seasonal climatic effects i.e. freeze-thaw action and snowmelt water infiltration explicitly.

Case studies of soil slope failures in Hokkaido have been studied using the recommended approach. Site investigations, monitoring of weather and related parameters, geotechnical data assessments, soil characterisations and soil property estimations have been performed as a limited part of this study. It has been found that the freeze-thaw action and snowmelt water infiltration both influence the soil slope stability significantly. The investigation of the slope failures using the recommended numerical modelling approach revealed the robustness of the approach in analysing soil slope instabilities in seasonal cold regions.

The second part of the study focused on soil slope failure predictions. For the prediction of snowmelt induced soil slope failures in seasonal cold regions, an early warning criterion is required. The applicability of existing Japanese early warning criteria i.e. 60-minute cumulative rainfall and Soil-Water-Index (SWI) relationships, Effective Rainfall (ER) indexes to predict the snowmelt induced soil slope failures are examined using the recommended slope stability assessment approach. An empirical method to quantify the amount of snowmelt water is presented. As a result, a revision for the SWI and ER index incorporating the amount of snowmelt water with rainfall is introduced and the slope failure scenarios are examined.

In conclusion, a new criterion Effective Precipitation (EP) index is proposed for the prediction and early warning of snowmelt induced soil slope failures. It is found that the new criterion introduced in this study perform well for the prediction of slope failure disasters in cold regions.

< This dissertation is a modified and revised form of the following original journals and proceedings>

1. Siva Subramanian, S., Ishikawa, T., and Tokoro, T. Stability assessment approach for soil slopes in seasonal cold regions, ***Engineering Geology***, Vol., No, 221, pp. 154–169, April, 2017.

2. Siva Subramanian, S., Ishikawa, T., Tokoro, T. (2017). An early warning criteria for the prediction of snowmelt induced soil slope failures in seasonal cold regions. ***Soils and Foundations*** (Submitted).

3. Siva Subramanian, S., Ishikawa, T., Yokohama, S., and Tokoro, T. Numerical simulation of volcanic soil slope failure under coupled freeze-thaw and rainfall infiltration effects. ***Japanese Geotechnical Society Special Publication***, Vol., No, 1, pp. 5–10. August, 2015.

4. Siva Subramanian, S., Ishikawa, T., and Tokoro, T. Climatic effects on the stability of unsaturated soil slopes in cold region. ***19 th International Conference on Soil Mechanics and Geotechnical Engineering*** (19th ICSMGE). September 17-22, 2017. Seoul, Republic of Korea.

5. Siva Subramanian, S., Ishikawa, T., and Tokoro, T. Evaluation of applicability of numerical modelling tools for complex slope stability problems in Hokkaido. ***55th Annual Meeting of Hokkaido Branch Japanese Geotechnical Society***. Vol., No, 1, pp. 215-224. January, 2015.

ACKNOWLEDGEMENTS

Firstly, I would like to express my sincere gratitude to my supervisor Prof. Tatsuya Ishikawa for his continuous support during my doctoral study and related research, for his patience, motivation and immense knowledge. His guidance helped me in all the time of my research and writing of this thesis.

Sincere thanks are also due to all members of the doctoral committee, Prof. Yoshiaki Fujii and Prof. (Assoc.) Satoshi Nishimura for their invaluable comments and help all time.

I am sincerely grateful to Emeritus Prof. Seiichi Miura for introducing me to Prof. Tatsuya Ishikawa. I am also extremely grateful to Prof. (Assoc.) Satoshi Nishimura for his inspirations in teaching advanced soil mechanics, guidance in geotechnical field works and for his continuous assessments of my research and for his tremendous support for the justification of this thesis.

I want to express my sincere thanks to Prof. (Assoc.) Koichi Isobe and Prof. (Asst.) Shoji Yokohama for their big support and advice in performing numerical simulations and experiments. I am also greatly indebted to Dr. Satoshi Matsumura formerly of Hokkaido University who was always forward to help me and suggesting valuable advice for my work. I gratefully acknowledge the students of Laboratory of Analytical Geomechanics for their help during these three years.

I would like to thank Prof. (Assoc.) Tetsuya Tokoro, who taught me techniques and useful tricks in geotechnical element tests. I gratefully acknowledge Emeritus Prof. Hiroyuki Tanaka formerly of Hokkaido University for his valuable advice, critics and comments about my research.

I would also like to thank and express my sincere gratitude to my Professors in my home country, Principal Scientist Dr. John Loui Porathur of CSIR-CIMFR (Council of Scientific and Industrial Research - Central Institute of Mining and Fuel Research), India and Emeritus Prof. Arangaswamy Ganesh formerly of Bharathidasan University, India for their incessant support and guidance all through my career.

This research was made possible through the financial support from MEXT (The Monbukagakusho Scholarship) and English Engineering Education (e^3) Program of Hokkaido University.

Finally, my special thanks are extended to my beloved wife Aarthi Srikrishnan, my parents, family and friends. Without their encouragement, support and confidence in me all through these years, it would not be possible for me to arrive Japan and complete my doctoral study.

TABLE OF CONTENTS

LIST OF FIGURES

LIST OF TABLES

CHAPTER 1

1 INTRODUCTION

1.1 Background

Under the context of global climate change, the threat of natural disasters in cold regions are ever increasing. Since Japan is a high latitude country, and Hokkaido is the northern most Island, snow and rain-induced natural disasters i.e. landslides, debris flows, sediment disasters and slope failure etc. occur frequently. Between 1978 to 1997 more than 15 large-scale snowmelt induced slope disasters were recorded causing small to large scale damages to the road transport in northern regions of Japan possessing an extreme threat to human life (Ishida et al., 2000). More than 15 small to large scale slope disasters were reported between 1999 – 2015 in and around Hokkaido (Iwakura et al., 2000). Since 2000, more than 62 % of the natural and man-made slopes along the Highways of Hokkaido required urgent special inspections for the prevention against collapses induced by rainfall and snowmelt water (Ishikawa et al., 2015). These disasters were also influenced by freeze-thaw action and snowmelt water infiltration.

Japan being geologically not very old, the terrain and surface soil are not well stabilised and will quickly react to mass movements by rainfall, snowfall, snowmelt and earthquake etc. Furthermore, considerable areas of Japan are covered by volcanic soils, which have been produced since the quaternary period. Likewise, in Hokkaido, volcanic soils are broadly spread over 40 % of the total area. With a decrease in the air temperature during the winter season, a surface layer of soil slope freezes vertically from the ground surface, and with an increase in air temperature during the spring season the frozen soils contrariwise thaw from the ground surface. This freeze-thaw action correspondingly affects the seepage flow inside the soil slope since the frozen soil layer will become partially/completely impermeable under negative temperatures. Accordingly, the stability assessment and prediction of slope failure during snow melting season are indispensable for the disaster prevention measures in Hokkaido.

The seasonal climatic factors persuading the soil moisture conditions in snowy cold regions could be explained by a conceptual figure as shown in Figure 1.1. In snowy cold regions like Japan, the annual climate has four distinct seasons, i.e. a winter from December to February, a Spring from March to May, a Summer from June to August and an Autumn from September to November.

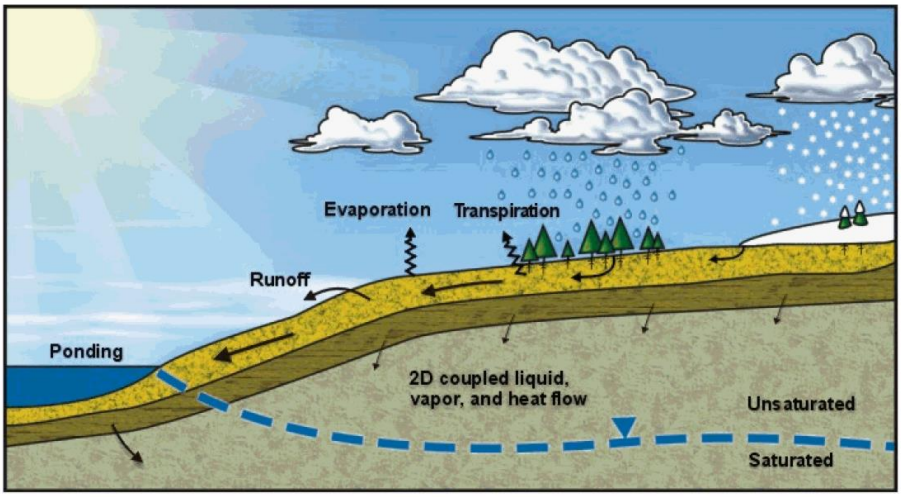

Figure 1.1 Physical processes related to seepage regarding snowy cold regions (after Krahn, 2007)

As shown in Figure 1.1. the surface soil moisture in snowy cold regions is affected by snowmelt water, freezing and thawing, evaporation and transpiration etc. Ishikawa et al. (2015) classified the mechanism and types of slope failures occurring in Hokkaido as explained from Figure 1.2.

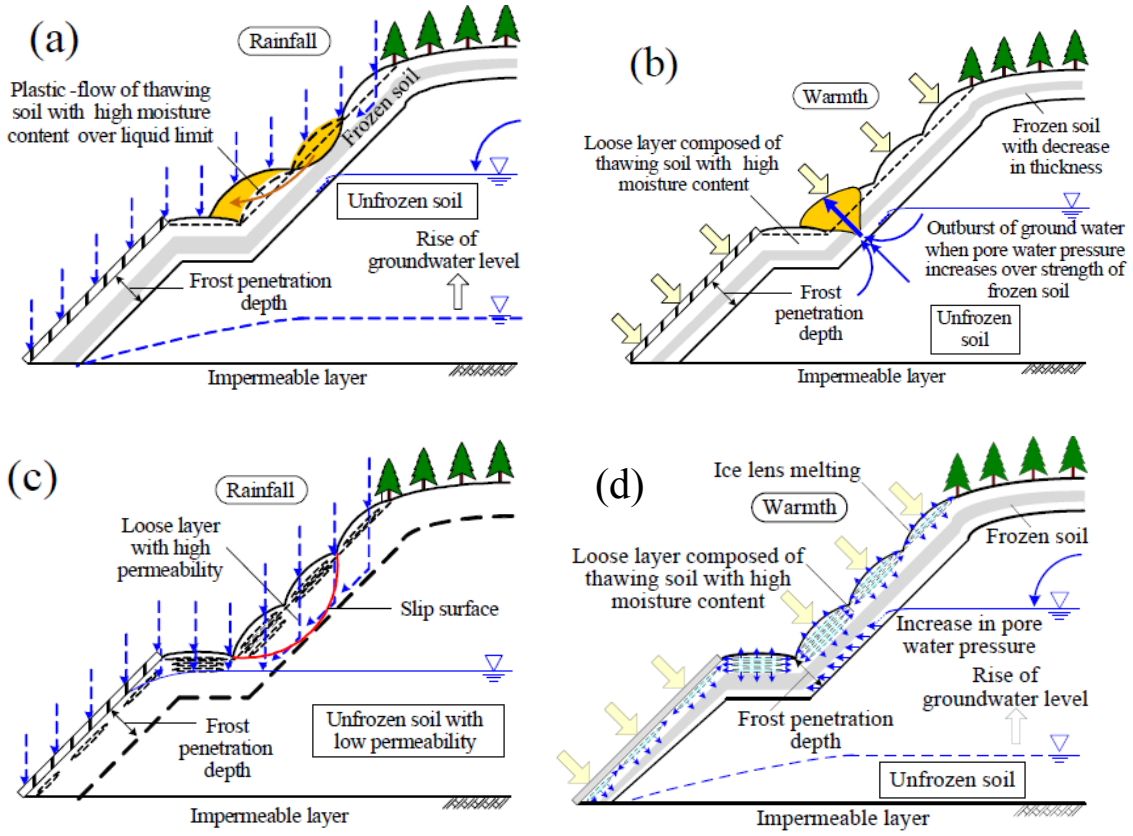

Figure 1.2 Mechanisms of soil slope failures occurring in Hokkaido (Ishikawa et. al., 2015)

1.2 Objective, purpose and methodology of the study

The objectives of this study are,

1. Identifying the effects of seasonal variations of weather on the stability of soil slopes in Hokkaido.
2. Finding a suitable method to analyse and estimate the stability of soil slopes in seasonal cold regions.
3. Proposal of a stability assessment approach for soil slopes in seasonal cold regions.
4. Proposing an early warning criteria for snowmelt induced soil slope failures in Hokkaido.
5. Performance evaluation of the stability assessment approach and the early warning criteria to make use in practice.

The purpose of this study are as follows.

An enormous number of studies have been done to identify the factors that affect the soil slope stability in cold regions (McRoberts and Morgenstern 1974a, 1974b; Mackay, 1981; Goodrich, 1982; Burgress, 1993; Niu, 2005). McRoberts and Morgenstern (1974b) investigated the failure mechanism of thaw-induced landslide slope failures observed in permafrost regions of Canada. Unlike permafrost regions, seasonal cold regions like Hokkaido experience abrupt weather changes throughout the year, which in turn fluctuates the ground temperature and water content of the soil. The excess water content originating from the snowmelt water and rainfall may induce a slope failure. Since most of the slopes are unsaturated, the key factor that determines the stability of this type of slope failures is the soil water content distribution. Ishikawa et al. (2015) comprehensively summarised the distinction between slope failures in seasonal cold regions and warm temperate regions and pointed out the important factors that need to be considered in the stability assessment of unsaturated soil slopes in seasonal cold regions. To date, an applicable stability assessment approach considering all the seasonal changes of water content, for soil slopes in cold regions has not been adopted in geotechnical practice.

Many studies have been done to standardise an early warning criterion to predict the oncoming slope disasters in snowy cold regions by using metrological data i.e. rainfall and snowmelt water etc. (Okimura and Ichikawa, 1985, Berris and Harr 1987, Singh et al. 1997, Williams et al. 1999, Matsuura 1998, Matsuura 2000, Matsuura et al. 2005, Matsuura et al. 2008, Matsuura et

al. 2013 and Nakatsugawa et al. 2015). According to many of the above-mentioned studies, the Japanese early warning criteria i.e. Soil-water index (SWI) and Effective rainfall index etc. need to be revised for the prediction of slope failures in seasonally cold regions. These criteria do not consider the soil water content supplied from the snowmelt. Compared to the hourly rate of rainfall precipitations, the hourly rate of snowmelt water is relatively very small. Instead, the snowmelt process is continuous during thawing season resulting in a continuous supply of water to the soil surface. As the cumulative amount of snowmelt water is large and its effects on soil instabilities are higher, the above-mentioned criteria fail to predict the oncoming soil slope failures and debris flows due to the larger pre-determined rainfall threshold values (Ishida et al., 2000). For these reasons, a method to quantify the hourly rate of snowmelt is necessary so that it can be incorporated in these early warning criteria. Based on this background, a criterion which can be used for the early warning of soil slope failures and debris flow disasters is proposed in this study. Two case studies of soil slope failures occurred in Hokkaido are studied. The applicability of the existing early warning systems is studied by applying those criteria to the case studies. An empirical method to estimate the hourly snowmelt rate is presented. A new early warning criterion to predict the snowmelt induced soil slope failures in seasonal cold regions is introduced. The applicability and validity of the new criterion is examined through detailed parametric numerical simulation studies.

1.3 Organisation of thesis

The organisation of the thesis is as follows. This thesis is drafted into a total of six chapters.

Chapter 1 Introduces the research background of the study briefly. The objectives, purpose and methodology of the research is outlined here. The organisation of the thesis is outlined at the end of Chapter 1.

Chapter 2 Presents the case examples of soil slope failures analysed in this study. The background, geotechnical setting and meteorological conditions of the failures are discussed deliberately. A review of the soil slope failures occurred in Hokkaido, Japan is included.

Chapter 3 Introduces the proposed/recommended slope stability assessment approach. At first, a review of the studies towards understanding the mechanism of slope instability problems in Hokkaido is done. Then, a brief review of the state of the art sophisticated thermo-hydro-mechanical models proposed for frozen soils is deliberated. Finally, the

recommended slope stability assessment approach is explained. A discussion about the consideration and non-consideration of factors in comparison to THM models is shown. The concept of the coupled thermo-hydro analysis under unsaturated conditions is explained. Modelling atmospheric-ground coupling is discussed. Mechanical behaviour of soil is explained.

Chapter 4 Presents the analysis of soil slope failures using the proposed stability assessment approach. At first, the numerical modelling and stability assessment of a volcanic soil embankment slope is explained. Then, a case study of slope failure along a national highway in Hokkaido is discussed. Finally, parametric studies performed to analyse the influence of climatic factors on soil slope stability is discussed.

Chapter 5 Presents the prediction and early warning of soil slope failures in snowy cold regions. At first, an overview of the current slope failure early warning systems used in Japan is shown. Among those, prime consideration was given to the Soil Water Index (SWI) and Effective Rainfall (ER) index. A review of studies concerned to the early warnings in cold regions is included. The applicability of the early warning criteria SWI and ER for the cases of slope failures occurred in Hokkaido are examined. An empirical model to predict the amount of snowmelt water is suggested. A new early warning criteria Effective Precipitation (EP) index is proposed.

Chapter 6 Summarises the findings and conclusions of the study. Recommendations for the analysis and prediction of soil slope failures in Hokkaido have been outlined. A brief discussion for the design and mitigation measures of soil slope failure disasters in snowy cold regions is included.

CHAPTER 2

2 CASE STUDIES OF SOIL SLOPE FAILURES IN HOKKAIDO

2.1 A review of slope disasters occurred in snowy cold regions of Japan

Between 1978 to 1997 more than 15 large scale snowmelt induced slope disasters were recorded causing small to large scale damages to the road transport in northern regions of Japan possessing extreme threat to human life (Ishida et al., 2000). More than 15 small to large scale slope disasters were reported between 1999 – 2015 in and around Hokkaido (Iwakura et al., 2000). These disasters were triggered by freeze-thaw action and snowmelt water infiltration. Table 1 summarises major occurrences of slope failures occurred during thawing season in snowy cold regions of Japan.

Table 2.1 List of sediment disasters occurred and recorded in snowy cold regions of Japan (after Iwakura et al. 2010)

S. No.	Date of occurrence	City	Type of sediment-related disasters	Cause
1	1999-4-1	Lee County	Landslides	Snow melting
2	1999-4-14	Otaru City	Landslides	Rainfall and snow melting
3	1999-4-15	Shakotan-gun	Landslides	Snow melting
4	1999-4-18	Kamikawa-gun	Landslides	Snow melting
5	2000-5-01	Nakayama pass	Landslides	Rainfall and snow melting
5	2004-2-22	Western County	Landslides	Rainfall and snow melting
6	2004-2-22	Western County	Sediment discharge	Rainfall and snow melting
7	2004-3-17	Western County	Debris flow	Rainfall and snow melting
8	2004-3-17	Kodaira County	Landslides	Rainfall and snow melting
9	2007-4-30	Otaru	Debris flow	Snow melting
10	2007-5-2	Otaru	Landslides	Snow melting
11	2012-5-01	Nakayama pass	Sediment discharge	Rainfall and snow melting
12	2013-04-07	Nakayama pass	Embankment collapse	Rainfall and snow melting

2.2 Case study of trial embankment slope

The first case example of soil slope failure discussed in this thesis is an embankment slope constructed using a volcanic soil at an angle of 45° with 5 m elevation and 7.7 m length at the base. Many kinds of volcanic soils are widely deposited in Hokkaido, and thus those have been often used as useful embankment materials. The site of the embankment slope is located at Latitude 42°57′13″ North and Longitude 141°21′46″ East in Hokkaido, Japan. The place is at the typical area inside the Shikotsu pumice flow deposit, denoted as "Spfl" near Shikotsu Volcanic caldera. As shown in Figure 2.1 thermometers, tensiometers, moisture content sensors, rainfall gauges and a snow gauge were installed in the slope to monitor the ground temperature, pore water pressure, soil water content, rainfall and snowfall respectively. To avoid disturbance to the surface soil of the slope, the monitoring instruments were installed in three different cross sections namely Left (L), Centre (C) and Right (R) as viewed from the bottom of the slope.

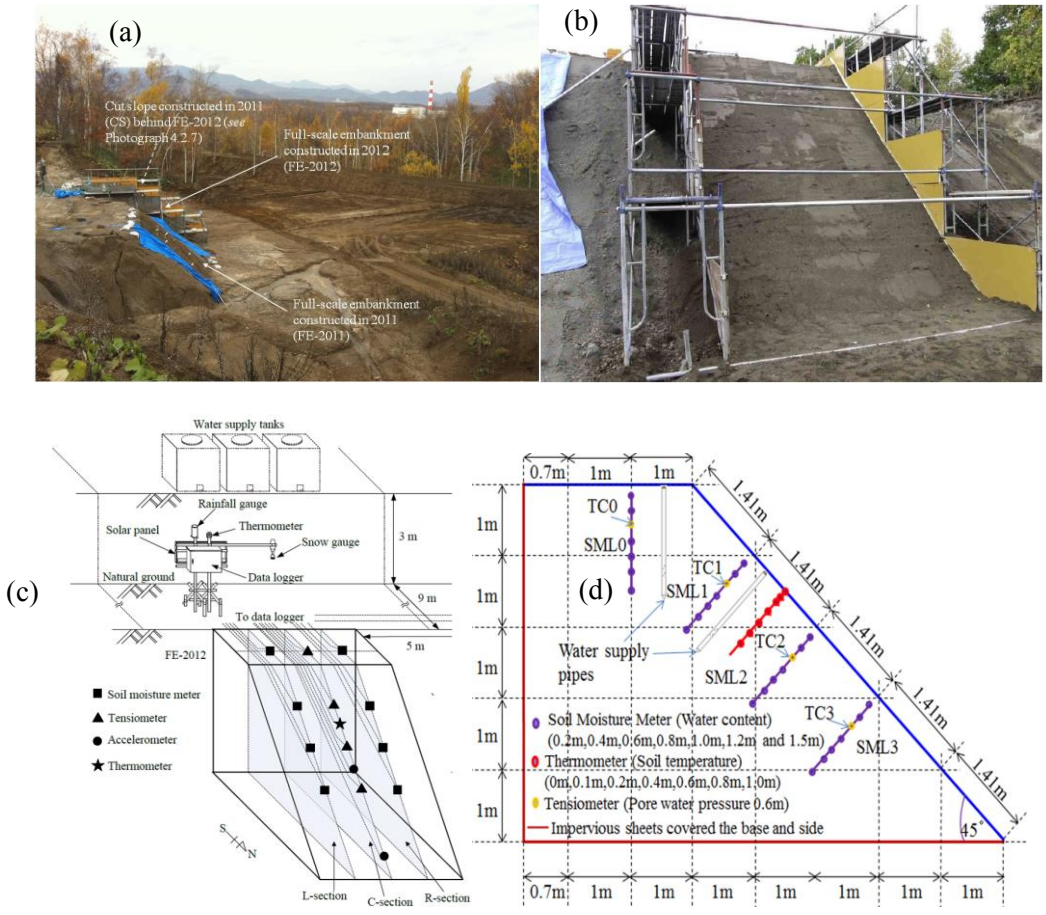

Figure 2.1 Photographs (a and b), 3D schematic view (c) and 2D cross-sectional view (d) of the embankment slope showing installed monitoring instruments (adapted from Matsumura, 2014)

The monitoring instruments installed in cross sections are shown in Figure 2.1 (c and d) in a three-dimensional and two-dimensional view. To prevent the mutual water exchange between the compacted embankment soil and ground surface, the embankment slope was covered by impermeable sheets made up of thin waterproof plastic materials at the bottom and side portions. A geomembrane liner is not used in this case, as it was understood that the water flow through the slope might not reach the slope bottom due to the soil's low permeability, and the purpose of impermeable sheets are to avoid some possible flow of water from the foundation soil. The foundation was also made up of the same volcanic soil material. In this case, no consideration was given to the interface friction that may occur between the impermeable sheets and soil layers. After placing the sheets at the bottom and the back side, the soil is compacted layer by layer with a constant depth of 0.25 m per layer up to 5 m height, using a hand-guided roller compactor.

A prescribed volume of water (approximately 1 m^3/day) was supplied to the slope using water supply pipes at constant intervals through different cross sections. The amount of the water supplied is determined based on the storage of water supply tanks. The intervals at which water was supplied through Left (L) section are 27-07-2013 to 06-08-2013 (10 to 11 days) and 11-10-2013 to 17-10-2013 (6 to 7 days). The construction and setting up of monitoring instruments were finalised and monitoring started on November 9, 2012 (09-11-2012). The monitoring continued until the day of slope failure on October 17, 2013 (17-10-2013). Total monitoring time was around 343 days. Further details about the slope monitoring program can be found from Matsumura, (2014) and Kawamura et al. (2016).

The air temperature, ground temperature and measured rainfall and snowfall amounts during the entire monitoring period is shown in Figure 2.2. The monitored pore water pressures and water content at different locations are shown in Figure 2.3. A photograph is shown in Figure 2.4 detailing the shape of the slope failure. Figure 2.5 depicts the shape of the outlined slip surface. The measured water content through section L and section R are shown in Figure 2.6 and Figure 2.7 respectively. Using these monitored data, the behaviour of the slope is studied through performing detailed slope stability analysis which will be explained in later chapters of this thesis.

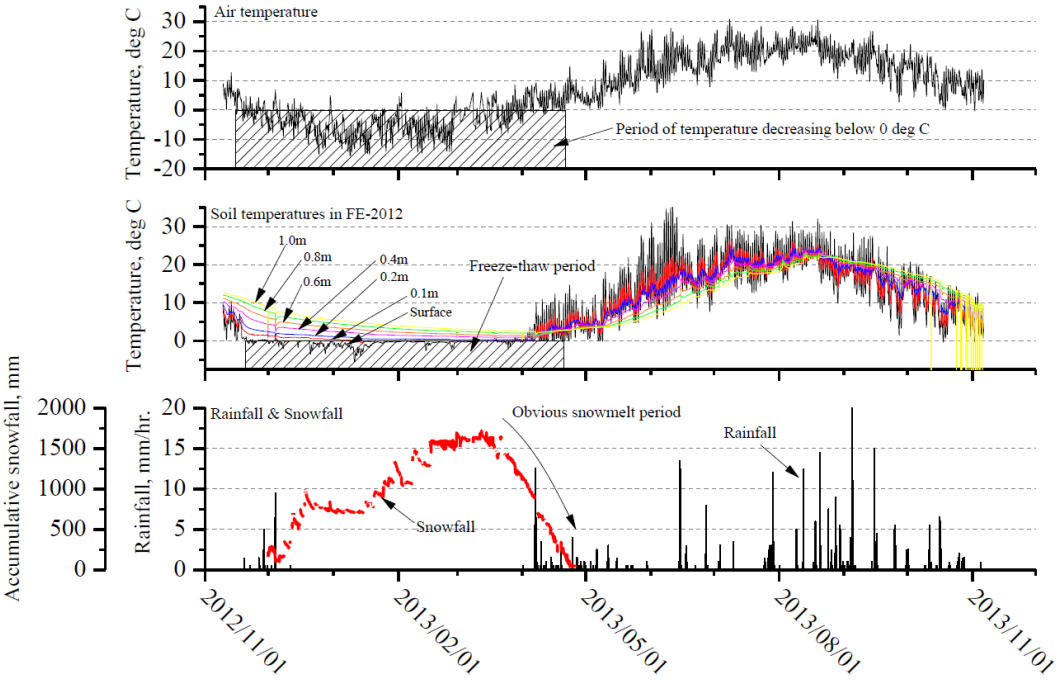

Figure 2.2 Temperature and precipitation monitored at the embankment site (after Matsumura, 2014)

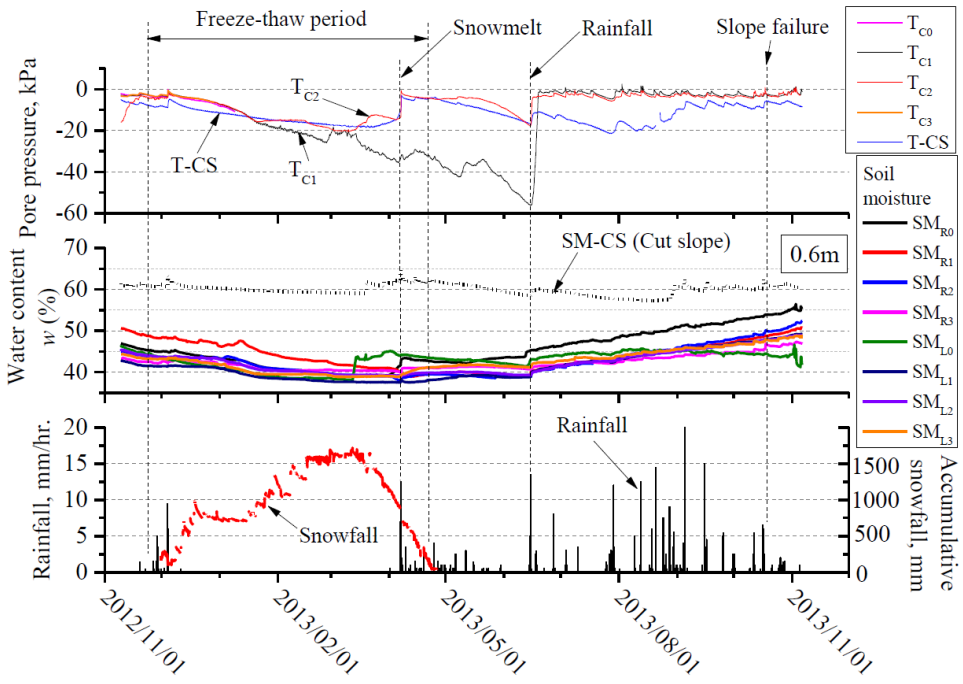

Figure 2.3 Soil water content and pore water pressure time series viewed against occurred precipitation (after Matsumura, 2014)

Figure 2.4 Picture of the occurred soil slope failure on 17-10-2013 (after Matsumura, 2014)

Figure 2.5 Slip surface identified on 15-11-2013 (after Matsumura, 2014)

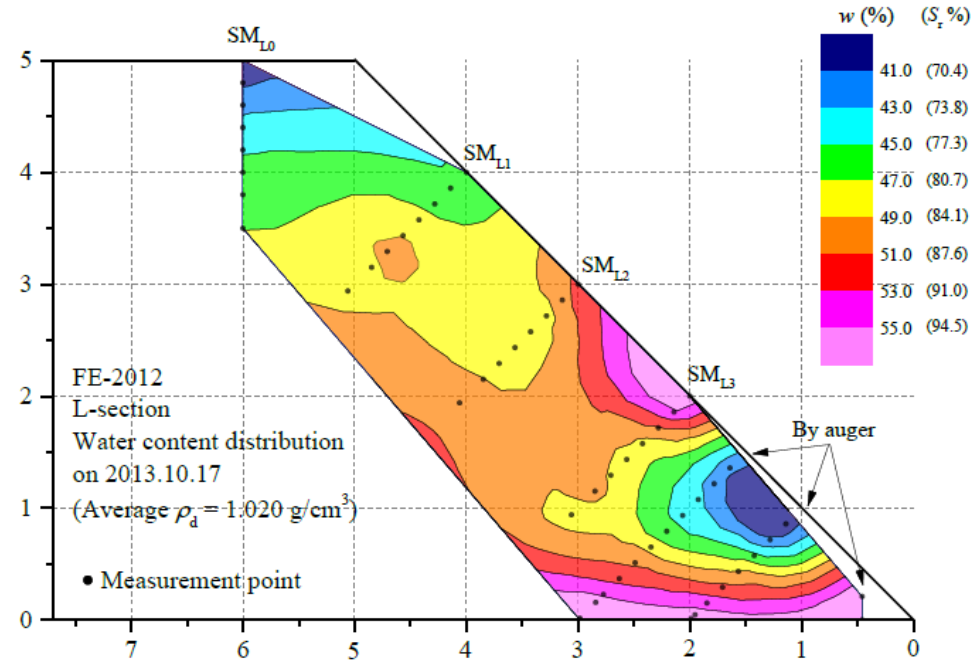

Figure 2.6 Distribution of water content on the day of slope failure along L- section (Matsumura, 2014).

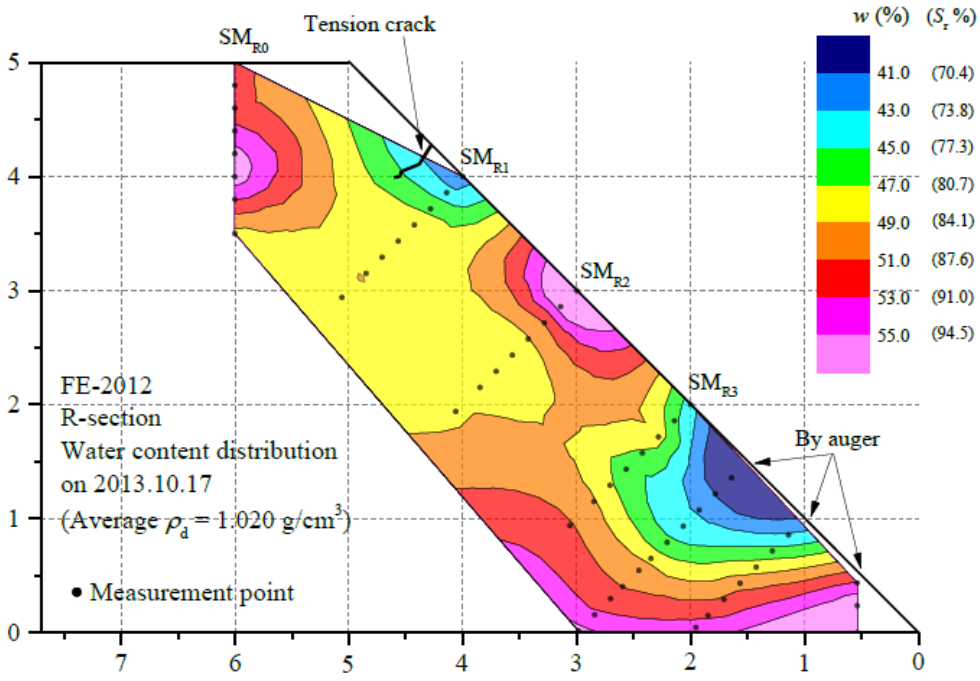

Figure 2.7 Distribution of water content on the day of slope failure along R- section (Matsumura, 2014).

2.3 Case study of slope failure occurring along national highway route 230

On April 7, 2013, at 11:20 A.M., a slope failure happened along the national highway route No.230 near 42° 54' 52" North Latitude and 141° 07' 22" East Longitude in Hokkaido, Japan. The national highway connects Sapporo city with Setana, a town in the Hiyama sub prefecture of Hokkaido. Hereafter, the slope failure will be referred as highway slope failure. The slope failure occurred in the embankment filling along the roadway. The size of the slope failure was around 40 m wide along the road and 19 m in vertical depth along the failure plane. Approximately 11000 m^3 of sediment, containing embankment filling material and accumulated snow above the soil ground together flowed out downward to the slope foot up to 40 to 50 m length, as shown in Figure 2.8 (a).

The slope failure was induced by the combined action of heavy rainfall and snowmelt water (Hokkaido Regional Development Bureau, 2013). The cumulative daily rainfall that occurred on the day of slope failure was 92 mm and the cumulative snowmelt was 31 mm, as recorded in a nearby meteorological telemetry, maintained by Ministry of Land, Infrastructure, Transport and Tourism, Hokkaido Regional Development Bureau (MLIT) shown in Figure 2.8 (b). The maximum hourly rainfall recorded on 07-04-2013 was 12 mm. The rainfall was continuous from 07-04-2013 00:00 to 07-04-2013 11:00. The cumulative daily rainfall along with the cumulative snowmelt water caused the failure of the slope. The cumulative daily rainfall and snowmelt water, which together amounted to 123 mm, is a considerable intensity to make the slope fail.

(a)

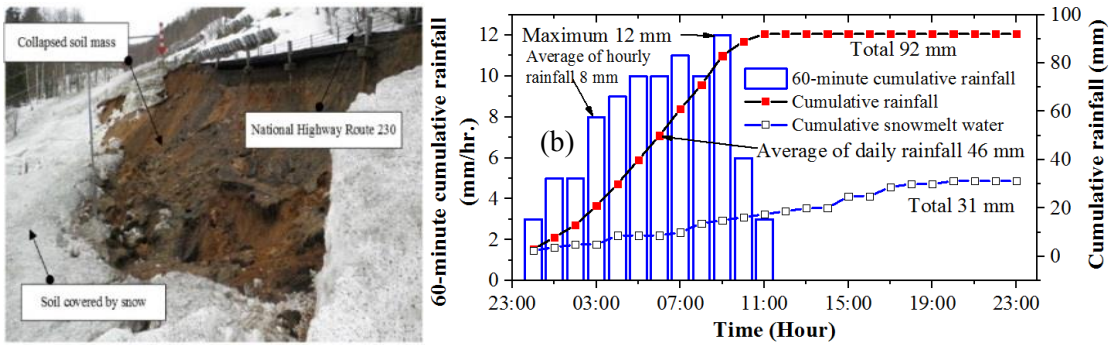

Figure 2.8 (a) Panoramic view of the slope failure (after Hokkaido regional development bureau, 2013) and (b) Rainfall and snowmelt recorded on 07-04-2013 at Mui Ne meteorological telemetry.

Geological survey of the slope failure has been performed by Hokkaido Regional Development Bureau and the geological stratigraphy are shown in Figure 2.9 and Figure 2.10.

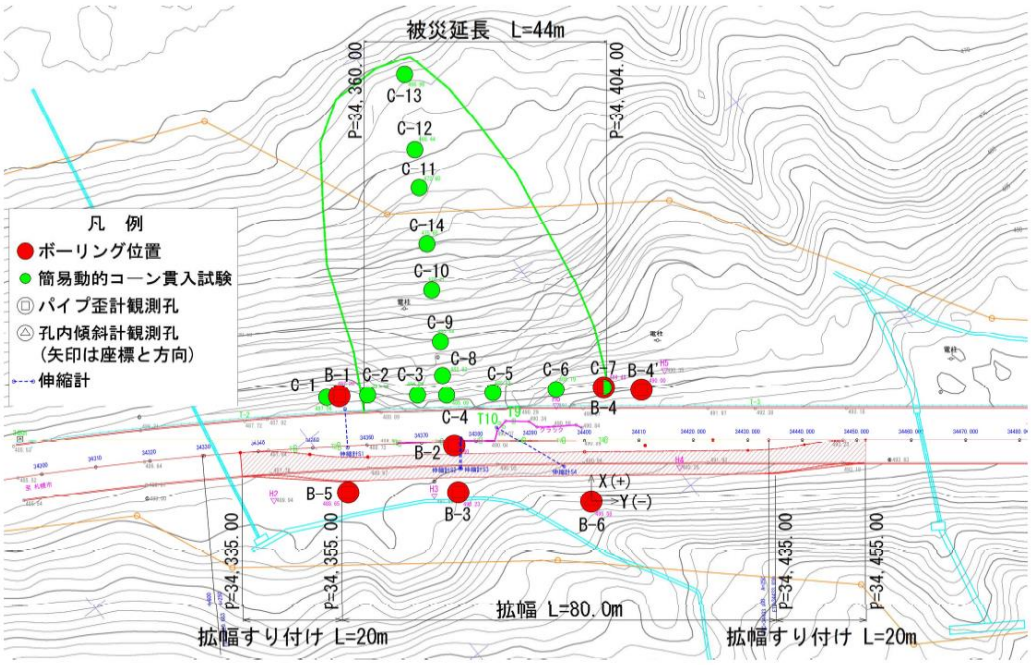

Figure 2.9 Map showing the aerial sketch of the slope failure and targeted bore hole sections (after Hokkaido regional development bureau, 2013)

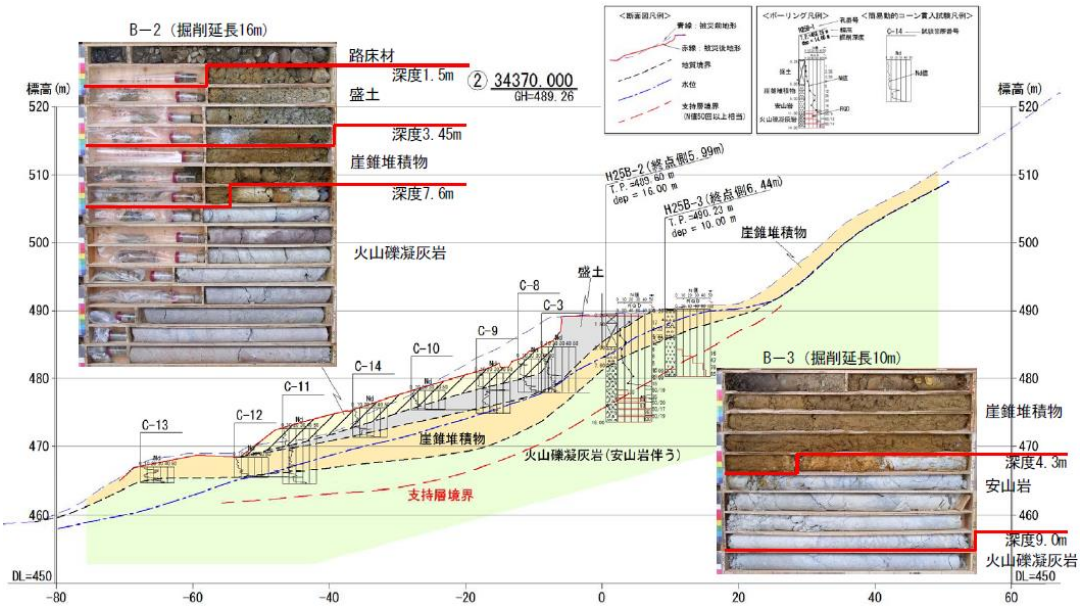

Figure 2.10 Two-dimensional cross section along bore hole number B-2 (after Hokkaido regional development bureau, 2013)

Grain size distributions and other index properties of the embankment filling and talus materials were made as shown in Figures 2.11 to 2.19.

Figure 2.11 Core soil samples at depth 0 m to 3 m (Talus sediments)

Figure 2.12 Core samples at depth 3 m to 6 m (Up to 4 m Talus sediments and after 4 m depth Andesite bedrock)

Figure 2.13 Mass measurements of cylindrical samples randomly selected at each 1 m depth for water content tests

Figure 2.14 Measurement of length and diameter of selected cylindrical samples for dry density test

Figure 2.15 Picture showing collapsed soil at depths 1.0 m to 2.0 m

Figure 2.16 View of crushing of samples for soil density tests

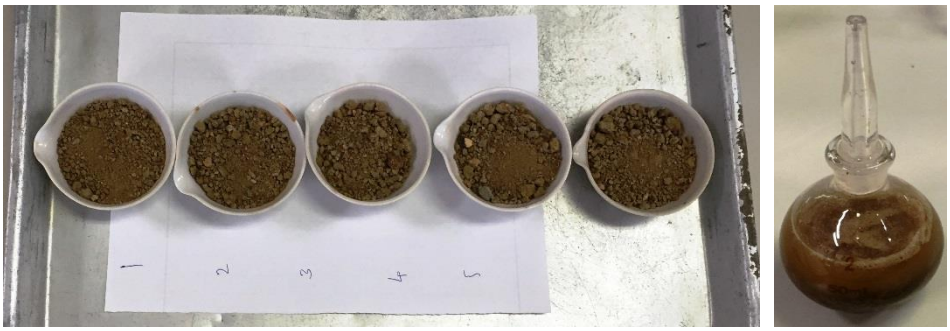

Figure 2.17 (a) Specimens used for solid density tests and (b) a view of a pycnometer filled with distilled water and soil specimen kept for reaching a steady room temperature

Figure 2.18 Photo showing collapsed soil from cores taken at depth 1.0 m to 2.0 m and cores taken at depths 3.0 m to 4.0 m

Figure 2.19 Photographs showing soil particles remained in (a) 2 mm sieve and (b) soil particles remained in 75 µm sieve (soil corresponding to core specimens at depth 3.0 m to 4.0 m

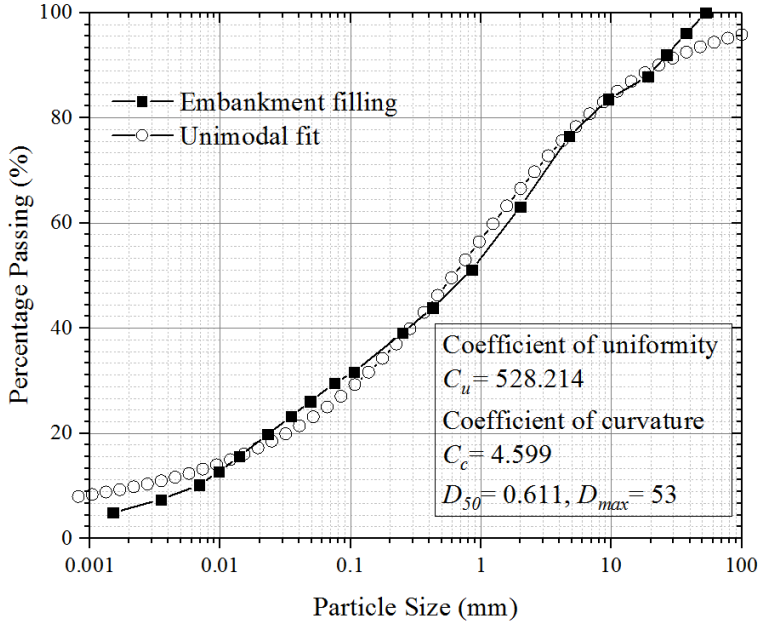

Figure 2.20 Grain size distribution curve of the Embankment filling material

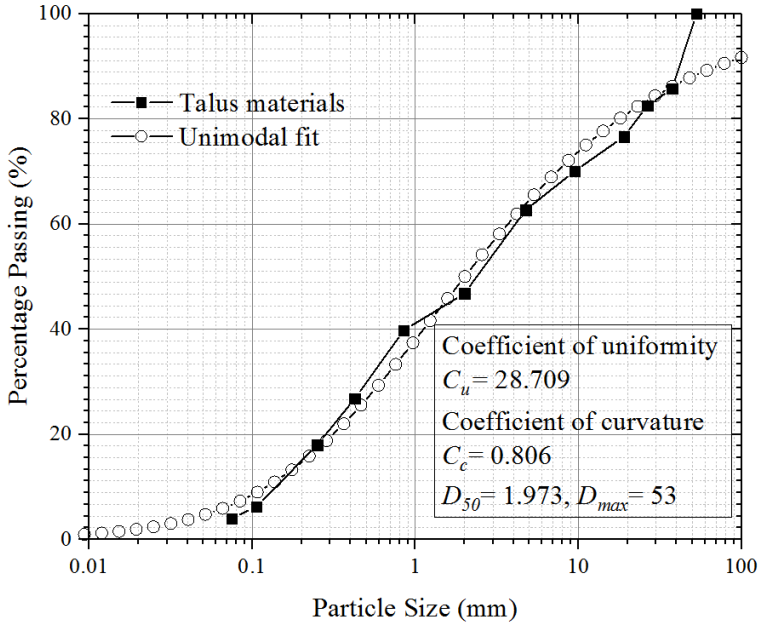

Figure 2.21 Grain size distribution curve of the Talus material

The index properties of the soil material Embankment filling and Talus were measured in laboratory and as summarised in Table 2.2. The Grain Size Distributions (GSD), Solid Densities, Porosities etc. were independently measured for both types of soils. These index properties are used as the base for soil property estimations for both Embankment and Talus materials which are explained detailly in Chapter 4 and used in the following numerical analyses.

Table 2.2 Index properties of Embankment filling and Talus materials

Property	Embankment filling	Talus materials
Volumetric Water Content	0.29 m^3/m^3	0.037 m^3/m^3
Porosity	47.00 %	52.00 %
Void Ratio	0.89	1.115
Water Content	20.60 %	3.00 %
Dry Density	1423.00 kg/m^3	1220 kg/m^3
Total Density	1716.14 kg/m^3	1256.6 kg/m^3
Total Unit Weight	16.84 kN/m^3	12.327 kN/m^3
Specific Gravity	2.68	2.58

2.4 Case study of series of sediment disasters occurred in Hokkaido during Typhoon 2016

In addition to the snowmelt induced soil slope failures mentioned above, many occurrences of rainfall induced slope failures were also reported in Hokkaido. It is indispensable to discuss the applicability of early warning criteria for the prediction of rainfall induced soil slope failures as well as snowmelt induced soil slope failures. Therefore, a series of rainfall induced sediments disasters happened along many of the expressways and national highways of Hokkaido during August 2016, by Typhoon 10 were studied. Figure 2.22 show some of the large-scale sediment disasters captured along Doto expressway and National Highway route 274. The maximum amount of cumulative rainfall occurred in some stations exceeded 700 mm within just 3 days of typhoon. The rainfall recorded during the typhoon at three different meteorological telemetries Nissho pass, Karikachi pass and Nozuka pass are shown in Figure 2.23. The rainfall has been continuous from 28-08-2016 17:00 to 31-08-2016 03:00. The maximum hourly rainfall occurred on 31-08-2016 00:00 at Nissho and Karikachi stations are 55 mm, 38 mm respectively. At Nozuka pass the maximum recorded hourly rainfall was 34 mm on 30-08-2016 19:00. The maximum cumulative rainfall during the typhoon was about 713 mm recorded at Nozuka pass telemetry as shown in Figure 2.33(c). At other telemetries Nissho and Karikachi pass 488 mm and 364 mm of cumulative rainfall were recorded.

Figure 2.22 Typhoon affected disasters in Hokkaido during the month of August 2016. Many occurrences of small to large sediment disasters along Doto Expressways and National Highway routes (Copyright@ NEXCO and Hokkaido regional development bureau, 2016)

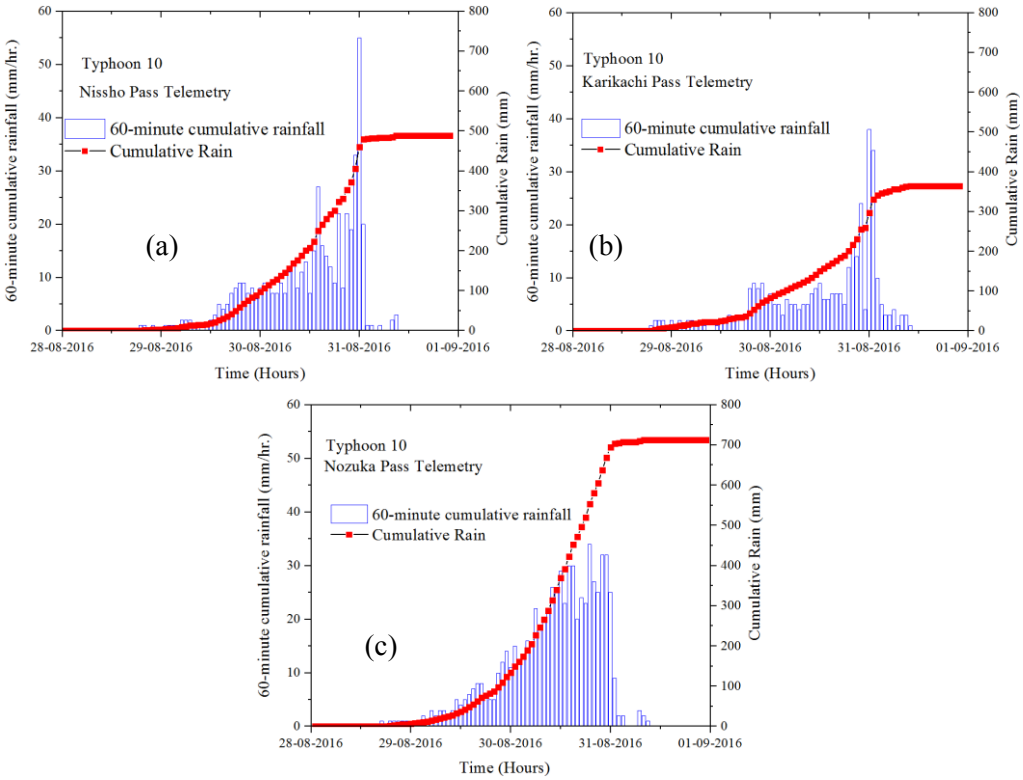

Figure 2.23 Rainfall recorded during typhoon at (a) Nissho pass meteorological telemetry (b) Karikachi pass meteorological telemetry and (c) Nozuka pass telemetry

CHAPTER 3

3 STABILITY ASSESSMENT APPROACH

3.1 Studies towards the understanding of slope instability problems in Hokkaido

Many studies have been performed earlier for slope failure problems in Hokkaido with special reference to volcanic soils. Volcanic soils are of interest here because 40 % of the surface soil of Hokkaido is covered by various type of volcanic soils and it has been widely used as a construction material. [1]According to Miura and Yagi (2003) the behaviour of volcanic soils are known to show different behaviour from that of clay or sand, and have been the subject of much research, as they have caused complicated geotechnical engineering problems in cold regions.

Long-term field monitoring on an actual cut slope, which was composed of a volcanic cohesive soil, was conducted beside national highway route 274 at Biman, Tokachi Shimizu-town in order to examine the behaviour of soil slope subjected to freeze-thaw and rainfall. A slope failure due to the increase in the degree of saturation caused by rainfall and snowmelt water occurred at a cut slope near the measurement site in the thawing season two years ago from the start of field measurement. The slope height is 23 m, and the slope angle is 34°. The soil is found to exhibit high void expansion through the results of frost heave tests. The monitoring period is from November 12, 2007 to November 13, 2009. The AMeDAS (Automated Meteorological Data Acquisition System) observation point closest to the field monitoring site, measured the 5-year average freezing index (F) in 2002–2006 as 494.2 °C·days and the average maximum snow depth is 0.86 m. Here, the freezing index is defined as the number of cumulative degree-days during freezing season. When the 0 °C isotherm gradually penetrates deep into the soil ground with time passing, the lateral displacement increases along with the growth of ice lens due to frost heave. If the frozen soil thaws from ground surface downward with a rise in air temperature, freeze-thaw of the soil slope causes the residual displacement parallel to the slope surface at a subsurface layer where frost heave occurs. Accordingly, the shear deformation is progressively developed at the subsurface layer by cyclic freeze-thaw actions. This indicates that a multistage-inclinometer is highly useful in the examination of the

[1] Information herein have been reproduced with the permission of the author of the paper. Ishikawa, T., Tokoro, T., Seiichi, M., 2015. Geohazard at volcanic soil slope in cold regions and its influencing factors. Japanese Geotech. Soc. Spec. Publ. 1:1–20

solifluction behaviour of frost-heaved soil slope at thawing season, and that for the precise prediction of subsurface failure, it is important to examine the influences of cyclic freeze-thaw actions on the thermo-hydro-mechanical behaviour of frost susceptible soil grounds in detail. In addition, Kawamura et al. (2009) examined the deformation behaviour of soil slope, which was composed of a volcanic coarse-grained soil, during freezing and thawing and during a rainfall test.

Ishikawa et al. (2010) developed a new triaxial apparatus that can simulate freeze-thaw sequences similar to those experienced by in-situ soils in cold regions. The influence of the freeze-thaw action on the mechanical behaviour of unsaturated volcanic coarse-grained soils, wherein significant particle crushing takes place during the loading processes, were studied by performing a series of freeze-thawing triaxial compression tests on volcanic coarse-grained soils under different freeze-thaw histories and different degrees of saturation. It was revealed that the cyclic freeze-thaw action induces severe particle breakage during freeze-thawing and shearing in crushable volcanic coarse-grained soils, thereby decreasing the shear strength and deformation modulus of the soil. Therefore, the freeze and thaw of pore fluid is a point to be specially considered in evaluating the risk of surface failure at soil slopes in cold regions, regardless of the frost heave characteristics of soil.

Ishikawa et al. (2010) developed a new permeability apparatus for unsaturated soils that could be used to reproduce a freeze-thaw sequence to a cylindrical specimen, as experienced by in-situ soils in cold regions. The influence of the freeze-thaw action on the infiltration behaviour of unsaturated volcanic coarse-grained soils were studied, wherein significant particle crushing takes place under low stress level, by performing a series of freeze-thawing water retention tests and freeze-thawing permeability tests along a drying process on two types of volcanic coarse-grained soils under different freeze-thaw histories and different degrees of saturation.

Later, Ishikawa et al. (2015) examined the influence of nonlinear factors such as the overburden pressure, freezing velocity, degree of saturation, and water supply system on the frost heave behaviour of volcanic fine-grained soils, which are considered as the factors that strongly influence the frost heave amount of soils. To this end, they performed a series of frost heave tests on a frost-susceptible geomaterial under different test conditions and performed a water retention test of the frost-susceptible geomaterial to examine the water retentivity characteristics of the soil in the unsaturated condition. Based on the test results, they discussed the influences

of the test conditions on the frost heave amount of the volcanic fine-grained soil. Additionally, they proposed an estimation method for the frost heave amount of unsaturated subsurface soils under low overburden pressure, and discussed the applicability and usefulness of the proposed estimation method by comparing the results of the frost susceptibility tests with the estimation results (Luo et. al., 2017).

Ishikawa et al. (2015) clearly distinguished the difference between soil slope failures in warm-temperate regions and snowy cold regions. A summary of the main conclusions of their study is reproduced here. By comparing the slope failure mechanism in cold regions with that in warm-temperate regions, the endogenous factors and the exogenous factors of slope failures in cold regions can be summarised as given in Figure 3.1. Note that there are two types of exogenous factors that produce the increase in the sliding force and the decrease in the shear resistance, respectively.

Factor type		Factor name	In warm regions	In cold regions
Endogenous factors		Slope inclination	Affected	Affected
		Shear strength of soil	Affected	Affected
		Weathering velocity of soil and its stability	Affected	Affected
		Existence of slip surface and its formation	Affected	Affected
		Water catchment topography and ground water level	Affected	Affected
		Snowy cold climatic conditions	–	Seriously affected
		Frost susceptibility of soil	–	Seriously affected
Exogenous factors	Increase in sliding force	Shape change of slope	Affected	Affected
		Seismic motion	Affected	Affected
		Increase in unit weight of soil	Affected	Affected
	Decrease in shear resistance	Decrease in shear strength of soil	Affected	Affected
		Increase in pore water pressure	Affected	Affected
		Formation of loose soil layer due to frost heave	–	Seriously affected
		Change in physical properties of soil due to freeze-thaw	–	Seriously affected
		Change in mechanical properties of soil due to freeze-thaw	–	Seriously affected
		Formation of impermeable frozen soil layer	–	Seriously affected

Figure 3.1 Influencing factors of slope failure in cold regions (after Ishikawa et. al., 2015)

(a) Important factors for slope failure in warm temperate regions are mainly summarised as follows:

[Endogenous factors]

- Slope inclination
- Shear strength of soil
- Weathering velocity of soil and its stability
- Existence of apparent and potential slip surface and its easiness for formation
- Water catchment topography and ground water level

[Exogenous factors]

- Shape change of slope due to erosion, excavation, and embankment
- Seismic motion
- Increase in unit weight of soil following increase in water content due to rainfall
- Decrease in shear strength of soil following increase in water content due to rainfall
- Increase in pore water pressure due to change in groundwater level and seepage flow and rainfall

(b) Important factors for slope failure in cold regions are mainly summarised below in addition to those in warm-temperate regions as follows:

[Endogenous factors]

- Snowy cold climatic conditions
- Frost susceptibility of soil

[Exogenous factors]

- Increase in unit weight of soil following increase in water content due to rainfall, snowmelt water and frost heave
- Influx of snowmelt water and thawing of ice lenses would cause an increment in water content of soils, thereby inducing the increase in unit weight which increases the sliding force.
- Decrease in shear strength of soil following increase in water content due to frost heave, freeze-thaw, and snowmelt water:

  Increment in water content caused by snowmelt and ice lens melting would induce decrease in matric suction, in other words, decrease in total cohesion of soil, which is directly related to the decrease in shear resistance.
- Changes in groundwater level and seepage flow, and increase in pore water pressure due to frost heave, freeze-thaw, and snowmelt:

  When an impermeable layer exists in soil slope, pore water pressure at the unfrozen soil ground behind the frozen soil layer will increase due to the rise of the ground water level. Furthermore, in soil ground where a loose soil structure has developed by freeze-thaw actions, streamlines are centralised due to high permeability of the soil, thereby increasing seepage force. These changes would influence the sliding force and shear resistance of soil. Formation of loose soil layer due to frost heave and freeze-thaw. Cavitation of ice lens inside frozen soil with thawing makes

the soil skeleton loose, and in other words, causes the decrease in soil density, thereby inducing the decrease in shear strength of soil.

- Changes in physical properties due to frost heave and freeze-thaw: Physical properties of clay and silt subjected to freeze-thaw actions tend to become hydrophobic, to decrease the amount of drying shrinkage, and further to decline the liquid limit as well as the water retentivity. These changes would affect the sliding force and the shear resistance of soils.
- Change in deformation-strength and water retention-permeability characteristics due to frost heave and freeze-thaw:

  Although the effect of freeze-thaw history differs depending on over consolidation ratio of clay, it does affect deformation-strength and water retention permeability characteristics of soils. These changes would affect the sliding force and the shear resistance of soils.
- Formation of impermeable frozen soil layer due to frost heave and freeze-thaw:

  Since frozen soil layer can be considered as an impermeable layer, water content of soil ground shallower than frost penetration depth increases due to ice lens melting and rainfall, which would induce the increase in unit weight of soils and the decrease in the shear strength. Besides, since thawing soil, which exhibits high fluidity and high water content, exists over the slippery frozen soil layer, the slope failure regarding the boundary of two-layer structure as a potential slip surface would occur easily in thawing season as compared with usual.

A brief review of the studies performed towards understanding slope instability problems in Hokkaido state that for the analysis of geotechnical structures i.e. fill slopes, embankments and natural slopes, a sophisticated analytical procedure accounting the above explained key influencing parameters is necessary. There are very few studies available regarding a numerical or analytical procedure to analyse frozen soil slope stability problems. Whereas, there are many numbers of numerical and analytical procedures developed in recent years for the analysis of frost heave induced soil behaviour. A concise review of the developments in the study of frost heave and its modelling on a numerical perspective is discussed in the next section.

3.2 Review of analysis methods for frozen soil behaviour

For the analysis of frozen soil/rock behaviour, many complex thermo-hydro-mechanical models (THM) were developed in the last three decades (Selvadurai et al., 1999; Li et al., 2000, Neupane and Yamabe 2001, Li et. al., 2002, Coussy, 2005, Michalowski and Zhu 2006, Li et. al., 2008; Nishimura et al., 2009; Thomas, H. R. et al., 2009, Liu and Yu, 2011, Kolditz et. al., 2012, Liu et. al., 2012, Zhou and Meschke, 2013, Lai et. al., 2014, Koniorczyk et. al., 2014, Wang and Liu, 2015, Zhang et. al. 2015, Zhang et. al., 2016, Ishikawa et al., 2016 and Bin et. al., 2017). Of these THM models listed above, the models proposed by Selvadurai et al., (1999), Li et al., (2000), Neupane and Yamabe (2001) and Nishimura et. al., (2009) are state of the art developments in frozen soil mechanics. Selvadurai et al., (1999) developed a novel computational approach to study the discontinuous frost heave within a frozen soil region. Li et al., (2000) introduced a coupled heat-moisture-mechanical model for frozen soil and demonstrated the applicability for a foundation problem. Neupane and Yamabe (2001) modelled the behaviour of frozen rock assuming Mohr-Coulomb yield criterion. Later, Nishimura et al., (2009) proposed a fully coupled THM model using finite element (FE) framework and developed a new critical-state elasto-plastic soil constitutive model to consider problems involving water-saturated frozen and unfrozen soils. Recently, Ishikawa et al., (2016) developed a coupled thermo-hydro-mechanical finite element (FE) analysis method to analyse freeze-thaw and deformation of unsaturated/partially saturated soils. The robustness of the THM models discussed above is well proven for the prediction of soil behaviour influenced by frost-heave.

Irrespective of the development of the above mentioned sophisticated and robust THM models, a brief review of the previous case studies handled by those models reveal that they were not been prepared and tested for the direct use in complicated and realistic geotechnical disasters such as slope failures, debris flows and landslides involving the freezing and thawing processes, snowmelt water infiltration etc. (Chen et. al., 2013, Siva Subramanian et. al., 2017). A review of frozen soil slope stability studies revealed that numerical modelling and simulations were short of field measurements and detailed experimental studies. On the other hand, the completely coupled heat and flow (or thermal-hydro, TH) approach in which the soil skeleton is assumed to be rigid has developed into a comparatively mature theory and has been widely recognised in fields such as hydrology, agriculture, environment science etc. since more than three decades.

Generally, two numerical methodologies are commonly utilised to study frozen soil slope stability, that is, pseudo-coupled and fully coupled numerical approaches. In the pseudo-coupled numerical approach, the coupled thermal-hydro (TH) field is analysed first, and then based on the thermal-hydro field the stress-deformation field is computed finally. The pseudo-coupled numerical approach is widely employed since the coupled thermal-hydro theories for unsaturated frozen soil are comparatively mature. Using an analogy between the mechanisms of water transport in partially frozen soils and those in unsaturated soils, Harlan (1973) analysed the coupled heat-fluid transport in frozen porous media and examined the soil-water redistribution and infiltration from a phenomenological viewpoint. Taylor and Luthin (1978) modified Harlan's model and compared the finite difference results with experimental results such as temperature, water and ice contents. To adequately model the water redistribution near the advancing freezing front, Newman (1995) developed an unsaturated soil freezing theory by modifying an existing non-freezing soil heat and mass transfer model. Hansson et al. (2004) proposed a new method based on the mixed formulation for both water flow and heat transport. By use of experimental data, the mixed formulation proved to be numerically stable and mass-conservative.

On a strict theoretical viewpoint, a fully coupled (THM) numerical approach should be utilised to analyse frozen soil slope instabilities. However, on a rational geotechnical viewpoint considering the balance between the laws of physics theory, practicality (code of practice) and computational efficiency, a pseudo coupled analysis would be appropriate depending on the nature of the problem. Since from a numerical perspective, frozen soil slope stability has not been well studied, which may be partially attributed to the still developing sophisticated coupled THM models as well as strength models of frozen soils, in this study a pseudo coupled approach is selected and utilised as discussed in the following section.

3.3 Slope stability assessment approach

In geotechnical design practice, for the long-term stability assessment of soil slopes i.e. embankment slopes and cut slopes along highways, the factors such as freeze-thaw action and snowmelt water infiltration are not considered. As found by previous research, for the design of soil slopes in seasonal cold regions the above-mentioned factors are significant (Ishikawa et al., 2015 and Siva Subramanian et al., 2015). Unlike geotechnical problems like frost heave, the

instabilities of soil slopes in Hokkaido are driven by the abrupt changes in soil water content distribution (Nakatsugawa et al., 2015).

Generally, THM models consider the phase mechanics of ice, soil solid and pore water relationships in a sophisticated manner. For slope instability problems in seasonal cold regions, the effects of ground-atmosphere interactions i.e. freeze-thaw action and snowmelt water infiltration are more significant because of the direct impacts of these factors on soil water content distribution. Computational difficulties may arise if the ground-atmosphere interactions are modelled using a THM model. Chen et al., (2013) pointed out the difficulties in performing a fully coupled THM analysis for frozen soil slope stability problems. Simultaneous numerical solutions of coupled unsaturated seepage, thermal and stress relationships including the ground-atmosphere interactions are very hard to achieve and computational methods for this purpose are not common in geotechnical engineering practice. Performing a stress based numerical simulation for a duration of one year including the time-dependent changes in soil water content, changes in temperature and including the atmospheric effects are extremely cumbersome. In addition, the dominant factor that influences the unsaturated soil slope stability in seasonal cold regions is the change in soil water content due to freeze-thaw action and snowmelt water infiltration (Ishikawa et al., 2015; Kawamura and Miura, 2013). Since the soil water content distribution inside the slope is the major factor determining the stability, it should be properly estimated for a precise stability assessment. For this purpose, a coupled thermo-hydro (TH) analysis would be appropriate, followed by a pseudo coupled mechanical analysis.

In view of these contexts, an approach to simulate the soil water content distribution subjected to freeze-thaw action and snowmelt water infiltration is recommended in this study. The approach is based on two-dimensional plane strain numerical modelling considering non-isothermal seepage simulation followed by a slope stability assessment as explained in the flow chart shown in Figure 3.2.

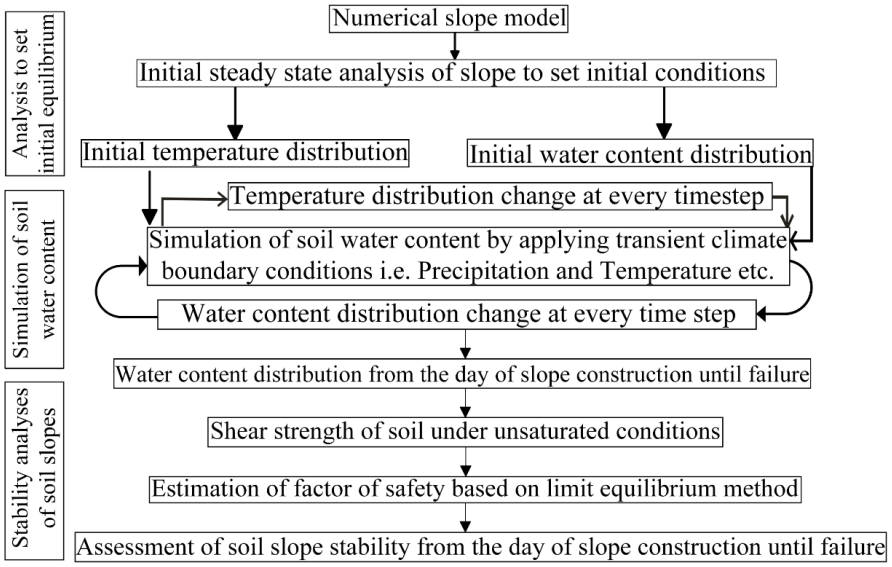

Figure 3.2 Recommended stability assessment approach for soil slopes in seasonal cold regions

There are three parts i.e. initial analysis, soil water content simulation and slope stability analysis. The first part is the initial analysis to configure the initial equilibrium of the soil slope in terms of soil water content distribution and temperature. The second part is the method used to estimate the water content distribution of the soil slope subjected to freeze-thaw action and snowmelt water infiltration. Non-isothermal seepage flow has been used to simulate the soil water flow in frozen and unfrozen soil. The interactions between the atmosphere and ground surface are modelled using a sophisticated numerical method which considers the climatic effects i.e. precipitation (rainfall and snowfall), evaporation effects and ground temperature estimations, using various governing equations as briefly explained in the following sections. The outcome of the soil water content simulation is the water content distribution inside the soil slope on a day to day basis. In the slope stability analysis, a traditional limit equilibrium technique based on the Morgenstern and Price (1965) method is used to calculate the factor of safety (FOS). The unsaturated shear strength of soil is also considered, as discussed below. The proposed numerical simulations were performed in a code GeoStudio using Vadose/W (Krahn, 2012a) and Slope/W (Krahn, 2012b) modules. As of author's knowledge, this study is the first attempt of this kind to investigate the effects of extreme climate conditions on non-frost susceptible soil slope stability in seasonal cold regions. The application of the recommended numerical approach is expected to contribute to the pre-design studies of soil slopes.

3.3.1 Coupled thermo-hydro analysis under unsaturated conditions

The governing equation for two-dimensional seepage flow is as given by Richards, (1931) and Childs and Collins-George, (1950),

$$\frac{1}{\rho_w}\frac{\partial}{\partial x}\left(D_v\frac{\partial P_v}{\partial x}\right)+\frac{1}{\rho_w}\frac{\partial}{\partial y}\left(D_v\frac{\partial P_v}{\partial y}\right)+\frac{\partial}{\partial x}\left(k_x\frac{\partial\left(\frac{P}{\rho_w g}+y\right)}{\partial x}\right)+\frac{\partial}{\partial y}\left(k_y\frac{\partial\left(\frac{P}{\rho_w g}+y\right)}{\partial y}\right)+Q=m_w\frac{\partial P}{\partial t} \quad \textbf{(3.1)}$$

where, ρ_w = density of water (kg/m^3), P = pressure (kPa), P_v = vapor pressure of soil moisture (kPa), k_x = hydraulic conductivity in the x direction (m/s), k_y = hydraulic conductivity in the y direction (m/s), Q = seepage boundary flux applied over a unit length (m/s), D_v = diffusion coefficient of water vapor through soil ((kg·m)/(kN·s)), y = elevation head (m), g = acceleration due to gravity (9.81 m/s^2), m_w = slope of the soil water characteristic curve SWCC (1/kPa), γ_w = unit weight of water (kN/m^3) and t = time (unit according to the numerical time step).

The governing equation for two-dimensional thermal flow is given by the concept based on Harlon (1973) and Harlan and Nixon (1978).

$$L_w\frac{\partial}{\partial x}\left(D_v\frac{\partial P_v}{\partial x}\right)+L_w\frac{\partial}{\partial y}\left(D_v\frac{\partial P_v}{\partial y}\right)+\frac{\partial}{\partial x}\left(k_{tx}\frac{\partial T}{\partial x}\right)+\frac{\partial}{\partial y}\left(k_{ty}\frac{\partial T}{\partial y}\right)+Q_t+\zeta V_x\frac{\partial T}{\partial x}+\zeta V_y\frac{\partial T}{\partial y}=\left(\zeta+L_w\frac{\partial\theta_{uw}}{\partial T}\right)\frac{\partial T}{\partial t} \quad \textbf{(3.2)}$$

where, T = temperature (°C), ζ = volumetric heat capacity of soil (kJ/m³-°C), k_{tx} = thermal conductivity in the x-direction (kJ/(s·m·°C)), k_{ty} = thermal conductivity in the y-direction (kJ/(s·m·°C)), V_x = the Darcy water velocity in x-direction (m/s), V_y = Darcy water velocity in y-direction (m/s), Q_t = thermal boundary flux applied over a unit length (kJ/(sec·m^3)) and L_w = latent heat of water during phase change either liquid to gas (vaporisation) or liquid to solid (fusion as ice) (kJ/kg) and θ_{uw} = unfrozen volumetric water content determined by the slope of soil freezing characteristic curve (SFCC) (m^3/m^3).

The seepage flow Equation. 3.1 and thermal flow Equation. 3.2 are linked by the relationships given by Edlefsen and Anderson (1943) and Joshi (1993),

$$P_v=P_{vs}\left(e^{\frac{-P.w}{\rho.R.T}}\right)=P_{vs}h_{rair} \quad \textbf{(3.3)}$$

where, P_{vs} = saturated vapor pressure of pure free water (kPa), ρ = density of water vapor or ice (kg/m^3), w = molecular mass of water vapor (kg/kmol), R = universal gas constant (kJ/kmol·˚C), T = temperature (˚C) and h_{rair} = relative humidity of air (%).

$$\nabla P_v = d_1 \nabla(-P) + d_2 \nabla T \quad \textbf{(3.4)}$$

The capacity to store heat is composed of two parts. The first part is the volumetric heat capacity of the material (either frozen or unfrozen) and the second part is the latent heat associated with the phase change. The latent heat associated with phase change is included in the thermal flow equation (3.2) in the form,

$$\lambda = \zeta + L_w \frac{\partial \theta_{uw}}{\partial T} \quad \textbf{(3.5)}$$

The volumetric heat capacity ζ is the slope of the energy curve in the frozen and unfrozen zones while the term $L_w \frac{\partial \theta_{uw}}{\partial T}$ represents the rate of change of the latent heat added to the heat storage component in the heat balance equation. The unfrozen water content of the soil is estimated using the relationships given by Black and Tice (1989).

$$\theta_{uw}(t) = \theta(C_f(-1110)t) \quad \textbf{(3.6)}$$

$\theta_{uw}(t)$ = unfrozen volumetric water content at temperature t, θ = function of volumetric water content against matric suction (shown in Equation 3.6) as, C_f = parameter ranges between 1 to 2.2 for fine to coarse grained soils.

Seepage analysis inside an unsaturated/partially saturated freezing ground/soil is highly complicated, especially in the direct vicinity of the phase change region. At this domain, it is possible for certain types of soils (fine grained soils) to experience cryogenic suction (ice suction) which results in very steep pressure gradients that can draw water towards the freezing front where it can accumulate and cause frost heave. The coupled TH formulation used in this study does not account for these mechanisms. While the suctions are estimated based on temperature and used to determine frozen ground hydraulic conductivity, therefore only change due to the solution of the seepage partial differential equation. As water turns to ice the negative pressures (or suction) in the ground can be quite significant which can lead to moisture redistribution towards a freezing front. This is a primary cause of frost heave in fine grained soils. The formulations/code used here does not allow negative pressures to increase in frozen ground, however, it does approximate (based on temperature and the Clausius-Clapeyron equation) what these pressures would be in order to compute a reduced hydraulic conductivity as ice replaces liquid water in frozen pores. The formulation limits the amount of ice that can exist in soil pores to be equal to the porosity of the soil. In other words, frost heave cannot exist.

3.3.2 Modelling atmospheric-ground interactions

The importance of accounting the physical laws of soil-atmosphere interactions in geotechnical engineering analysis are being understood in recent years (Gens, A. 2010). The range of problems that geotechnical engineers face is increasing in complexity and scope especially in cold regions where the climatic factors play a vital role in determining the life of any geotechnical structure. To consider the freeze-thaw action, snowfall during winter and other climatic effects in an unsaturated soil, a seepage flux boundary used in conventional seepage analysis may not be sufficient since the surface flux resulting from snowmelt and outgoing flux resulting from evaporation are needed to be properly considered in order to estimate the ground surface temperature, surface infiltration and soil water content etc. For this purpose, incorporation of other climatic variables in a seepage analysis are must. During the winter season, the precipitation occurs as snowfall in seasonal cold regions. The snow will accumulate above the soil ground until the air temperature is below 0 ˚C. Once the temperature rises high enough to melt the accumulated snow (> 0 ˚C), the snow will start to melt and will release water to the soil surface. The snow water equivalent is the water that is stored in the snowpack. The snow water equivalent is determined based on the following equation.

$$SWE_t = SWE_{t-1} + SF - SM \tag{3.7}$$

where, SWE_t = snow water equivalent at the present numerical time step (mm/day), SWE_{t-1} = snow water equivalent at the previous numerical time step (mm/day), SF = snowfall precipitation rate (mm/day), SM = snowmelt rate (mm/day).

The snowfall precipitation is calculated based on the amount of precipitation and air temperature according to the following relationships.

$$SF = Q_P \times P \tag{3.8}$$

where, Q_P = thermal factor, P = precipitation (mm/day). The thermal factor Q_p varies according to the average daily air temperature as,

$$Q_P = 0 \text{ (if } T_a > T_f \text{) and } Q_P = 1 \text{ (if } T_a < T_f \text{)} \tag{3.9}$$

where, T_a = average daily air temperature (˚C) and T_f = freezing point temperature (0˚C). The snowmelt rate (SM) is determined based on an energy balance approach used by Bras (1990), Liang et al. (1994), Flerchinger and Saxton (1989). For the estimation of snow precipitation, precipitation data (including rainfall and snowfall) and air temperature data are required.

To calculate the snow depth and density of snow the following relationships are used.

$$D_{sn} = \frac{\rho_w}{\rho_{sn}} SWE_{t-1} \; ; \; \rho_{sn} = \frac{SWE_{t-1}}{D_{sn}} + \beta(0.55 - \rho_{sn(t-1)}) \text{ and } \beta = \begin{cases} 0.002 & \because T_a < 1.0 \\ 0.002 \times T_a & \because T_a \geq 1.0 \end{cases} \quad \textbf{(3.10)}$$

where, D_{sn} = snow depth (mm), ρ_{sn} = density of snow (kg/m^3), $\rho_{sn(t-1)}$ = density of snow on the previous time step (kg/m^3), ρ_w = density of water assumed to be 1 (kg/m^3), SWE_{t-1} = snow water equivalent on the previous time step (mm), β = snow consolidation parameter and T_a = average daily air temperature (˚C).

The ground surface temperature when there is snow cover in the ground is estimated using the following relationship given by Bras (1990),

$$T_g = T_{sn} - \frac{D_{sn}}{\lambda_{sn}} q_{Tg} \quad \textbf{(3.11)}$$

where, T_g = ground surface temperature (˚C), T_{sn} = temperature of snow surface considered equal to the air temperature (˚C), D_{sn} = snow depth (mm), λ_{sn} = thermal conductivity of snow (kJ/(s·m·°C)) and q_{Tg} = energy flux at the ground surface (kJ/(sec·m^2)).

The maximum rate of evaporation from a pure water surface/saturated soil pore under given climatic conditions is defined as the potential rate of evaporation (PE). If the surface soil becomes unsaturated, the amount of water inside the soil pore will become limited and the rate of evaporation begins to decline. This phenomenon is defined as the actual rate of evaporation (AE). Actual evaporation is the actual rate of evaporative flux from a partially saturated soil pore. The actual evaporation from an unsaturated soil is modelled adopting the approach given by Wilson et al. (1994),

$$AE = \frac{\Gamma Q_n + \eta E_a}{\Gamma + \eta / h_s} \quad \textbf{(3.12)}$$

where, AE = actual vertical evaporative flux (mm/day), Γ = slope of the saturation vapor pressure versus temperature curve at the mean temperature of the air (kPa/˚C), Q_n = net radiant energy flux available at the water surface (mm/day), η = psychrometric constant, E_a = flux associated with vapor pressure mixing (mm/day) and h_s = relative humidity at the soil surface (%). For the estimation of actual evaporation from unsaturated soil, relative humidity of air and soil, wind speed and net radiation are required. To model the soil surface evaporation reasonably, Wilson et al. (1994) equation is appropriate.

The infiltration, runoff and actual evaporation are considered based on the following relationship.

$$I = P - AE - R \tag{3.13}$$

where, I = infiltration (mm/day), P = precipitation (mm/day), AE = actual evaporation (mm/day) and R = runoff (mm/day). The runoff R is defined as the amount of water that cannot infiltrate into the soil ground. The runoff is determined by the amount of precipitation, actual evaporation and infiltration. If the precipitation is less than the anticipated actual evaporation, then the applied surface flux boundary condition will be equal to the precipitation value minus the actual evaporation and a negative flux will be applied to the node. If the precipitation minus actual evaporation is a positive value, then a positive infiltrative surface flux will be applied as a boundary condition. The amount of total surface water flux near the ground surface is determined by the length of the sloping ground (length of the surface nodes along the slope surface). The slope angle will change the length of the slope surface which in turn affects the total surface flux. The total flux near the ground surface can be expressed simply using the following relationship,

$$Q_{surface} = P \times \sum L_n \tag{3.14}$$

where, $Q_{surface}$ = amount of total surface flux (m^3/day), P = precipitation (mm/day) and $\sum L_n$ = summation of length between nodes along the entire slope surface (m). The length of the slope surface is indirectly proportional to the slope angle as given by,

$$\sum L_n \propto \frac{1}{S_{angle}} \tag{3.15}$$

where, $\sum L_n$ = summation of length between nodes along the entire slope surface (m) and S_{angle} = slope angle (˚).

The amount of surface flux that is applied at the boundary strongly depends on the slope angle and the length of sloping ground. The assumption, by neglecting the slope angle effect in runoff calculations, is not valid in terms of surface water flow simulations and runoff through a mountain valley etc. Surface water flow and runoff caused by flooding cannot be simulated using these assumptions. The adopted numerical simulations do not track the route of surface water and flow speed etc. The infiltration boundary condition for the model is defined by Gitirana (2005). If the surface soil is saturated, the pore spaces will get filled with water and no

more water can get into the soil element. Conceptually, this effect is modelled considering the rate of applied surface flux *(q)* and saturated hydraulic conductivity of the soil *(k_s)*. If the soil surface is a flat ground, there is a possibility of surface ponding. If conditions for infiltration met later, the ponded water from the flat surface will infiltrate into the soil ground. To incorporate these conditions, the method given by Gitirana (2005) is useful. By this way, the effect of slope angle on surface infiltration is considered in the analysis.

3.3.3 Mechanical behaviour of soil

3.3.3.1 Shear strength of soil under unsaturated conditions

The shear strength of an unsaturated is expressed based on Bishop's effective stress principle through extended Mohr-coulomb failure envelope (Figure 3.3) by Vanapalli et al. (1996) as given by,

$$\tau = c' + \left(\sigma_n - u_a\right)\tan\phi' + \left(u_a - u_w\right)\left[\chi\tan\phi'\right] \quad \textbf{(3.16)}$$

where, τ = shear strength of soil (kPa), σ_n = net total stress (kPa), u_a = pore air pressure (kPa), u_w = pore water pressure (kPa), c' = effective cohesion (kPa), ϕ' = effective angle of internal friction (°) and χ = parameter related to the degree of saturation. According to Vanapalli et al. (1996) the magnitude of parameter χ can be expressed in terms of volumetric water content as,

$$\chi = \frac{\theta_w - \theta_r}{\theta_s - \theta_r} \quad \textbf{(3.17)}$$

where, θ_w = volumetric water content (m^3/m^3), θ_s = saturated volumetric water content (m^3/m^3) and θ_r = residual volumetric water content (m^3/m^3).

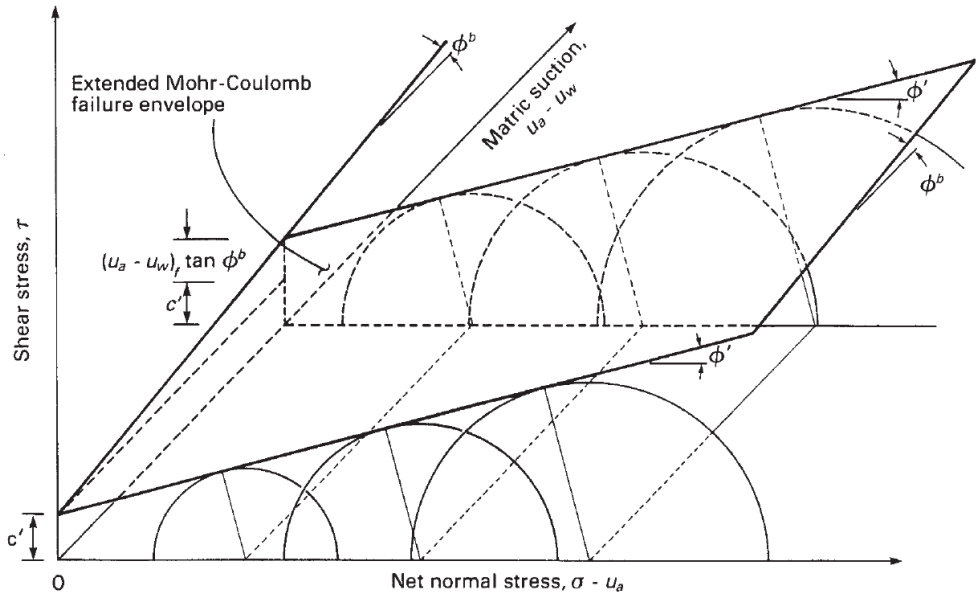

Figure 3.3 Extended Mohr-Coulomb failure envelope for unsaturated soils (after Fredlund et. al. 2012)

In an unsaturated soil, Mohr circles corresponding to failure conditions can be plotted in a three-dimensional manner, as illustrated in Figure 3.3. The three-dimensional plot has the shear stress τ as the ordinate and the two stress state variables $\sigma - u_a$ and $u_a - u_w$ as abscissas. The frontal plane represents saturated soil conditions where matric suction is zero. The $\sigma - u_a$ axis reverts to the $\sigma - u_w$ axis on the frontal plane since the pore-air pressure becomes equal to the pore-water pressure at saturation. The Mohr circles for an unsaturated soil are plotted with respect to the net normal stress axis $\sigma - u_a$ in the same manner as the Mohr circles are plotted for saturated soils with respect to effective stress axis $\sigma - u_w$. The location of the Mohr circle plot in the third dimension is a function of the matric suction. The surface tangent to the Mohr circles at failure is referred to as the extended Mohr-Coulomb failure envelope for unsaturated soils. The extended Mohr-Coulomb failure envelope defines the shear strength of an unsaturated soil. The intersection line between the extended Mohr-Coulomb failure envelope and the frontal plane is the failure envelope for saturated conditions. The inclination of the failure plane is defined by joining the tangent point on the Mohr circle to the pole point. The tangent point on the Mohr circle at failure represents the stress state on the failure plane at failure.

3.3.3.2 Factor of safety estimation for slope stability analysis

Slope stability has been analysed using limit equilibrium technique based on the method given by Morgenstern and Price (1965).

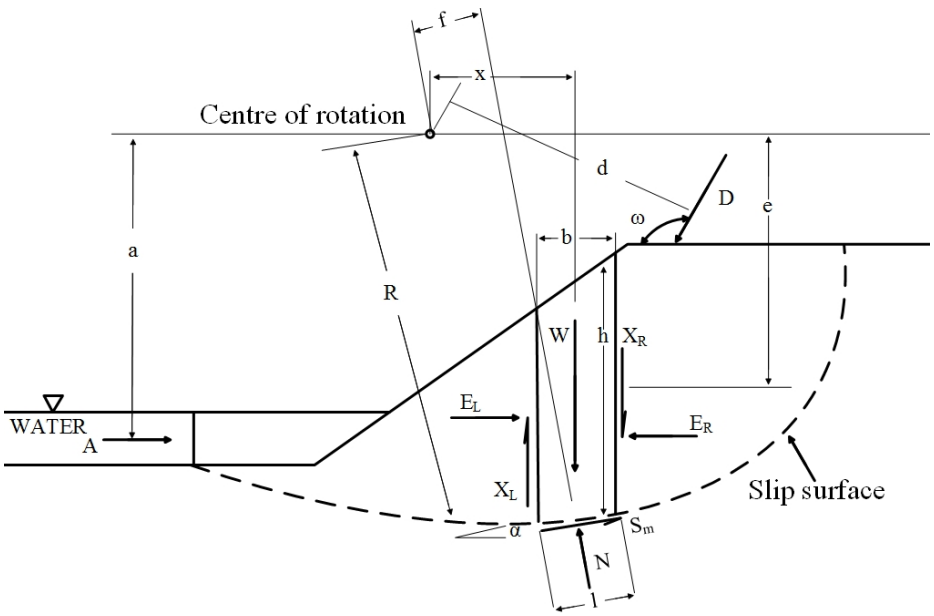

Figure 3.4 Forces acting on a slice through a sliding mass with a slip surface

The Morgenstern and Price method is a widely-used slope stability method in general geotechnical engineering practice. The factor of safety equations with respect to moment equilibrium (F_m) and force equilibrium (F_f) considering the unsaturated shear strength of soil are given in Equation. 3.17 and Equation. 3.18 respectively. The unsaturated soil shear strength in the factor of safety is considered based on the nonlinear relationship given by Vanapalli et al. (1996) as explained in Equation 3.15 and Equation 3.16.

$$F_m = \frac{\sum\left[c'lR + \left\{N - u_w l\chi - u_a l(1-\chi)\right\} R\tan\phi'\right]}{\sum Wx - \sum Nf \pm \sum Dd \pm \sum Aa} \quad \textbf{(3.18)}$$

$$F_f = \frac{\sum\left[c'l\cos\alpha + \left\{N - u_w l\chi - u_a l(1-\chi)\right\}\tan\phi'\cos\alpha\right]}{\sum N\sin\alpha - \sum D\cos\omega \pm \sum A} \quad \textbf{(3.19)}$$

where, W = the total weight of a slice of width b and height h (kN/m^2), N = the total normal force on the base of the slice (kN), D = an external point load (kN). R = the radius of a circular slip surface (m), x = the horizontal distance from the centreline of each slice to the centre of

rotation or to the centre of moments (m), d = the perpendicular distance from a point load to the centre of rotation or to the centre of moments (m), f = the perpendicular offset of the normal force from the centre of rotation or from the centre of moments (m), a = the perpendicular distance from the resultant external water force to the centre of rotation or to the centre of moments (m), A = the resultant external water forces (kN), ω = the angle of the point load from the horizontal (˚), α = the angle between the tangent to the centre of the base of each slice and the horizontal (˚) and l = the base length of each slice (m).

The shear mobilised and normal stresses need to be calculated in consideration with the effect of unsaturated shear strength. The Shear mobilised is written for unsaturated soil conditions (Fredlund and Krahn, 1977) in equation form,

$$S_m = \frac{l}{F}(c' + (\sigma_n - u_a)\tan\phi' + (u_a - u_w)\tan\phi^b \quad \textbf{(3.20)}$$

$$N = \frac{W + (X_R - X_L) - \frac{\left[c' l \sin\alpha + u_a b \sin\alpha(\tan\phi' - \tan\phi^b) + u_w l \sin\alpha \tan\phi^b\right]}{F} + D\sin\omega}{\cos\alpha + \frac{\sin\alpha\tan\phi'}{F}} \quad \textbf{(3.21)}$$

S_m = the shear force mobilized on the base of each slice, E = the horizontal interslice normal forces. Subscripts L and R designate the left and right sides of the slice, respectively, X = the vertical interslice shear forces. Subscripts L and R define the left and right sides of the slice, respectively, R = the radius for a circular slip surface or the moment arm associated with the mobilized shear force, S_m for any shape of slip surface, e = the vertical distance from the centroid of each slice to the centre of rotation or to the centre of moments. It is assumed that f distances on the right side of the centre of rotation of a negative slope (i.e., a right-facing slope) are negative and those on the left side of the centre of rotation are positive. For positive slopes, the sign convention is reversed. h = the height of a slice along the slip surface.

A relationship can be obtained from equating the unsaturated soil shear strength equations given by Vanapalli et al. (1996) and Fredlund et al. (1978).

$$\tan\phi^b = \chi\tan\phi' \quad \textbf{(3.22)}$$

CHAPTER 4

4 ANALYSIS OF SOIL SLOPE FAILURES USING THE RECOMMENDED METHOD

4.1 Case example of volcanic soil embankment slope failure

The case example of failure on embankment slope constructed using Shikotsu Komaoka volcanic soil is analysed using the recommended approach.

4.1.1 Numerical model

The two-dimensional numerical finite element mesh with the slope geometry adopted for the embankment slope is given in Figure 4.1.

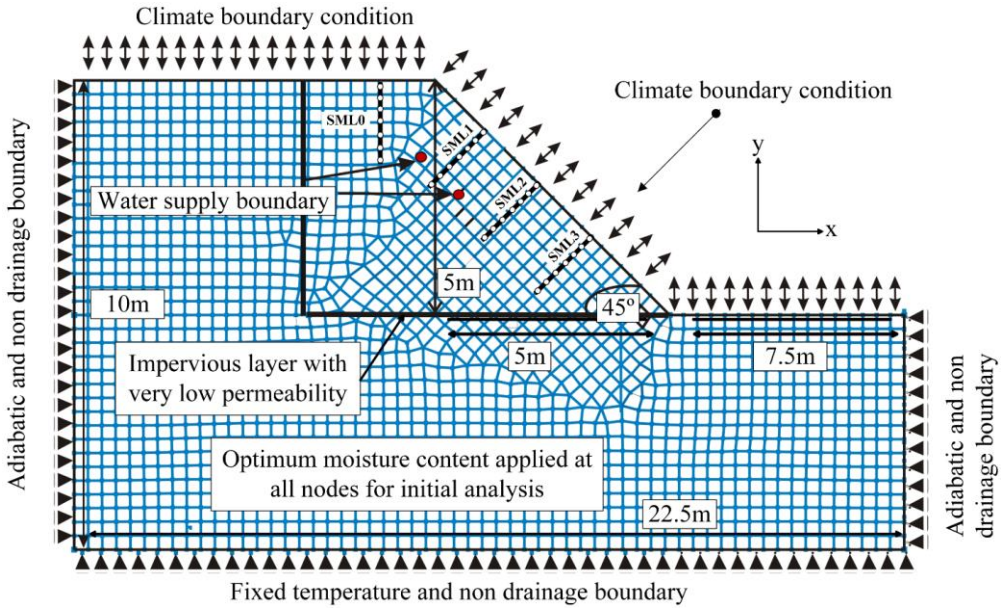

Figure 4.1 Two-dimensional numerical model with applied boundary conditions and FEM mesh for volcanic soil slope

4.1.2 Soil properties

Shikotsu Komaoka volcanic soil has been used as the slope material in the embankment slope. The soil parameters used for the numerical simulation of embankment slope are summarised in Table 4.1. The parameters i.e. dry density (ρ_d), hydraulic conductivity of saturated soil (k_s), effective cohesion (c') and effective angle of internal friction (ϕ') have been obtained from laboratory element tests (Matsumura et al., 2015). The parameters for which no laboratory measurements are available, i.e. thermal conductivity (λ), volumetric heat capacity (ζ) and

volumetric water content of soil at 0°C (θ_{wf}), have been estimated using equations given by Kersten (1949), Jame (1977) and Black and Tice (1989), respectively. The soil-water characteristic curve (SWCC) was obtained from laboratory element tests by Matsumura et al. (2014).

Table 4.1 Soil properties used for the simulation of volcanic soil embankment slope

Property name	**Volcanic soil**
Dry density of soil *(ρ_d)*	1020 kg/m^3
Porosity *(n)*	0.63
Hydraulic conductivity of saturated soil *(k_s)*	6.00 ×10^{-06} m/s
Volumetric water content of soil at 0°C *(θ_{wf})*	0.19 m^3/m^3
Volumetric water content of saturated soil *(θ_s)*	0.63 m^3/m^3
Residual volumetric water content of soil *(θ_r)*	0.33 m^3/m^3
Unfrozen thermal conductivity *(λ_u)*	107.8 kJ/(Day·m·°C)
Frozen thermal conductivity *(λ_f)*	171.7 kJ/(Day·m·°C)
Unfrozen volumetric heat capacity *(ζ_u)*	3372 kJ/(m³·°C)
Frozen volumetric heat capacity *(ζ_f)*	1193 kJ/(m³·°C)
Effective cohesion *(c')*	0 kPa
Effective angle of internal friction *(ϕ')*	35°

The hydraulic conductivity in a freezing soil k (m/s) depends on the amount of available free water (unfrozen volumetric water content). In fully coupled thermo-hydro models, the relationship of permeability, thermal conductivity and heat capacity under negative temperatures are inherently obtained from the description of unfrozen volumetric water content versus temperature. The unfrozen water content of the soil is estimated using the relationships given by Black and Tice (1989).

$$\theta_{uw}(t) = \theta(C_f(-1110)t) \quad \textbf{(4.1)}$$

$\theta_{uw}(t)$ = unfrozen volumetric water content at temperature t, θ = function of volumetric water content against matric suction as, C_f = parameter ranges between 1 to 2.2 for fine to coarse grained soils.

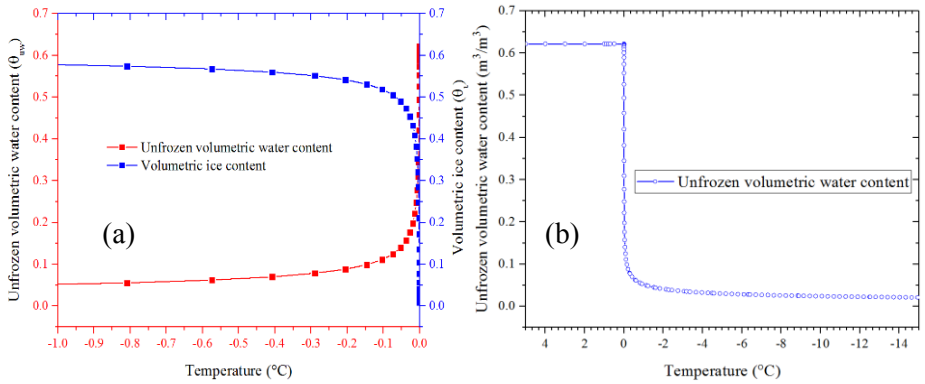

Figure 4.2(a) Unfrozen volumetric water content function and volumetric ice content of K-Soil (b) Volumetric water content against temperature

Black and Tice (1989) have suggested a value of 2.2 for C_f which is suitable for coarse grained soils. The unfrozen volumetric water content and volumetric ice content is estimated based on the relationships and as given in Figure 4.2. The soil water characteristic curve is derived from the van – Genuchten and Mualem equation (1976) as following:

$$\theta = \theta_{rm} + (\theta_s - \theta_{rm}) \left[\frac{1}{\left[1 + (a_m \psi)^{n_m}\right]^{\left[1 - \frac{1}{n_m}\right]}} \right] \tag{4.2}$$

where, θ_w = volumetric water content at any soil suction; θ_{rm} = residual volumetric water content; θ_s = saturated volumetric water content; a_m = a material parameter which is primarily a function of the air entry value of the soil in kPa; n_m = a material parameter which is primarily a function of the rate of water extraction from soil once the air entry value has been exceeded and Ψ = soil suction.

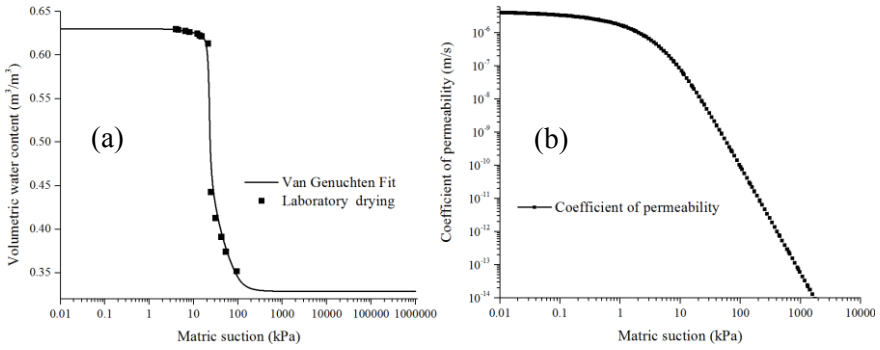

Figure 4.3 (a) SWCC of K-Soil and (b) permeability function

Referring to the values of available free water inside frozen soil (unfrozen volumetric water content), the equivalent matric suction is obtained at every time steps from the SWCC (Figure 4.3a). The equation proposed for estimating the coefficient of permeability is,

$$k(\psi) = k_s \left[\frac{\left\{ 1 - (a\psi)^{nm} \left[1 + (a\psi)^n \right]^{-m} \right\}^2}{\left[1 + (a\psi) n \right]^{m/2}} \right] \tag{4.3}$$

where, k = hydraulic conductivity or permeability of the water phase; k_s = saturated hydraulic conductivity or permeability of the water phase; a = van Genuchten soil-water characteristic curve fitting parameter; m = van Genuchten soil-water characteristic curve fitting parameter and; Ψ = soil suction. The permeability at each equivalent matric suction are calculated using the permeability function (coefficient of permeability vs matric suction) (Figure 4.3 b). The coefficient of permeability vs volumetric water content is shown in Figure 4.4 (a), coefficient of permeability against unfrozen water is shown in Figure 4.4 (b) and coefficient of permeability against temperature is shown in Figure 4.4 (c). These curves are prepared by relating the coefficient of permeability and matric suction with unfrozen water content curve (Figure 4.2)

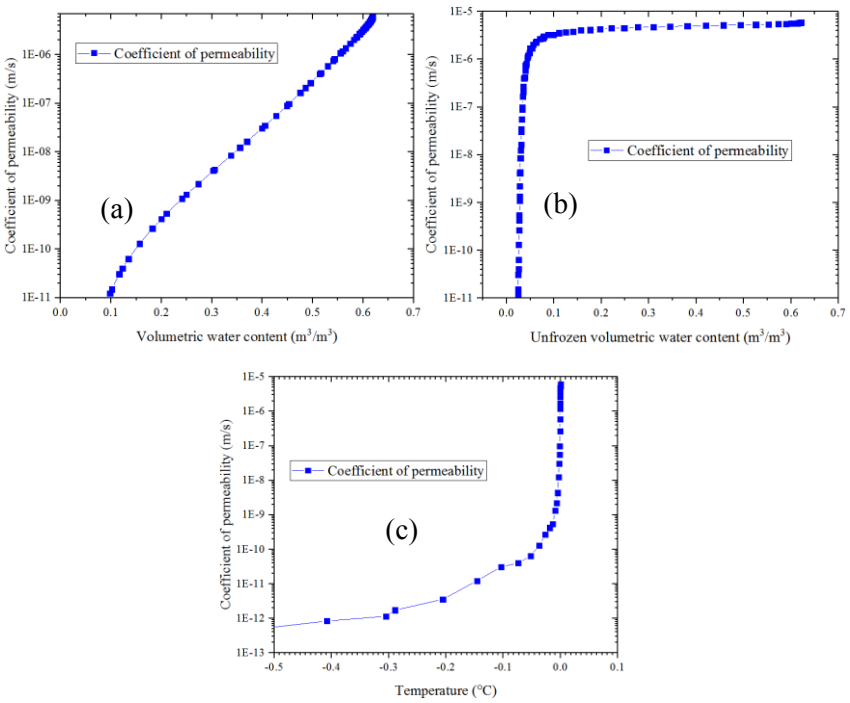

Figure 4.4 Coefficient of permeability against (a) Volumetric water content, (b) Unfrozen volumetric water content and (c) Temperature.

Thermal conductivity of saturated soil is estimated using the following formula. The unfrozen thermal conductivity (λ_u) is estimated based on its dry density (ρ_d) and water content (w) using the following equation (Kersten, 1949).

$$\lambda_u = \left\{ (0.7 \log w + 0.4) \times 10^{0.6242\rho_d - 3.4628} \right\} \times 418.6 \qquad \textbf{(4.4)}$$

Frozen thermal conductivity of saturated soil λ_f is estimated based on its dry density (ρ_d) and water content (w) using the following equation (Kersten, 1949).

$$\lambda_f = \left\{ 0.011 \times 10^{1.320\rho_d - 3.4628} + 0.026w \times 10^{0.9114\rho_d - 3.4628} \right\} \times 418.6 \qquad \textbf{(4.5)}$$

The parameters in Table 1., unfrozen thermal conductivity estimated is 1.249J/sec•m•°C (107.8 KJ/day•m•°c) and frozen thermal conductivity of Shikotsu Komaoka volcanic soil is estimated as 1.98J/sec/m/°C (171.74 KJ/day•m•°c) using Equation 4.4 and 4.5. Based on the frozen and unfrozen thermal conductivity, the relationship between thermal conductivity and temperature is drawn as shown in Figure 4.5 (a).

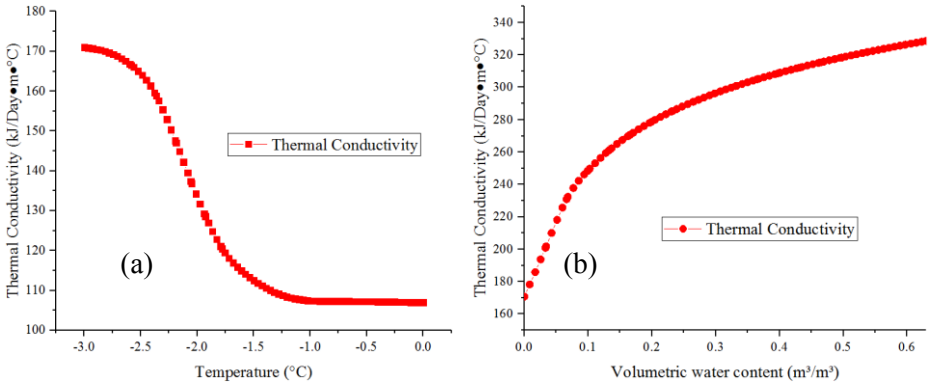

Figure 4.5 (a) Thermal conductivity of K-Soil against temperature and (b) water content

The Kersten (1949) equation does not account for unfrozen water content when calculating thermal conductivity of frozen soil. For coarse grained soils the unfrozen water content are typically negligible when there is no temperature change over time. And these values are used only in the steady state analysis where there is no temperature drop below zero. As we can see the drop in thermal conductivity is smoothed from frozen to unfrozen states without consideration of the change in water content and unfrozen water content. Figure 4.5 (a) assumes that all the water content will be frozen once the temperature reduces less than 0. Whereas when

performing non-isothermal coupled seepage analysis, the consideration of unfrozen water content is essential. This has been done by a function of thermal conductivity against volumetric water content as shown in Figure 4.5 (b). The function in Figure 4.5 (b) is derived using the method given by Johansen (1975) explained as follows.

For a saturated unfrozen soil, the thermal conductivity λ_{sat} is estimated based on the thermal conductivities of its components and their respective volume fractions. Here the presence of air is neglected.

$$\lambda_{sat} = (\lambda_s)^{1-n}(\lambda_w)^n \tag{4.6}$$

where, λ_s is the thermal conductivity of the soil particles, and λ_w is the thermal conductivity of the pore water and n is soil porosity. If the ice content is greater than zero, the program back calculates the soil particle conductivity. The frozen soil thermal conductivity ($\lambda_{sat\text{-}f}$) for saturated soil at the given water content is estimated according to the amount of water that is frozen (per Equation 4.1) as follows (Johansen, 1975).

$$\lambda_{sat-f} = (\lambda_s)^{1-n}(\lambda_i)^{n-w_u}(\lambda_w)^{w_u} \tag{4.7}$$

where, λ_i is the thermal conductivity of ice. Once the fully frozen conductivity is known, the partially frozen thermal conductivity of the ground is assumed to be linearly partitioned between the unfrozen and frozen states by the ratio of ice content to water content.

For an unsaturated soil, the thermal conductivity λ_{unsat} under frozen and unfrozen states are estimated based on its saturated conductivity, dry conductivity and degree of saturation (θ/n) using the following equation

$$\lambda_{unsat} = (\lambda_{sat} - \lambda_{dry})\lambda_e + \lambda_{dry} \;;\; \lambda_{unsat-f} = (\lambda_{sat-f} - \lambda_{dry})\lambda_e + \lambda_{dry} \tag{4.8}$$

λ_e = 0.7 Log(θ/n) + 1.0 for unfrozen coarse grained soil, λ_e = Log(θ/n) + 1.0 for unfrozen fine grained soil, λ_e = (θ/n) for frozen soil and λ_{dry} = ((0.135ρ_d+64.7)/(2700-0.947ρ_d)) ±25%.

The volumetric heat capacity of frozen and unfrozen soil are estimated using the Jame-Newman formulation (Jame, 1977; Johnston et al. 1981; Newman and Wilson, 1996). The unfrozen and frozen heat capacity of soil are given by,

$$\zeta_u = \rho_d\left[\zeta_s + \zeta_w w_u\right] \tag{4.9}$$

$$\zeta_f = \rho_d \left[\zeta_s + \zeta_i w_f + \zeta_w w_u \right] \quad \textbf{(4.10)}$$

ζ_u = volumetric heat capacity of unfrozen soil, ζ_f = volumetric heat capacity of frozen soil, ζ_s = specific heat capacity of soil solids, ζ_w = mass specific heat capacity of unfrozen water (4184 J/kg•˚C), ζ_i = mass specific heat capacity of ice (2100 J/kg•˚C), w_u = unfrozen gravimetric water content, w_f = frozen gravimetric water content (ice content). The unfrozen and frozen water contents w_u and w_f are calculated from specific gravity (ρ_s) and volumetric water content at unfrozen (θ_{uw}) and frozen states (θ_f). Both the unfrozen and frozen water contents are referred from the function given by Equation 4.1 at every time step. The component of air is ignored in both unfrozen and frozen soils. The frozen and unfrozen volumetric heat capacity of Shikotsu Komaoka volcanic soil is estimated as 1193 KJ/m^3•°C and 3372 KJ/m^3•°C respectively. The volumetric heat capacity against temperature and volumetric water content are shown in Figure 4.6 (a) and (b).

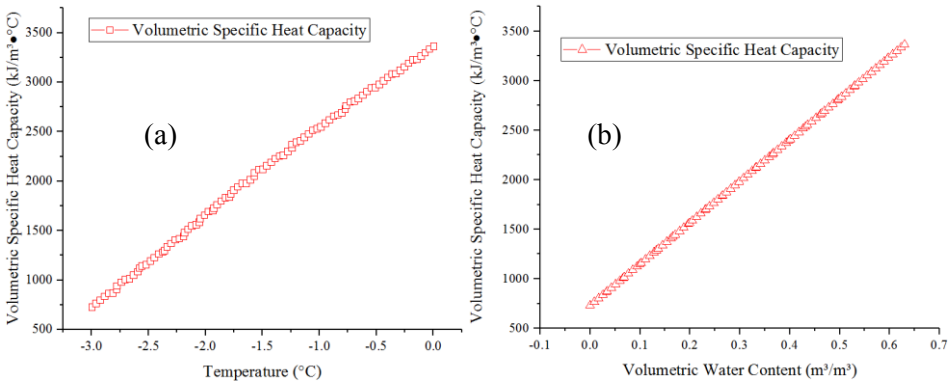

Figure 4.6 Volumetric heat capacity against (a) temperature and (b) volumetric water content.

4.1.3 Analytical conditions

The initial distribution of the volumetric water content and temperature of the slope has been configured based on the soil water content and temperature data recorded during day 1 (09-11-2012) as shown in Figure 4.7 (a) and (b) respectively. To derive an equilibrium of volumetric water content distribution corresponding to day 1 (09-11-2012), the average volumetric water content recorded at locations SML0, SML1, SML2 and SML3 (as shown in Figure 2.1 and Figure 4.1) are specified exactly at the corresponding locations in the numerical model. For the temperature distribution on the initial day (09-11-2012), the measured temperature has been specified at the depths of 0 m to 1 m.

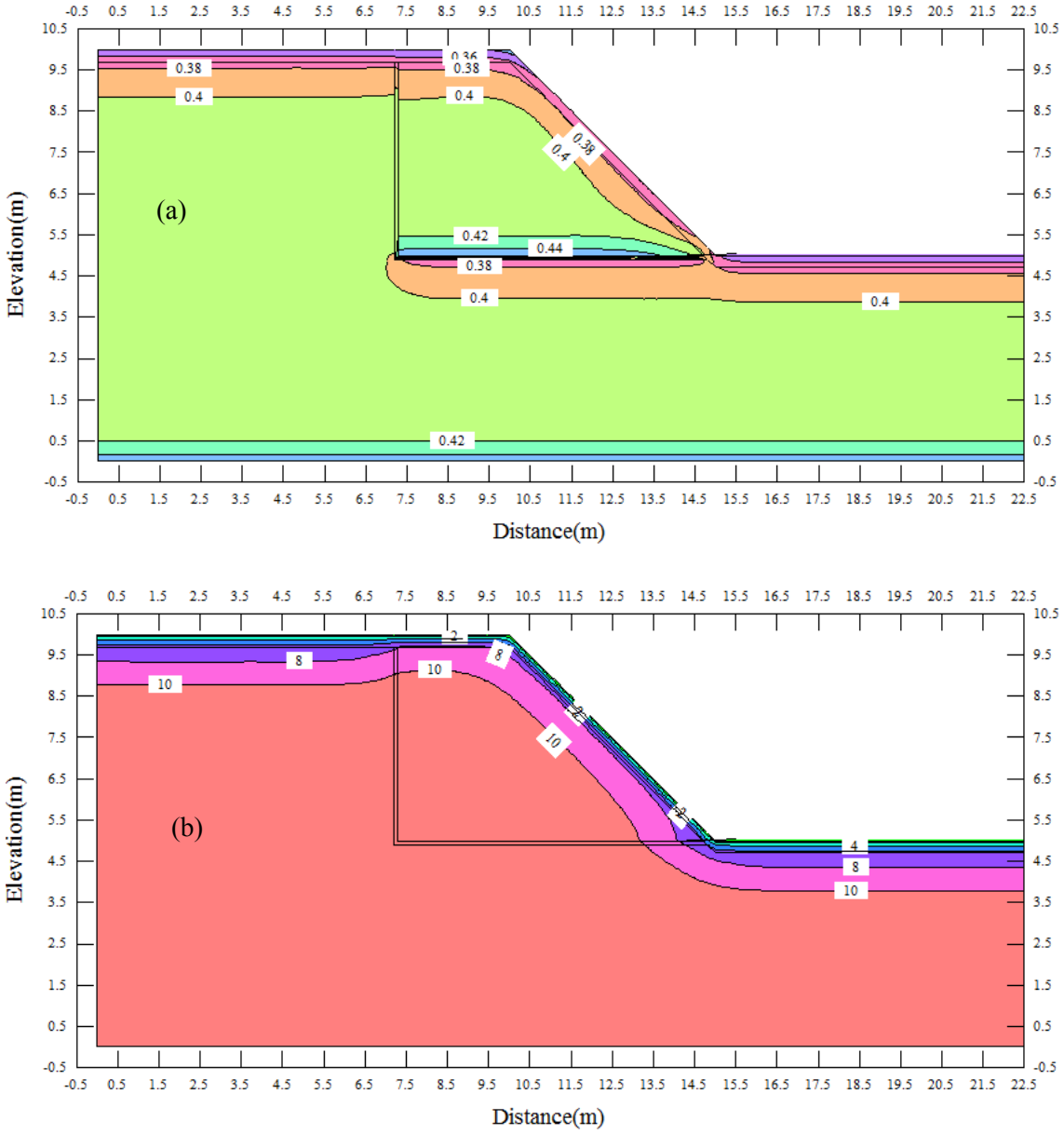

Figure 4.7 Distribution of (a) volumetric water content (m^3/m^3) and (b) temperature (°C) on day 1 (09-11-2012)

The volumetric water content and temperature during the initial day at location SML0, SML1, SML2 and SML3 are configured based on the measured data as shown in Figure 4.8 and Figure 4.9. A close similarity with the measured values are obtained with respect to the volumetric water content and temperature. After this initial set of analyses the model is put forth for the transient non-isothermal seepage analysis as explained in the successive sections.

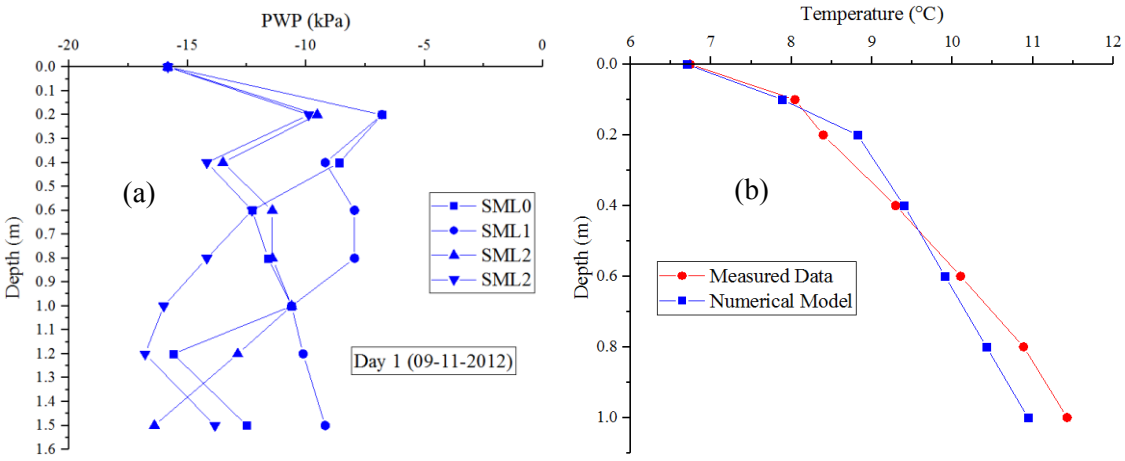

Figure 4.8 (a) Initial configuration of PWP distribution at corresponding locations of monitoring instruments SML0, SML1, SML2 and SML3 (b) Initial configuration of temperature at corresponding locations along the installed thermometers

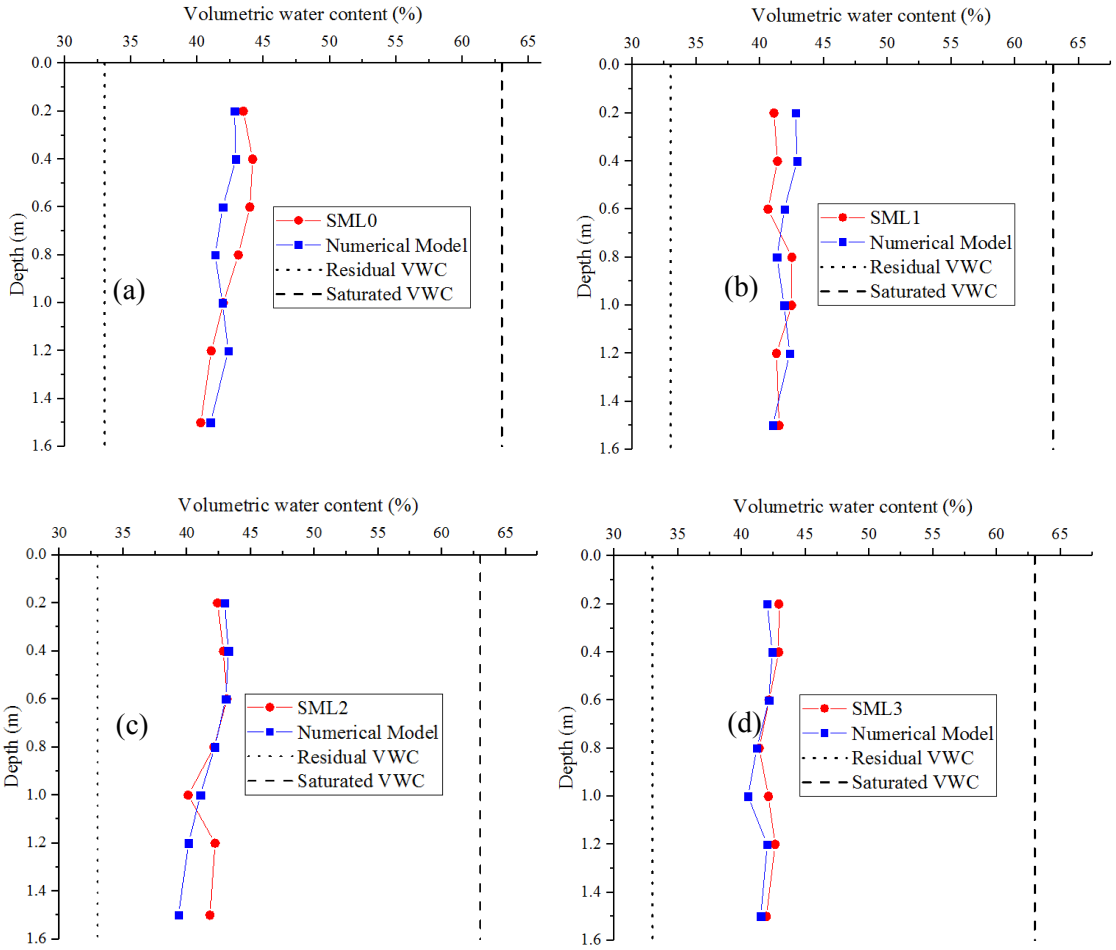

Figure 4.9 Configuration of volumetric water contents at (a) SML0, (b) SML1, (c) SML2 and (d) SML3 during the initial day (09-11-2012)

For the climatic boundary conditions used in the transient non-isothermal seepage model, climate data i.e. maximum and minimum air temperature, average daily rainfall, maximum and minimum relative humidity, average daily wind speed and average daily net radiation are required. During the monitoring of the volcanic soil embankment slope, the temperature and rainfall were monitored. Additional required climatic data were obtained from the AMeDAS (Automated Meteorological Data Acquisition System) data provided by the Japanese Meteorological Agency (JMA) and as given in Figure 4.10.

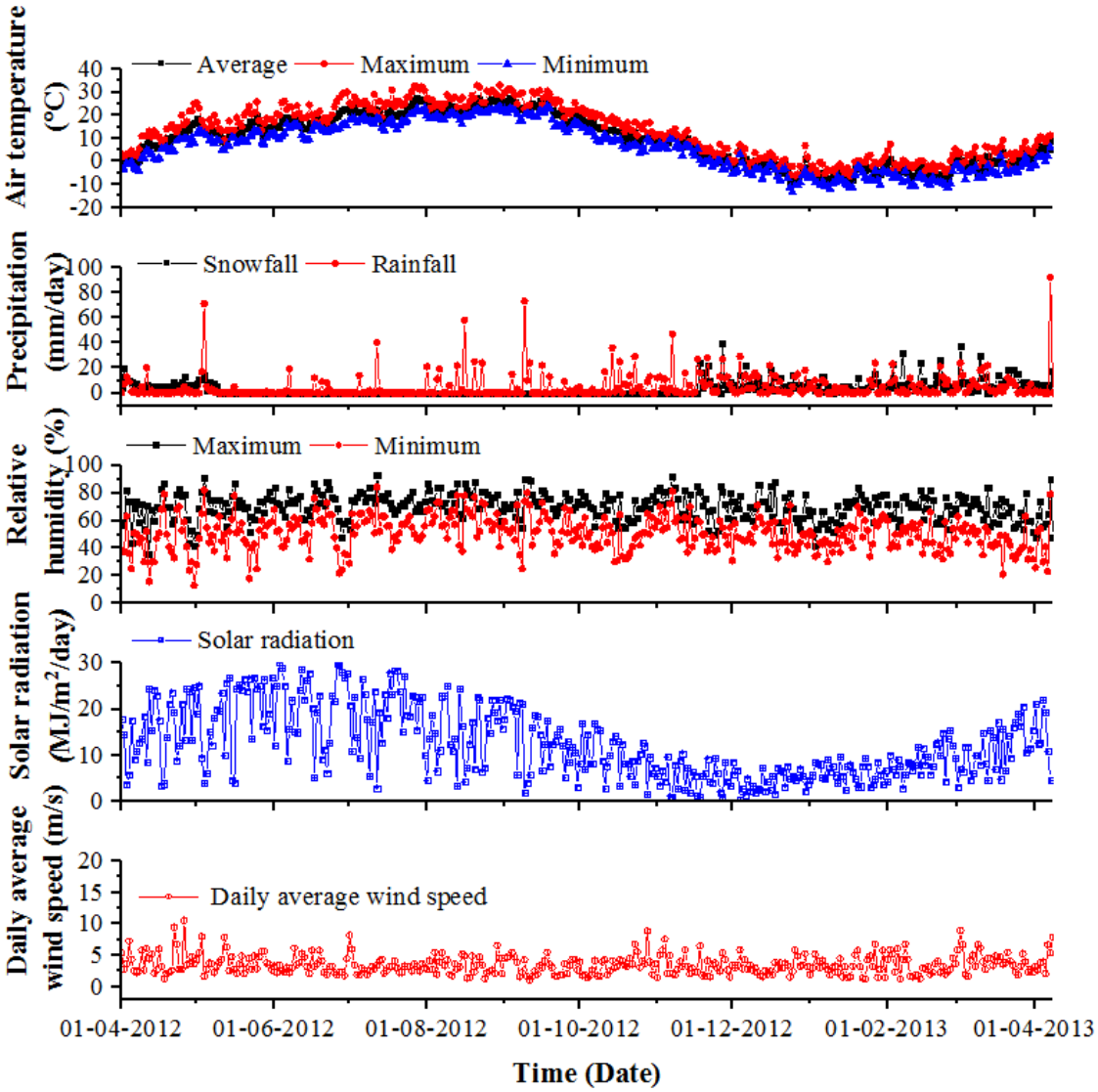

Figure 4.10 Climate data used for the numerical simulation of embankment slope

4.1.4 Results and discussions

From the numerical simulations, the magnitude of the various influencing factors i.e. precipitation, accumulated snow depth, snowmelt water, ground temperature, net surface infiltration etc. was analysed and finally the factor of safety of the slope was estimated. The numerical results are compared with the measured data.

A comparison of volumetric water content has been made from the numerical results and monitoring data as given in Figure 4.11(a), Figure 4.12 and Figure 4.13 showing the comparison between numerical estimation and measurement of the average volumetric water content of the soil water content sensors at SML0, SML1, SML2 and SML3 installed at depths 0.2 m to 1.5 m. The ground temperature estimated from the numerical simulation is compared with the measured data as given in Figure 4.11(b). The numerically estimated snow depth and measured snow depth is compared and given in Figure 4.11(c).

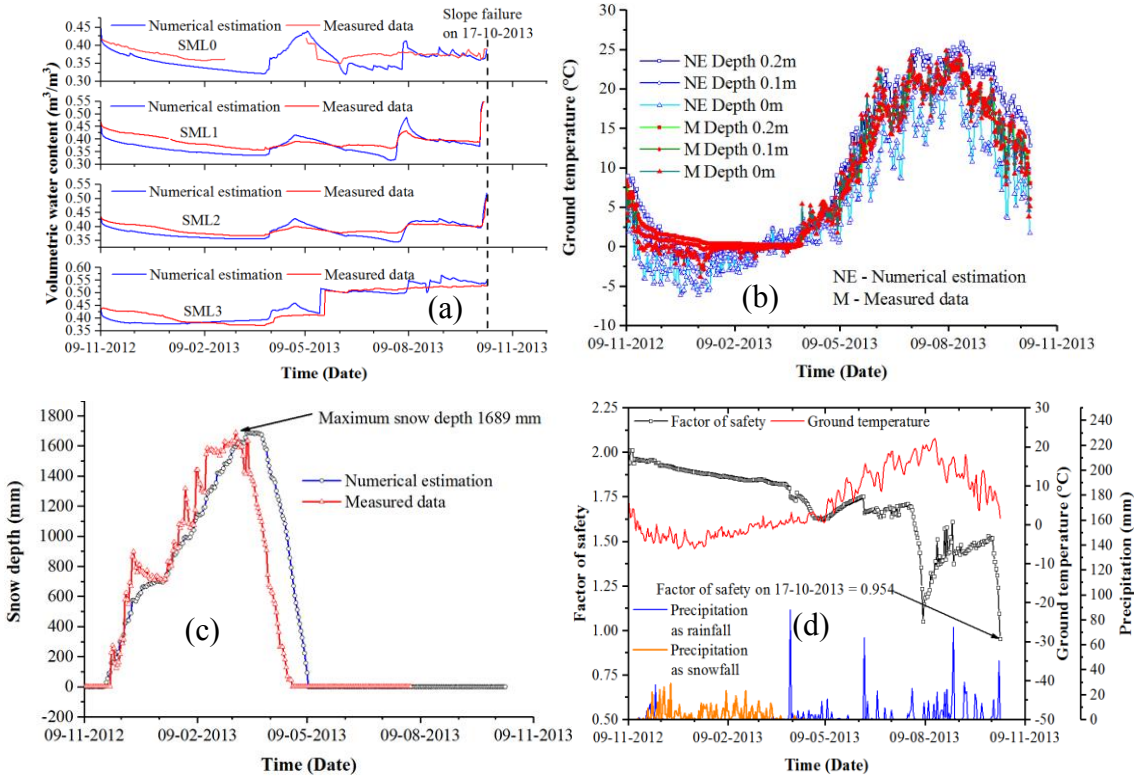

Figure 4.11 (a) Comparison of estimated volumetric water content and measured volumetric water content at locations SML0, SML1, SML2 and SML3, (b) Comparison of estimated ground temperature and measured temperature and (c) estimated snow depth and measured snow depth (d) Stability of soil slope from the day of slope construction until failure

A close similarity between the numerical estimation and measured data has been found. Slope failure will occur if the soil is saturated near the slope surface and the failure may trigger along the slip surface. In such circumstances, the reason for failure could be judged by estimating the average volumetric water content. The average volumetric water content is compared here in order to visualise the saturation of the slope. It may be seen that the average volumetric water content at locations SML1, SML2 and SML3 reaches to a range of 0.52 m^3/m^3 to 0.56 m^3/m^3. The saturated volumetric water content of the soil is 0.63 m^3/m^3 as given in Table 1. From this observation, it could be said that during the day of the slope failure the degree of saturation (S_r) was up to 85 % on the slip surface. The numerical simulation results match well with the trend of the measured data. The maximum difference found between the numerically estimated volumetric water content and measured volumetric water content is 0.02.

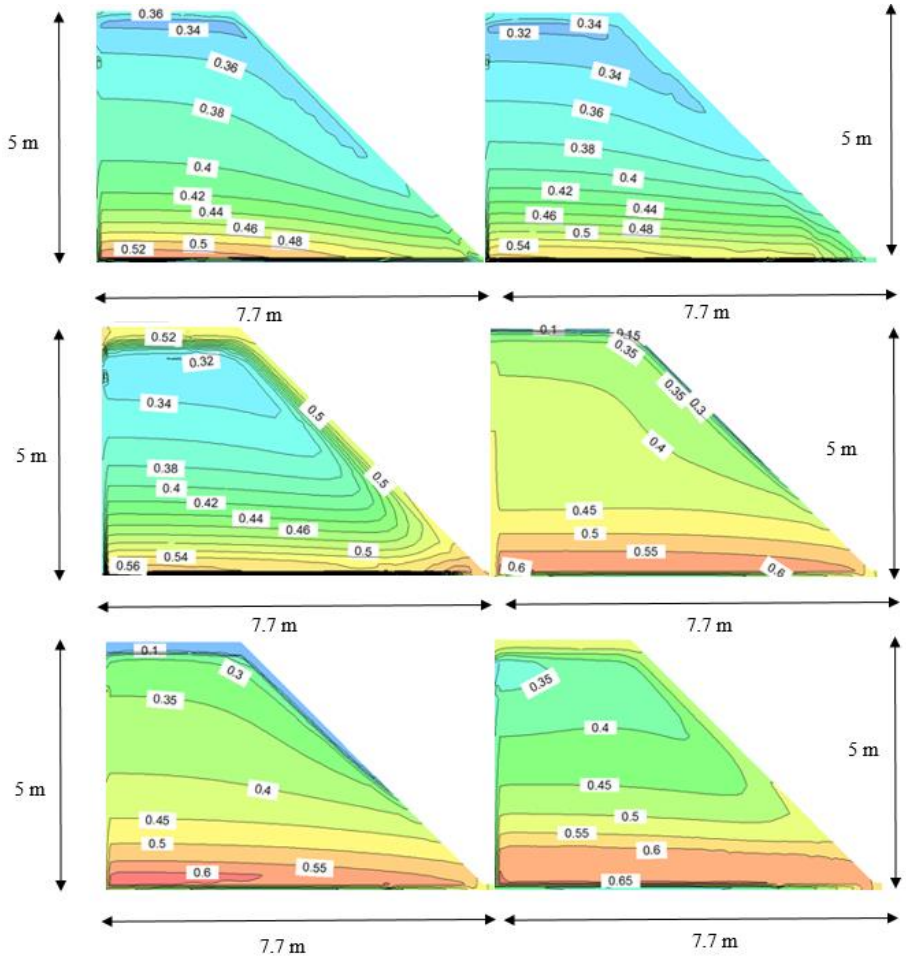

Figure 4.12 Distribution of volumetric water content VWC (m^3/m^3) at (a) day 50 (29-12-2012), (b) day 100 (17-02-2013), (b) day 150 (08-04-2013), (c) day 200 (28-05-2013), (d) day 250 (17-07-2013) and (e) day 300 (05-09-2013)

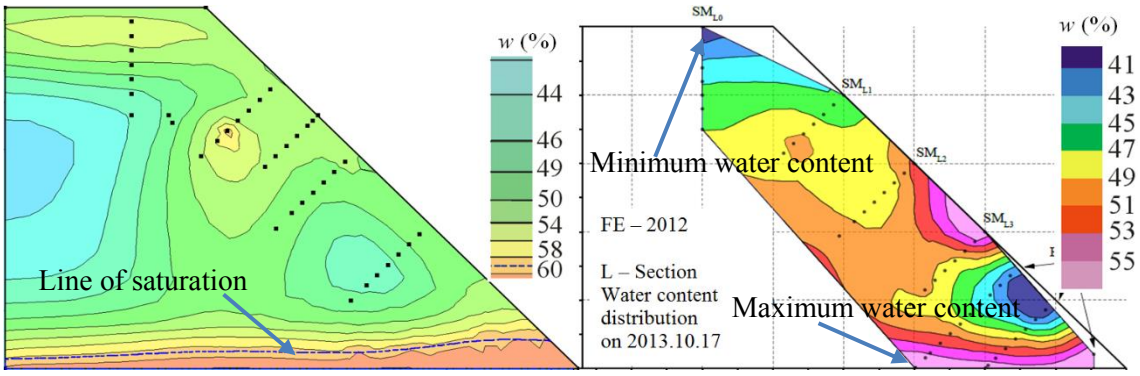

Figure 4.13 Distribution of gravimetric water during the day of slope failure day 343 (17-10-2013)

(a) numerical model (b) physical slope model

The stability of the soil slope starting from the day of slope construction until the failure is expressed as a factor of safety and has been plotted in Figure 4.14(d). The factor of safety during the day of slope failure is 0.954. The slip surface estimated using the limit equilibrium method is compared with the field slope failure data, as shown in Figure 4.14 (a) and (b) respectively.

(a)

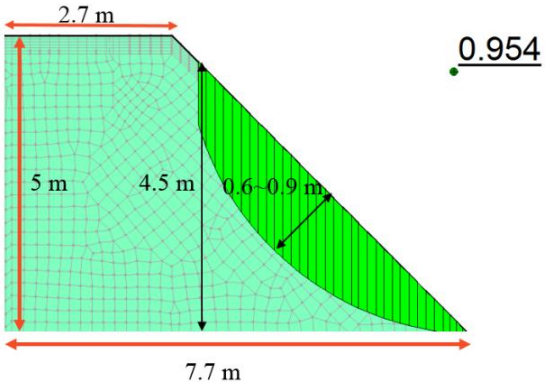

(b)

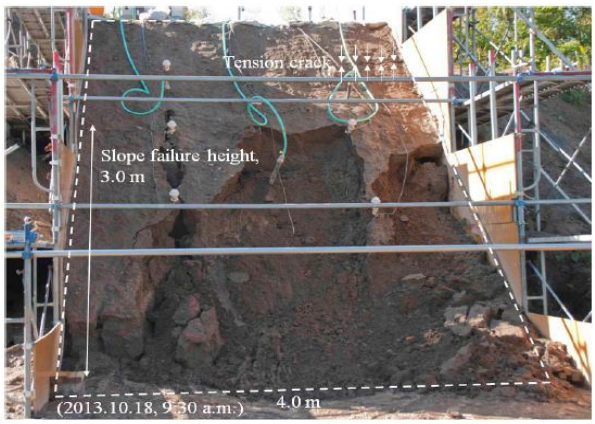

Figure 4.14 Comparison between (a) estimated limit equilibrium slip surface with (b) actual slope failure (adapted from Matsumura, 2014)

In field conditions, the failure surface was about 3 m in height and 0.6 m to 0.8 m in depth. From the numerical simulation, the failure surface is estimated as 4.5 m in height and 0.6 m to 0.9 m in depth. The numerical simulation demonstrated close similarity in estimating the influencing parameters i.e. net surface infiltration, snow depth, snowmelt water and ground temperature etc. and could predict the soil water content distribution of the slope appropriately. The numerically estimated data closely matches with the measured data almost in all circumstances. Through these observations, it could be claimed that the adopted approach is reliable to predict the soil slope stability in seasonal cold regions.

4.2 Study of the highway slope failure using the recommended approach

The slope failure that occurred along the national highway route 230 (highway slope failure), is analysed using the recommended approach. The two-dimensional numerical model, boundary conditions and material properties were considered to be similar to the embankment slope failure model and are discussed in the following section.

4.2.1 Numerical model

The two-dimensional numerical model for the highway slope failure is designed using the geological cross-sectional data. The two-dimensional numerical model with the soil/rock stratigraphy and surveyed ground water table are given in Figure 4.15.

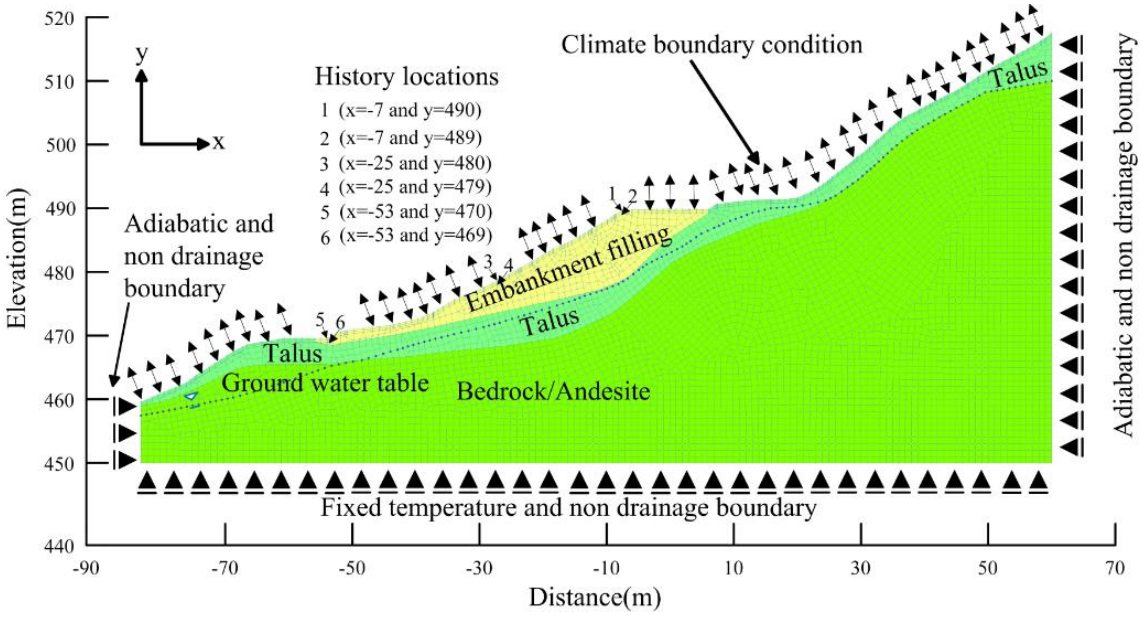

Figure 4.15 Two-dimensional numerical model for the highway slope with boundary conditions

The slope stratigraphy has three soil/rock types, namely embankment filling, talus slope materials and the bedrock (Andesite). The surveyed ground water table is at an average depth of 8 m from the ground surface.

4.2.2 Soil properties

The soil material properties used for the numerical simulation of the highway slope model are given in Table 4.2. The parameters i.e. dry density (ρ_d), hydraulic conductivity of saturated soil (k_s), and undrained shear strength (q_u) have been obtained from laboratory measurements (Hokkaido Regional Development Bureau, 2013). The parameters for which no laboratory measurements are available, i.e. thermal conductivity (λ), volumetric heat capacity (ζ), volumetric water content of soil at 0°C (θ_{wf}), effective cohesion (c') and effective angle of internal friction (ϕ') have been estimated using methods given by Kersten (1949), Jame (1977), Black and Tice (1989) and Hoek and Brown (1977), respectively. The SWCC of the embankment filling material and Talus sediments were estimated from the grain size distribution curve based on the method given by Fredlund et al. (2002). For the embankment filling and talus material, the unsaturated shear strength data is not available so that the available undrained shear strength is considered for the embankment filling and saturated shear strength is estimated for the talus slope material. The bedrock is modelled as a low permeability material.

Table 4.2 Soil properties used for the simulation of highway slope

Property name	**Embankment filling**	**Talus materials**
Dry density of soil *(ρ_d)*	1400 kg/m^3	1200 kg/m^3
Porosity *(n)*	0.47	0.53
Hydraulic conductivity of saturated soil *(k_s)*	5.62×10^{-7} m/s	1×10^{-4} m/s
Volumetric water content of soil at 0°C *(θ_{wf})*	0.15 m^3/m^3	0.10 m^3/m^3
Volumetric water content of saturated soil *(θ_s)*	0.47 m^3/m^3	0.53 m^3/m^3
Residual volumetric water content of soil *(θ_s)*	0.12 m^3/m^3	0.05 m^3/m^3
Unfrozen thermal conductivity *(λ_u)*	127.04 kJ/(Day·m·°C)	103.7 kJ/(Day·m·°C)
Frozen thermal conductivity *(λ_f)*	132.24 kJ/(Day·m·°C)	135.7 kJ/(Day·m·°C)
Unfrozen volumetric heat capacity *(ζ_u)*	2237 kJ/(m³·°C)	2398 kJ/(m³·°C)
Frozen volumetric heat capacity *(ζ_f)*	1624 kJ/(m³·°C)	1392 kJ/(m³·°C)
Undrained shear strength (q_u)	52 kPa	-
Effective cohesion *(c')*	9.75 kPa	52 kPa
Effective angle of internal friction *(ϕ')*	35˚	11.36°

For the long-term slope stability analysis, drained shear strength parameters are needed. The effective cohesion (c') and effective angle of internal friction (ϕ') for the embankment filling material were derived using rigorous back calculation methods given by Duncan and Stark (1992), Okui et al. (1997) and Zhang et al. (2013). Several values of cohesion and angle of internal friction are given initially. By setting the FOS = 1 and using the reference ground water table derived from the non-isothermal seepage simulation and using the pre-known dimensions of the slope failure, several iterations of calculations have been made from which different cohesion and angle of internal friction values are obtained. In consideration to the height of the failure surface, the effective cohesion and effective angle of internal friction for the embankment soil were derived as shown in Figure 4.16 (a) and (b). Back-calculation of shear strength parameters may have some limitations concerning with the precision of the estimated shear strength (Tang et al. 1999; Duncan and Wright, 2005; Deschamps and Yankey, 2006).

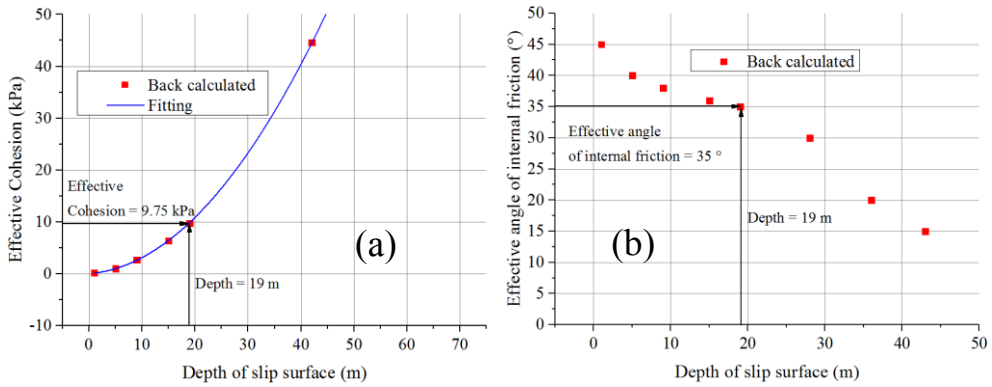

Figure 4.16 Back calculation of effective cohesion (a) and effective angle of internal friction (b) of the failed embankment material

Since the major objective of this study is to examine the influencing parameters of slope failure, the problems with the precision of the estimated shear strength may be negligible and these values can be used as a basis for a parametric study. The shear strength of the Talus materials was intentionally kept larger so that the steep portions of the mountain slope located far away from the embankment does not influence the factor of safety calculations.

4.2.3 Analytical conditions

Prior to the transient non-isothermal coupled seepage analysis, an initial equilibrium condition in terms of pore water pressure and the ground temperature is necessary. The ground water table has been measured from the geological survey performed after the slope failure. The ground

water table line from the geological survey is kept as a reference and an average of 10-year climate data recorded between years 2002 to 2012 obtained from a meteorological telemetry at Mui Ne, Hokkaido, Japan maintained by the Ministry of Land, Infrastructure, Transport and Tourism, Hokkaido Regional Development Bureau (MLIT) has been used and to derive the initial equilibrium as shown in Figure 4.17 and Figure 4.18.

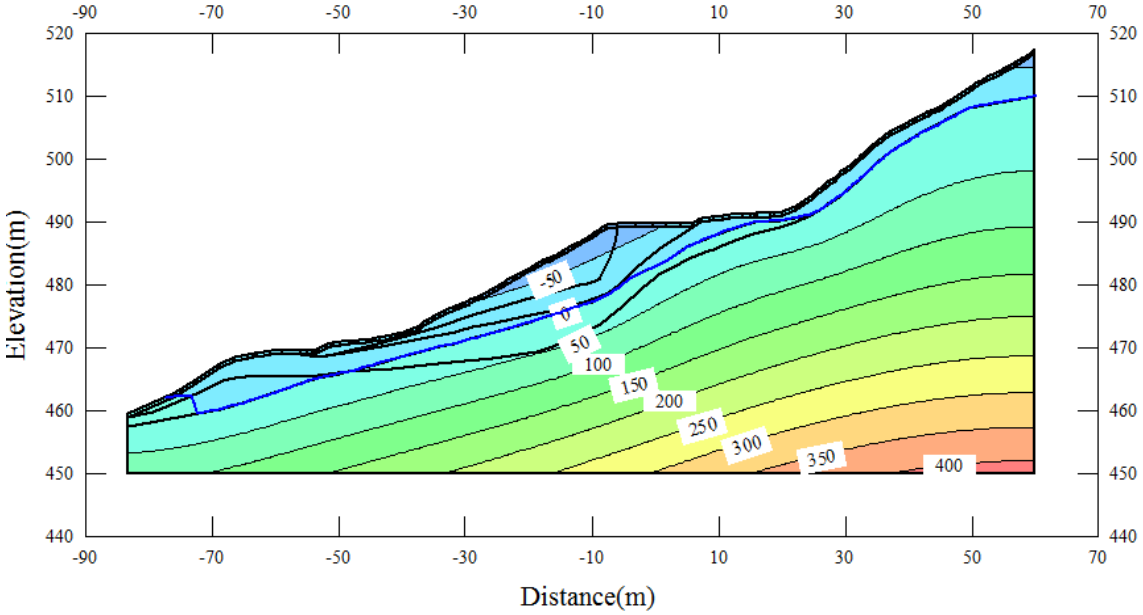

Figure 4.17 Distribution of pore water pressure (kPa) during initial day 01-04-2012

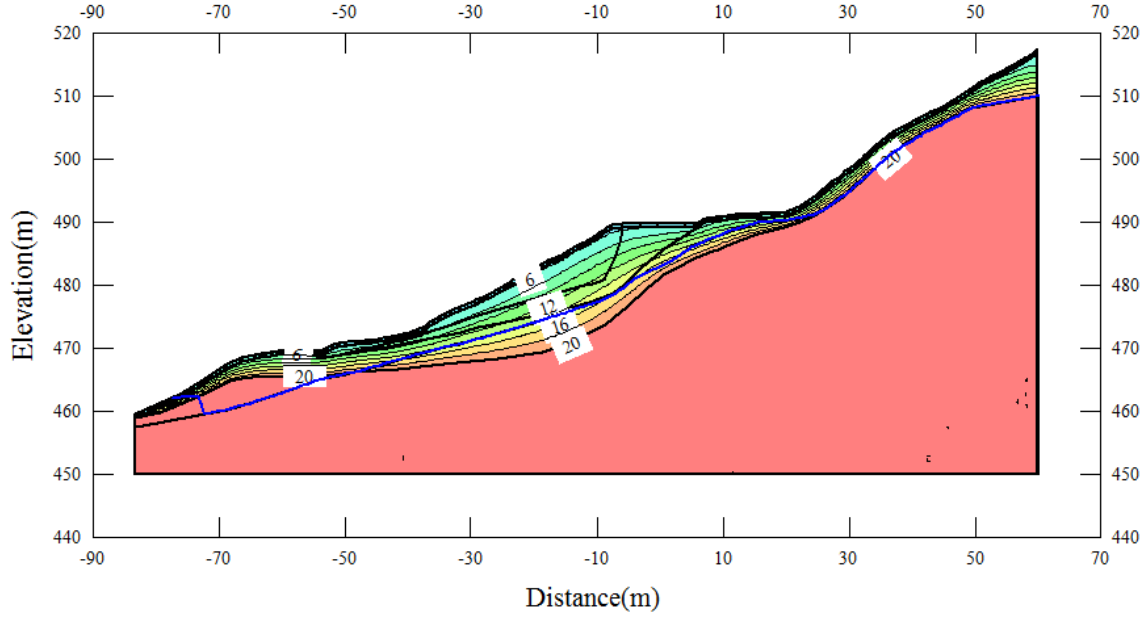

Figure 4.18 Distribution of ground temperature (°C) during initial day 01-04-2012

The climate data used for the numerical simulation is also obtained from the meteorological telemetry at Mui Ne which is closest to the disaster site. The climate data is given in Figure 4.19.

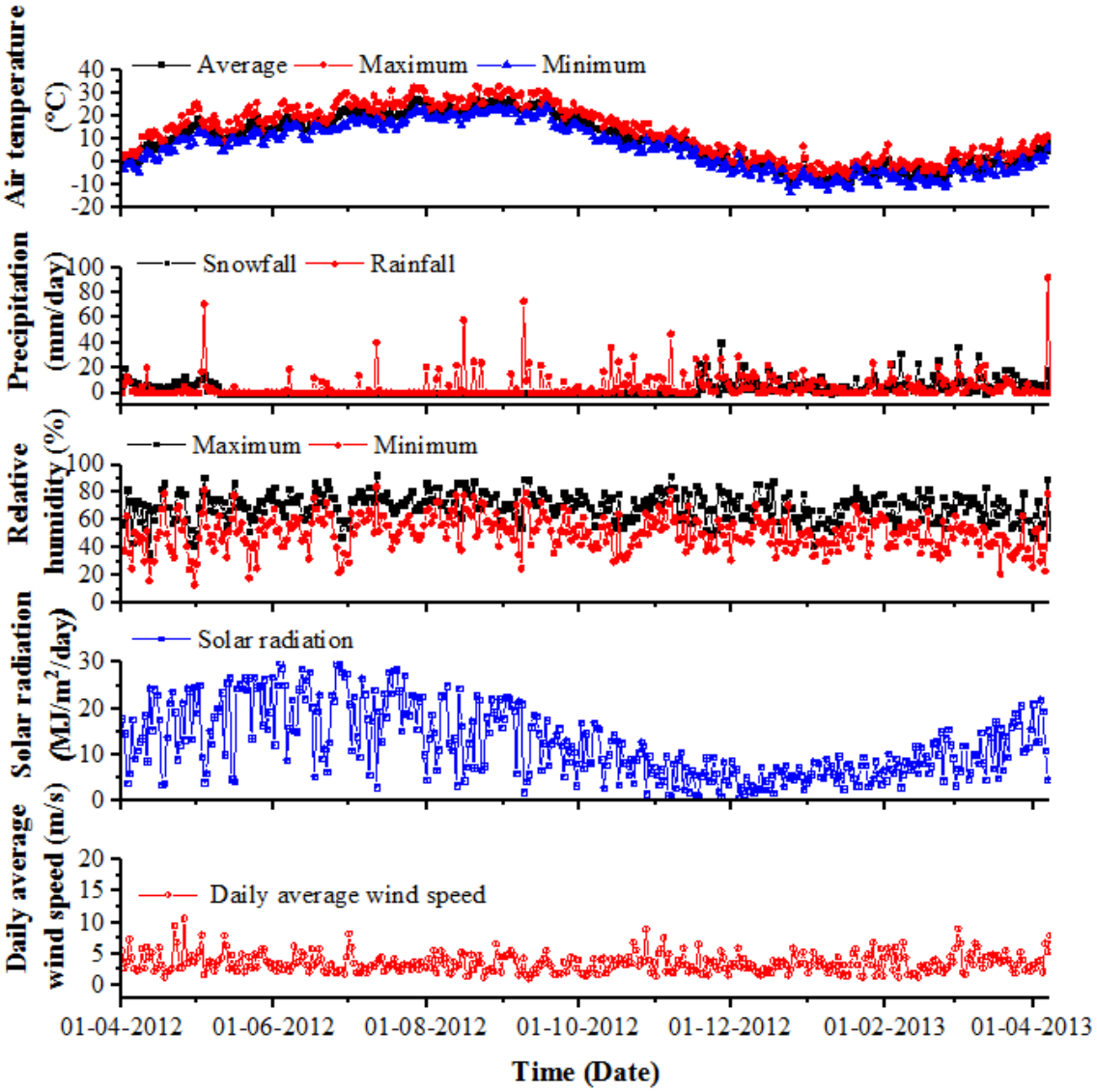

Figure 4.19 Climate data used for the simulation of highway slope

The air temperature on the day 1 (01-04-2012) is just close to 0˚C and it increases during the thawing period. The maximum rainfall of 92 mm/day occurred during the day of slope failure 07-04-2013.

4.2.4 Results and discussions

To study the changes in pore water pressure and volumetric water content of the embankment, histories were given at particular locations 1 to 6 in the numerical model, as shown in Figure

4.16. The variation in volumetric water content and pore water pressure are given in Figure 4.20 (a) and Figure 4.20 (b) respectively. From Figure 4.20, it could be seen that there is a higher fluctuation of soil water at locations 1 and 2. During the day of slope failure, the volumetric water content and pore water pressure at all locations of the embankment reaches 0.47 m^3/m^3 and 0 kPa respectively, as shown in Figure 4.20 (a) and (b). The saturated volumetric water content of the slope is 0.47.

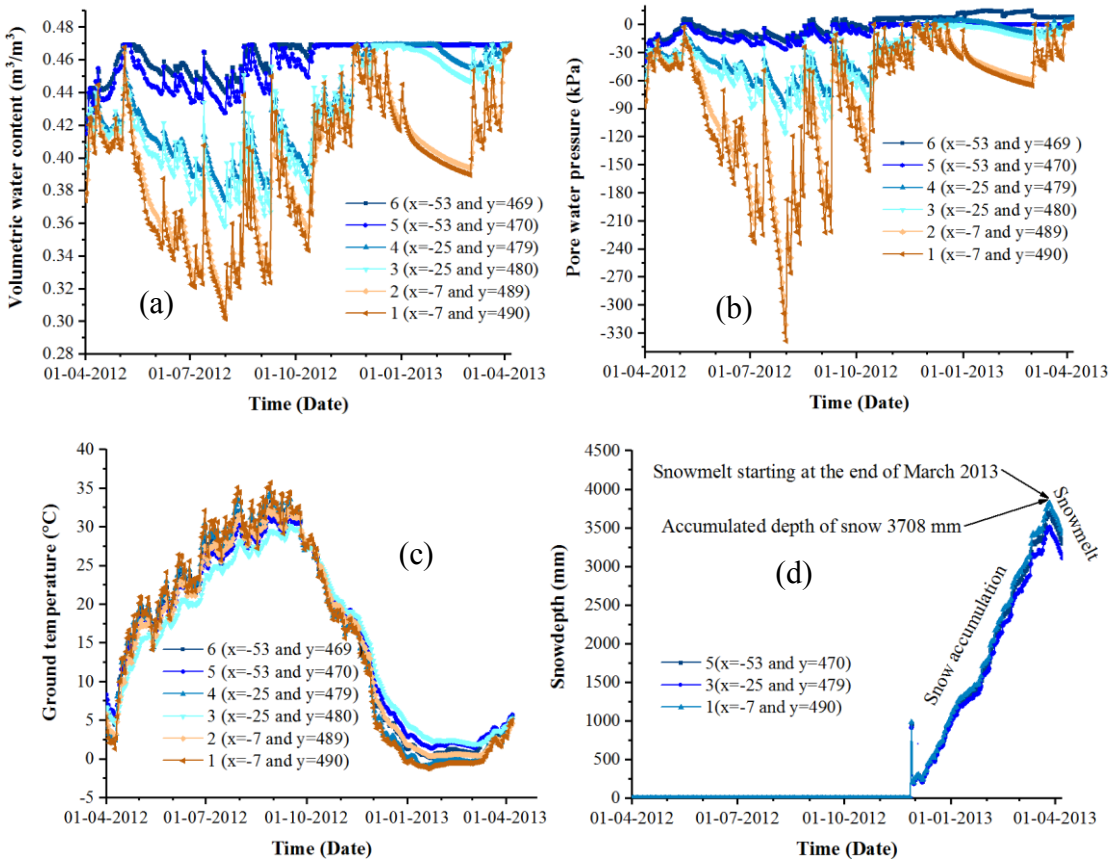

Figure 4.20 Variation in volumetric water content, (b) Variation in pore water pressure (c) Variation in ground temperature and (d) accumulation of snow depth

The ground temperature and accumulated snow depth measured at locations 1 to 6 are given in Figure 4.16(c) and (d). The ground temperature rises above 0˚ after March 12, 2013. The maximum accumulated snow depth is 3708 mm at location 1 (x=-7 and y=490). A comparison of snowmelt with the measured data could not be obtained in this case because the snow depth varies with location. The accumulated snow started to melt from March 12, 2013. During this period, the stability may get reduced due to the snowmelt water. The factor of safety estimated from the simulation is plotted in Figure 4.21(a).

During initial days from 01-04-2012, the stability of the slope reduced rapidly due to continuous precipitation until early May 2012. During the month of June 2012, there is not much precipitation observed and hence an increasing trend in safety factor is estimated. Further, the factor of safety reduces whenever there is continuous precipitation. During the month of October to November 2012, the stability reduces rapidly due to continuous precipitation. A similar trend continues until December 2012.

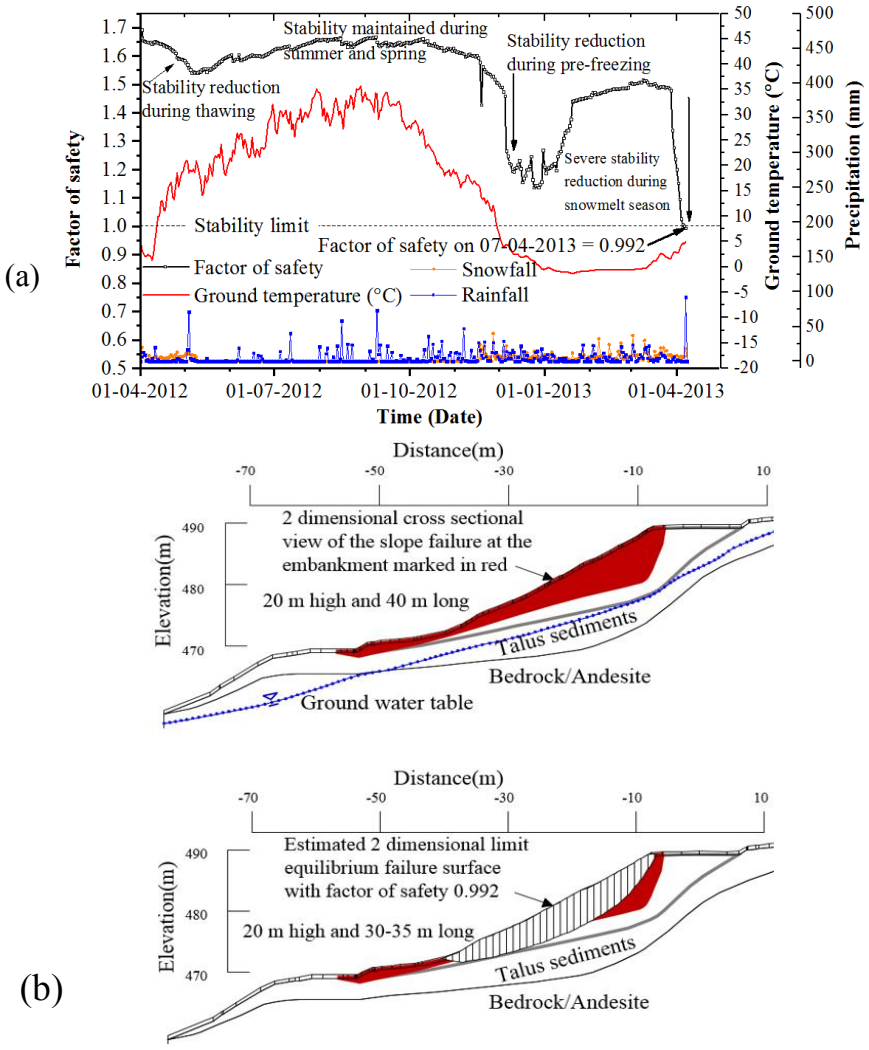

Figure 4.21 (a) Stability of slope expressed as factor of safety along with ground temperature and precipitation (b) Two-dimensional geological cross section showing the slope failure area compared with numerically estimated two-dimensional failure surface with factor of safety

The ground temperature reduces below 0° C during January 2013 and the soil surface remains frozen until March 12, 2013. During this period, an increase in the factor of safety is observed and later the factor of safety value keeps nearly constant. The reduction in the factor of safety

commences once the ground temperature increases above 0˚ C, exactly on March 12, 2013. The reduction continues markedly, and on the day, April 07, 2013, the factor of safety reaches a value 0.992 which denotes the slope failure. The surveyed failure surface and the numerically estimated failure surface with the factor of safety on April 07, 2013 is given in Figure 4.21(b). The height of the numerically estimated slip surface is 19 to 20 m and 30 to 35 m in length. From the geological survey, the length of the failure is around 40 m with a height of 20 m. The minimum safety factor 0.992 has been found for the critical slip surface passes through the embankment portion.

4.3 Parametric studies

The effects of the factors i.e. freeze-thaw action, snowmelt water infiltration and the weight of the accumulated snow need to be known for the precise assessment of the long-term stability of soil slopes i.e. embankment and cut slopes along the highways. Based on this purpose, in this study, a series of parametric studies using the recommended numerical simulation method has been performed using the embankment slope model and highway slope model with the analytical conditions as given in Table 4.3.

Table 4.3. Analytical conditions for parametric studies

Targeted parameter for investigation	Case study	Additional factors and analytical conditions considered in simulations					
		Rainfall	Freeze -thaw action	Snowfall/ snowmelt water	Weight of snow	Change in slope angle	Shear strength of frozen soil
Effect of increased amount of rainfall	ES	O (Twice and Thrice)	O	X	X	X	X
Effect of increased amount of snowfall	ES	O	O	O (Twice and Thrice)	X	X	X
Effect of Freeze-thaw action	ES and HS	O	O	O	X	X	X
		O	X	O	X	X	X
Effect of snowfall/snowmelt water	ES and HS	O	O	O	X	X	X
		O	O	X	X	X	X
Effect of weight of snow	ES	O	O	O	O	X	X
Effect of slope angle	ES	O	O	O	X	O	X
Effect of frozen soil shear strength	ES	O	O	O	X	X	O

Note: ES = Embankment slope; HS = Highway slope; O = parameter considered; X = parameter not considered.

4.3.1 Effect of increased magnitudes of rainfall on slope stability

The amount of rainfall has been increased twice and thrice in order to see the effect on slope stability using the embankment slope model. The twice and thrice considered rainfall magnitude significantly reduces the stability as given in Figure 4.22 (a).

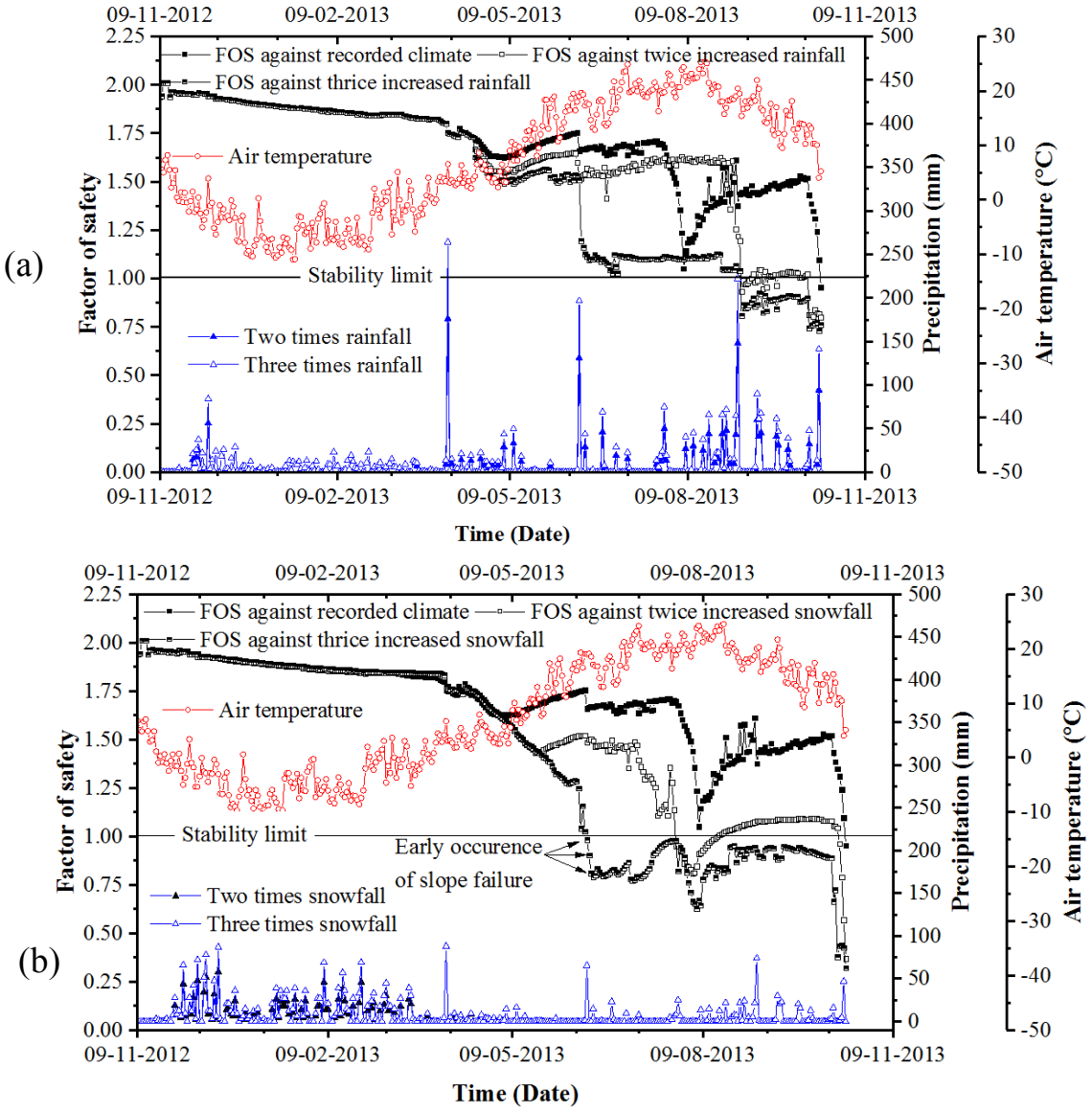

Figure 4.22 (a) Influence of increased magnitudes of rainfall on soil slope stability (b) Influence of increased magnitudes of snowfall on soil slope stability

4.3.2 Effect of increased magnitudes of snowfall on soil slope stability

To clearly visualise the effect of snowmelt on slope failure, the snowfall precipitation has been configured in different magnitudes, like twice and thrice for the embankment slope model. The

stability of the slope abruptly reduces during March-April-May months due to snowmelt and surface infiltration. It could be seen that as the depth of accumulated snow increases, the duration took to melt the snow also increases and finally it results in a reduction in safety factor as shown in Figure 4.22 (b). The failure-inducing factor is not only the rainfall or not the snowmelt water alone. The rainfall along with snowmelt water induces such a reduction in slope stability. Through the parametric studies, it is found that the accumulated snow depth increase may result in an excess amount of snowmelt water which may eventually reduce the soil slope stability.

4.3.3 Effect of freeze-thaw action on soil slope stability

Two different numerical simulations, one considering the freeze-thaw process and the second without considering the freeze-thaw process were performed using embankment slope model and highway slope model. When there is no freeze-thaw action considered, the effects of soil water freezing, the effect of the latent heat phase change and the temperature flow are neglected. The calculation of all other variables i.e. precipitation (rainfall and snowfall), air temperature, relative humidity etc. are kept same for both the analysis and the shear strength of frozen soil is not considered for this parametric study. For the simulation considering freeze-thaw action, the soil water content distribution is estimated using non-isothermal seepage flow and for the simulation without freeze-thaw action, the soil water content distribution is estimated using isothermal seepage flow. These analyses were performed for both the embankment slope model and highway slope model. The factor of safety for both the simulations was analysed and compared as given in Figure 4.23 (a) and (b).

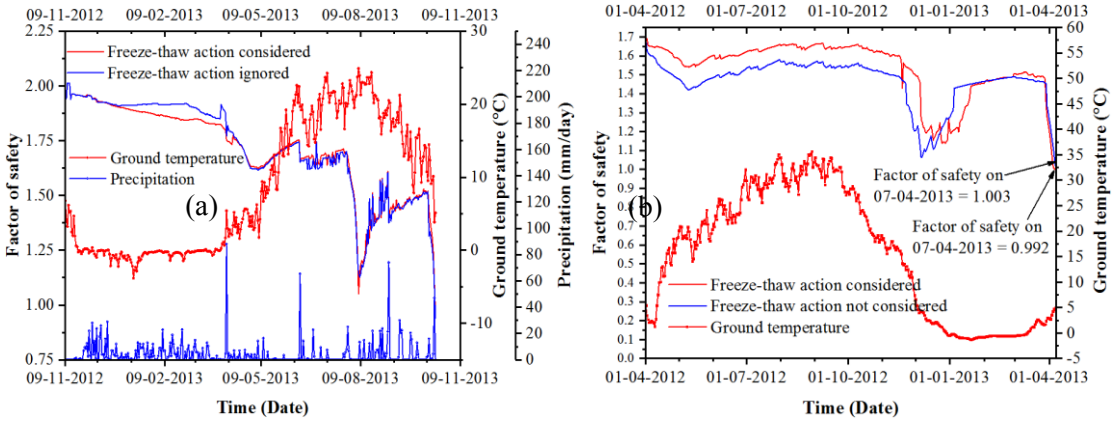

Figure 4.23 Comparison of slope stability considering freeze-thaw action and ignoring freeze-thaw action for (a) embankment slope model and (b) highway slope model

A stability difference could be seen between analysis considering freeze-thaw action and analysis without freeze-thaw action during the period when the ground surface temperature is below zero for both the cases. In the case example of embankment slope, the freeze-thaw action has very small impact on soil water content and factor of safety. Whereas, for the highway slope, a major difference in the factor of safety between analysis considering freeze-thaw action and analysis without considering freeze-thaw action is observed. On the day of slope failure, the factor of safety estimated by the analysis considering freeze-thaw action is 0.992 and the factor of safety estimated by the analysis without considering freeze-thaw action is 1.003. From this observation, it could be said that the freeze-thaw action has a considerable effect on soil water content fluctuation which in turn affects the slope stability and for the proper assessment of the stability of soil slopes in seasonal cold regions, the freeze-thaw action must be considered in estimating the soil water content distribution.

4.3.4 Effect of snowfall/snowmelt water infiltration on soil slope stability

The snowfall accumulated above the slope during the winter season will start to melt once the air temperature increases above the phase change temperature (0˚C). During this snow melting period, the snowmelt water will infiltrate into the soil or runoff above the slope based on the ground surface temperature. From Figure 4.24(a) and (b), it can be seen that the factor of safety does not get reduced during the months of March, April and May for the analysis without considering snowmelt water. The reason is due to the lack of snowmelt water. Whereas when snowfall is considered, the factor of safety abruptly reduces during the snow melting season. The contribution of snowmelt water in the net surface infiltration is high during the thawing season which abruptly reduces the slope stability. One more important observation made from the embankment slope model is that when there is no snow on the ground the safety factor starts deviating from the early February 2013 itself. The reason behind this phenomenon is, if there is no snow accumulated on the soil ground, the soil temperature may be much lower than it would be under the accumulated snow. There would not be a heat flux variation in this case. Due to this fact, the ground will freeze up to a certain depth more than it will freeze under the accumulated snow. If the ground is frozen over greater depth, it will become impermeable and there will not be any surface infiltration. The factor of safety will be high during the winter period if there is no snow accumulated on the soil ground. Due to the absence of snowmelt water, during snowmelt period, there will not be any reduction in stability. Similar behaviour

has been observed from the highway slope model as well. It is very interesting to note that for the highway slope if the snowmelt water infiltration is ignored, the factor of safety and stability of the slope is considerably higher throughout the year from 01-04-2012 to 07-04-2013. On the day of slope failure, the factor of safety of slope when the snowmelt water is ignored is 1.224 which emphasises considerable stability. In the case of simulation, in which the snowmelt water is included in the calculation of soil water content, the factor of safety on the day of slope failure is 0.992 which clearly denotes the slope failure. Based on this observation, it could be said that for the case of highway slope failure, the 92 mm cumulative rainfall alone would not have induced the slope failure. The water originating from the snowmelt that infiltrated into the soil ground together with the cumulative rainfall should have induced the disaster.

One more interesting observation found for the highway slope model is that the difference in the factor of safety during the month of December 2012 between analysis considering snowfall and analysis neglecting snowfall, as shown in Figure 4.24(b). The air temperature fluctuates below and above 0˚C during the starting of the freezing season, November and December 2012. In this situation, there is a possibility of rainfall and snowfall together. If there is accumulated snow above the soil ground originating from the previous day snowfall, on the next day if the air temperature is above 0˚C and there will be precipitation in terms of rainfall. The factor of safety reduces to 1.137 on December 25, 2012, when the effect of snowmelt water is considered in the analysis. Whereas, for the analysis without the effect of snowmelt water, the factor of safety is 1.507 on December 25, 2012. Based on this observation it could be said that the snowfall that occurs during the initial stages of freezing (November and December months) will also influence the slope stability considerably.

From these parametric studies, it is very clear that snowmelt water infiltration seriously affects the soil slope stability and it should be considered in long-term slope stability analysis of embankment structures and cut slopes along the highways in seasonal cold regions.

(a)

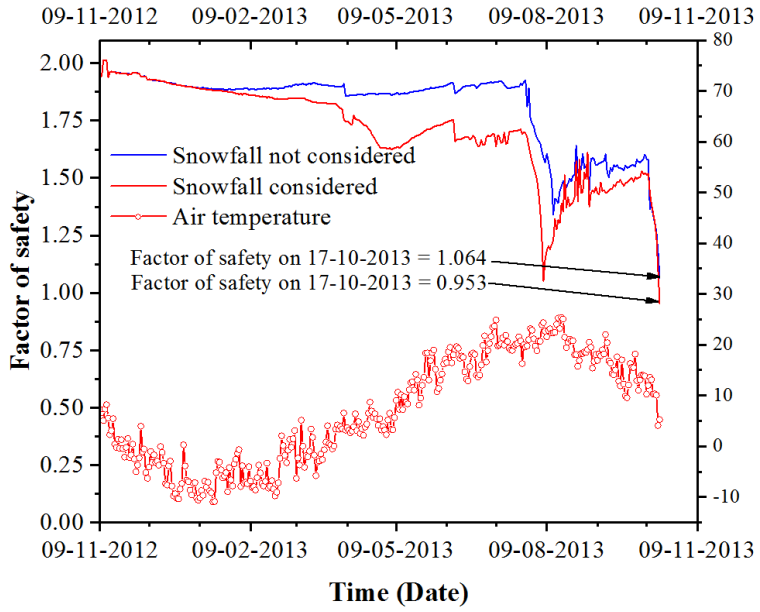

(b)

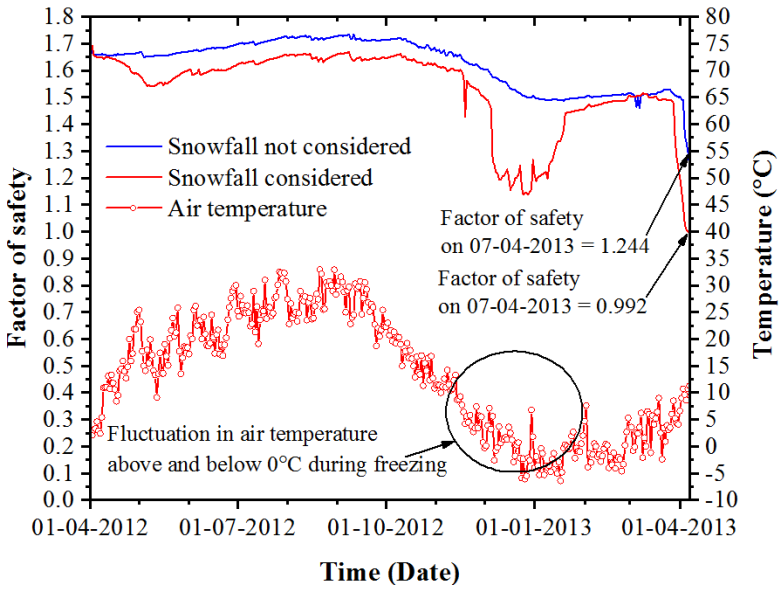

Figure 4.24 (a) Variation in factor of safety with and without considering snowfall for embankment slope (b) Variation in factor of safety with and without considering snowfall for highway slope

4.3.5 Effect of weight of snow on soil slope stability

The snow accumulated on top of the slope surface has its own weight. In such cases, it may induce a reduction in slope stability. To analyse this effect, the weight of the snow is considered as a surcharge load. The snow load is estimated using the snow density (ρ_{sn}) and accumulated snow depth. As the accumulated snow depth increases, the snow load starts to build up. The maximum snow load calculated for 1689 mm snow depth is 7 kN/m^2. To see whether this snow

load will affect the slope stability or not, the load is considered as a surcharge pressure in the slope stability analysis. Since it is not possible to consider the increasing snow load day by day in a safety factor calculation, a 25 days averaging has been adopted, as given in Figure 4.25 (a). The safety factor seems to be affected much by the accumulated snow weight, as given in Figure 4.25 (b).

(a)

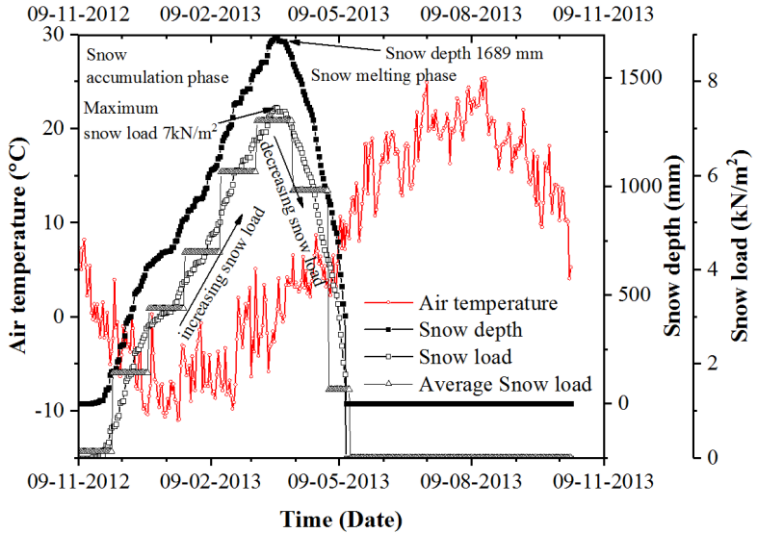

(b)

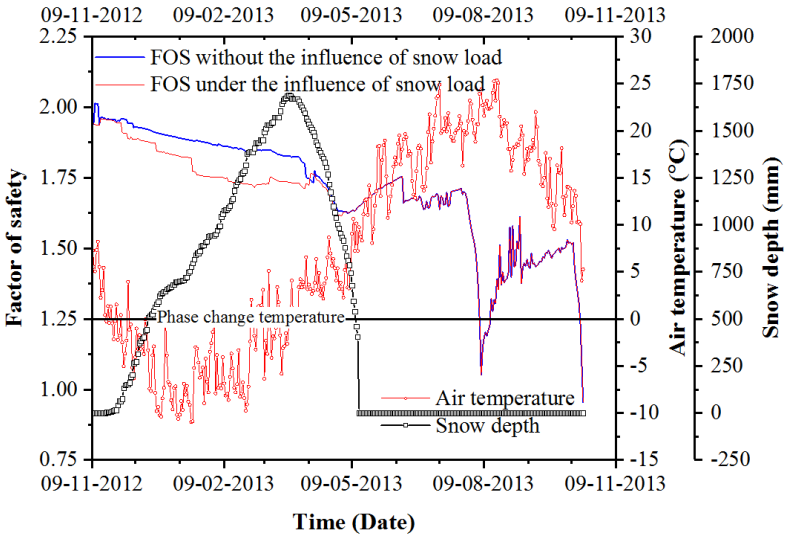

Figure 4.25 (a) Accumulated snow depth and calculated average snow load for every 25 days, (b) Effect of snow load on soil slope stability

In Figure 4.25, the factor of safety obtained with and without snow load both considers the effect of snowmelt water. It seems the weight of snow combined with the snowmelt water may affect the slope stability to a considerable amount during the freezing and snow melting seasons,

respectively. The maximum difference in safety factor is observed during the month of March 2013 when the snow load reaches its maximum. Once the snow starts melting, the load of the snow will decrease and diminish when all the accumulated snow is converted into water.

4.3.6 Effect of slope angle on soil slope stability

Kawamura and Miura (2013) performed experiments with small scale model soil slopes made up of volcanic soil material under different slope angles considering a slope angle range from 45˚ to 65˚. For the design of embankment slopes and cut slopes along the express highways in Japan, the NEXCO (Central Nippon Expressway Company Limited) has set some guidelines (Yasuda and Fujioka, 2012). For the design of embankment slopes in express highways, the standard slope would be 1:1.8 that is 29˚ and for highways other than the national expressways in Japan, a standard slope angle ratio of 1:1.5 to 1:1.8˚ is adopted depending on the soil/rock material type underlying the embankment. Further, for natural cut slopes along the highways, the slope may range up to a slope angle of 60˚ if the base of the soil is rock. In view of all these considerations, a study to evaluate the effect of slope angle is performed by making numerical slope models with different slope angles. The slope angles are considered to be 30˚, 35˚, 40˚, 45˚, 50˚, 55˚ and 60˚, though the physical embankment model considered in this study was built at an angle of 45˚. In order to study the effect of slope angle, 30˚, 35˚, 40˚, 45˚, 50˚, 55˚ and 60˚ numerical slope models are made and simulated with the recorded climatic measurements.

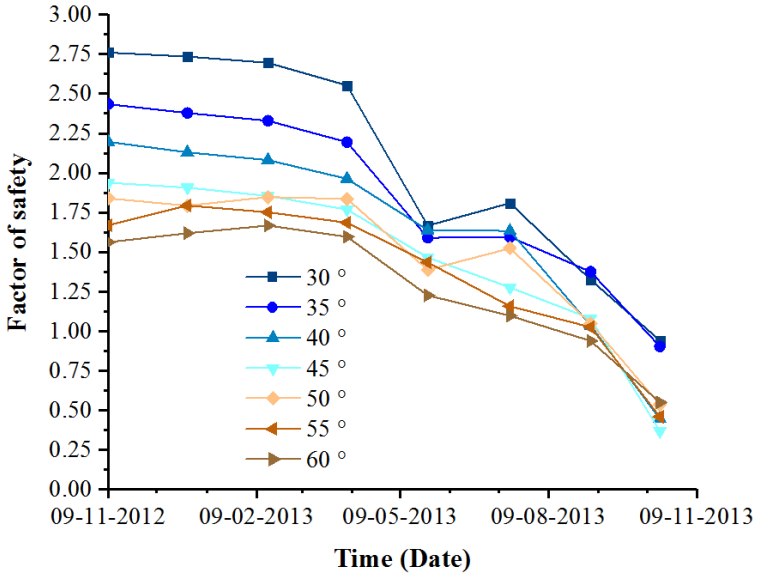

Figure 4.26 Safety factor of various inclinations of slope

It may be seen from Figure 4.26 that the safety factor of the slope varies with different slope angles. During the slope failure day, October 17, 2013, the safety factor for slope angles 45˚ to 60˚ are lesser than slope angles 30˚, 35˚ and 40˚. For shallow slopes, 30˚, 35˚ and 40˚, the factor of safety is more than 1. Interestingly, the reduction in safety factor during the snow melting season is more for the shallow slopes 30˚, 35˚, 40˚ than 45˚, 50˚, 55˚ and 60˚ slopes. The variation in the factor of safety between different slope angles is governed by the infiltration and runoff which will vary significantly according to the slope angle.

4.3.7 Effect of shear strength of frozen soil

Chen et al. (2013) analysed the effect of shear strength of frozen soil on soil slope stability conceptually. When the soil is frozen, it will gain additional shear strength depending on the ice content. Many studies have shown the dependency shear strength of frozen soils on negative temperatures (Hooke et. al., (1972), Anderson and Ladanyi, (2004), Arenson and Springman (2005) and Wang et. al., (2017)). In the case study of volcanic soil embankment, during the freezing months, a maximum freezing depth of 0.2 m is observed from the embankment monitoring (Matsumura, 2014). The region where the soil water is frozen would have gained additional shear strength which could result in an increase in stability. In any case, in this study so far this phenomenon is not considered due to the following reasons,

1. The additional shear strength will only increase the stability which will eventually increase the factor of safety.
2. Once the frozen water content of the soil melts, the additional shear strength will diminish.
3. Since the freezing depth in the present study is only 0.2 m (20 cm) it would not have strongly influenced the overall stability of 5 m tall slope.

In order to check the generality of the above-mentioned statements, a slope stability analysis considering additional shear strength in terms of effective cohesion and effective angle of internal friction is performed. Due to non-availability of frozen shear strength data, basic empirical equations as referred from the literature is adopted to calculate the frozen soil shear strength parameters. The frozen soil shear strength is estimated as given by Arenson and Springman (2005) and Chen et al. (2013), assuming that the effective angle of internal friction ϕ'

is independent of temperature and strain rate, and the effective cohesion *c'* is independent of strain rate.

$$\phi_f = \phi' - \phi'(\theta_i)^{2.6} \tag{4.11}$$

ϕ_f= angle of internal friction of frozen soil (˚), ϕ'= effective angle of internal friction (˚), θ_i= volumetric ice content (m^3/m^3). For the estimation of frozen shear strength, two variables viz. unfrozen water content and unfrozen ice content of the soil are needed. The unfrozen water content of the soil is estimated using the relationships given by Black and Tice, (1989).

A simple empirical estimation for cohesion of frozen soils is given by Chen et al. (2013),

$$C = \begin{cases} c_f(T,\theta_{uw}) = (\beta_1.T + \chi_1)(\beta_2.\theta_{uw} + \chi_2), T_g < 0°C \\ c', T_g \geq 0°C \end{cases} \tag{4.12}$$

C = cohesion (kPa), c'= effective cohesion at unfrozen state (kPa), C_f= cohesion at frozen state (kPa), T = Temperature (˚C), θ_{uw} = unfrozen volumetric water content (m^3/m^3), β_1 = 0.074, β_2 = −5.14, χ_1 = −0.015, χ_2 = −1.23 fitting parameters for the cohesion function for coarse grained soils.

Since the motivation of considering the estimation equation in this study is to only see the effect of frozen shear strength on slope stability, the maximum cohesion value and minimum angle of internal friction are specified to the frozen soil zone up to 0.2 m depth and a slope stability analysis has been performed.

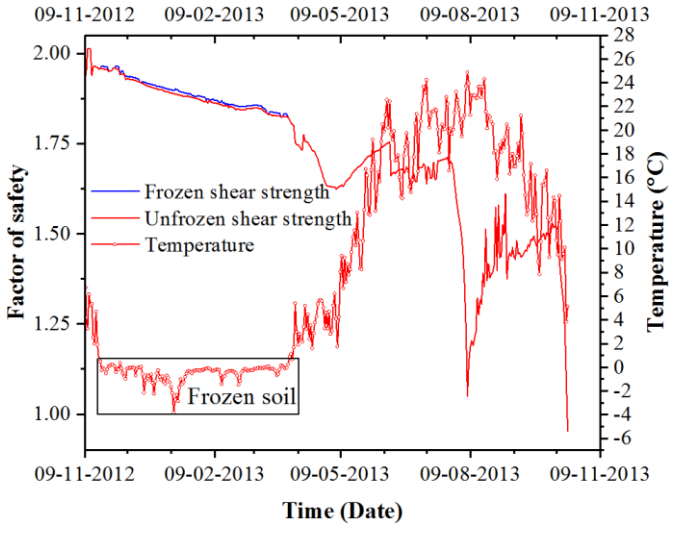

Figure 4.27 Effect of frozen soil shear strength on soil slope stability

The increment in safety factor due to frozen shear strength seems to be very minimal and it has very little impact on the safety factor for the analysis performed, as shown in Figure 4.27. There could be two possible reasons behind this behaviour. The increased frozen shear strength is too low (only 0.67 kPa) and the freezing depth is very small (0.2 m) comparing with the overall slope geometry. However, if the frozen soil occupies an adequate amount of the slope slip surface, the frozen shear strength should be properly considered for the estimation of slope stability.

CHAPTER 5

5 PREDICTION AND EARLY WARNING OF SOIL SLOPE FAILURES IN SNOWY COLD REGIONS

5.1 Overview of the current early warning system in Japan

For the prediction of slope failures in cold regions, whose mechanism is different from warm region slope failures and rainfall induced slope failures, a stability criteria or an early warning system should consider at least some of the influencing factors like freeze-thaw action, snowmelt water infiltration etc. so that a proper warning can be made. For the prediction of rainfall induced slope failures, the Soil Water Index (SWI) is widely used by Japanese Meteorological Agency (JMA) and the effective rainfall index (ER) is used by East Japan Railway Company (JR East). Whereas, the slope failures in seasonally cold regions like Hokkaido are not only influenced by the rainfall. There are other factors than the rainfall to induce a slope failure in cold regions. In consideration to these aspects, a method to predict the soil slope failures in cold regions is developed in this study.

5.1.1 Relationship between 60-minute cumulative rainfall and Soil Water Index (SWI)

In Japan, Japanese Meteorological Agency (2012) performs the early warning of slope failures induced by the rainfall based on the relationship between 60-minute cumulative rainfall and Soil Water Index (SWI) (Osanai et al. 2010). The calculation of 60-minute cumulative rainfall and Soil-water index is referred from Okada, (2005). The Soil Water Index is a concept model that uses a calculated value of the total water depth of a three-layer tank model estimated using the coefficients of the model as given in Figure 5.1.

According to the research of Okada (2005), the Soil–Water Index remains unchanged in many cases even when the parameters of the tank model are changed. The fixed parameters are identified by statistical analysis as confirmed by Okada (2005) for the relationship between rainfall and discharge in a Granite region in Japan as listed in Figure 4. The inflow for the model includes the rainfall amount of the target period. The outflow from the model is calculated based on the equations below.

$$q_1(t) = \alpha_1\{S_1(t) - L_1\} + \alpha_2\{S_1(t) - L_2\} \quad \textbf{(5.1)}$$

$$q_2(t) = \alpha_3\{S_2(t) - L_3\} \quad \textbf{(5.2)}$$

$$q_3(t) = \alpha_4 \{S_3(t) - L_4\} \tag{5.3}$$

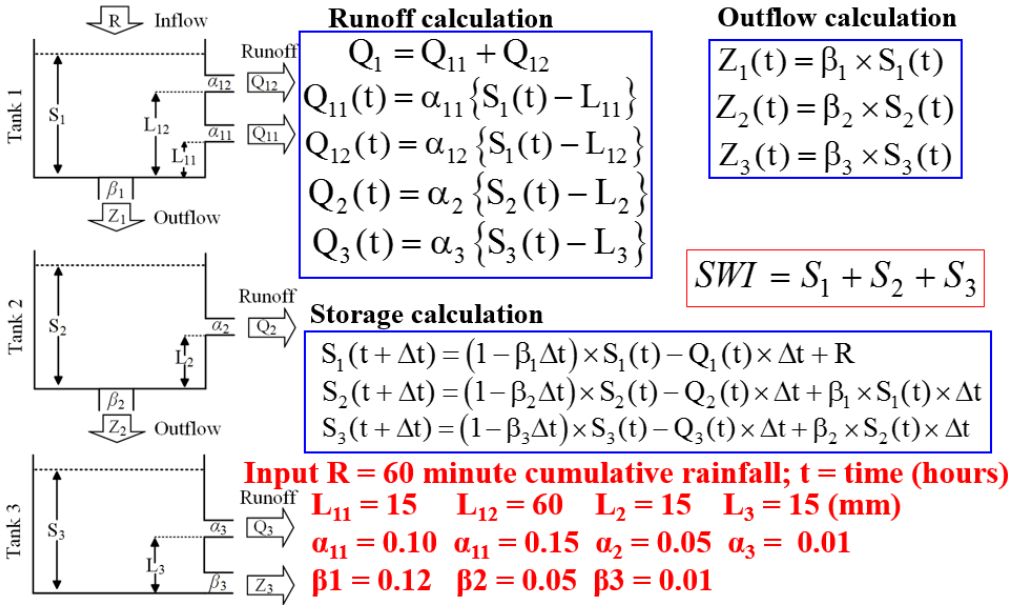

Figure 5.1 Three-layer tank model for Soil Water Index (adapted from Okada, 2005)

Standing water in each tank is represented as,

$$S_1(t+\Delta t) = (1-\beta_1\Delta t) \times S_1(t) - q_1(t) \times \Delta t + R \tag{5.4}$$

$$S_2(t+\Delta t) = (1-\beta_2\Delta t) \times S_2(t) - q_2(t) \times \Delta t + \beta_1 \times S_1(t) \times \Delta t \tag{5.5}$$

$$S_3(t+\Delta t) = (1-\beta_3\Delta t) \times S_3(t) - q_3(t) \times \Delta t + \beta_2 \times S_2(t) \times \Delta t \tag{5.6}$$

$$SWI = S_1 + S_2 + S_3 \tag{5.7}$$

where α_1, α_2, α_3 and α_4 are the outflow coefficients of the tanks; L_1, L_2, L_3 and L_4 are the heights of the outflow holes of the tanks; β_1, β_2 and β_3 are the penetration volumes of the tanks; R is the cumulative hourly rainfall, t is current time and Δt is time step and in this case, it is 60 minutes. For the early warning of debris flows and slope failures, JMA uses a threshold line as a criterion for the relationship between 60-minute cumulative rainfall and Soil-water index. The concept of the early warning system currently adopted in Japan (Osanai et al. 2010) is given in Figure 5.2. The applicability of these criteria for the slope failures induced in seasonal cold regions due to the various influencing factors as discussed in this study should be verified.

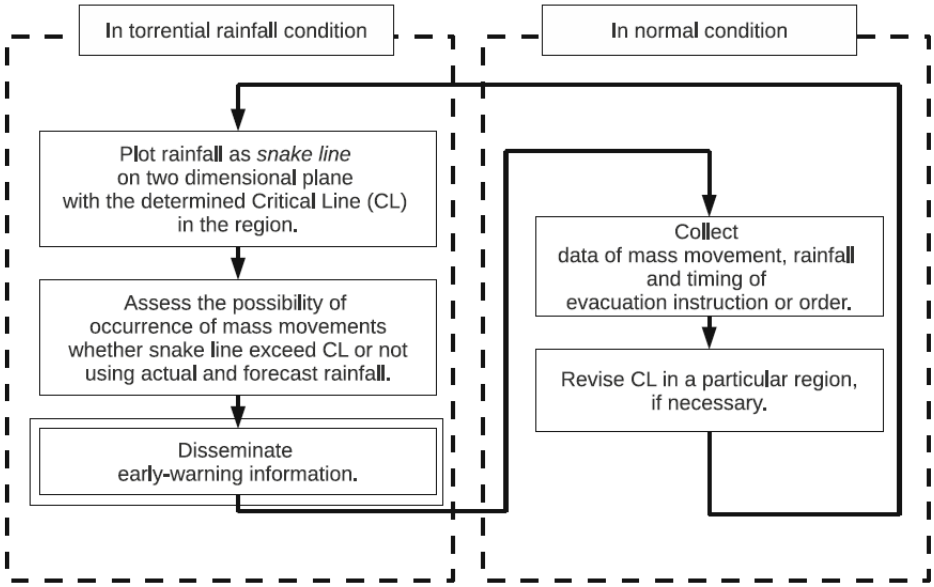

Figure 5.2 Basic concept of the currently operating Japanese early-warning system (after Osanai et al. 2010)

5.1.2 Effective rainfall index

The effective rainfall index is calculated based on the below given method. In the conventional method given by Yano (1990), two half-lives i.e. 1.5 hours and 24 hours were used. The effective rain is then calculated as follows,

$$ER = \left[\left(\sum \alpha_{1i} \right) \times R_{1i} \right] \quad \textbf{(5.8)}$$

ER= Effective rainfall (mm), $\alpha_{1i} = 0.5^{i/T}$ the reduction coefficient i hours beforehand, R_{1i} = current 1-hour rainfall amount (mm/hr.) and T = half-life.

There are various half-life periods determined i.e. 1.5 hours, 6 hours, 24 hours and 72 hours. Sudden heavy rainfall exceeding 30 mm/hr. rate will result in shallow and surface erosion type slope failures which can be predicted using effective rainfall with half-lives 1.5 hours and 6 hours or 24 hours. Large slope failures like deep seated landslides, which result from continuous surface infiltration due to small to medium amount of rainfall (0 - 30 mm/hr.) can be predicted using 72 hr. half-life. Matsuura et al. (2013) have suggested the use of 72 hours half-life along with 1.5 hours half-life, so that the slow infiltration process of snowmelt water can be accounted. The critical line (CL) for this effective rainfall index is determined based on the occurrence of small to large scale sediment disasters observed in a mountain area at Busuno, Japan during the

snowmelt seasons (Matsuura et al. 2013). The effective rainfall of a 72 hours half-life time on the X-axis and effective rainfall of 1.5 hours on the Y-axis are used as the standard rainfall indexes in this study with reference to Matsuura et al. (2013).

5.1.3 Accumulative rainfall index

The accumulative rainfall index criterion is used by NEXCO (2009) for monitoring real time slope failures. The relationship between the 1 hour rain and continuous rainfall is plotted in a two-dimensional plane and the occurrence of disasters are studied accordingly. Accumulated rainfall is plotted in X-axis and 1 hour rainfall is plotted in Y-axis. Anyhow the accumulative rainfall index is given here just to show its relative reliability comparing to the ER and SWI.

5.2 Review of studies concerned to the early warnings in cold regions

In seasonal cold regions, the climate effects i.e. freeze-thaw action and snowmelt water infiltration affect the moisture content of the soil (Ishikawa et al. 2015). The snowmelt water infiltrated into the soil ground through a long period results in large amount of surface water and may trigger landslides and debris flows (Nakatsugawa et al. 2015). The stability of soil slopes in seasonal cold regions are more sensitive to the amount of snowmelt water and ignoring the effect of snowmelt may not properly judge the stability (Siva Subramanian et al. 2017). Many studies have been done to standardise an early warning criterion to predict the oncoming slope disasters in snowy cold regions by using metrological data i.e. rainfall and snowmelt water etc. (Okimura and Ichikawa, 1985, Berris and Harr 1987, Singh et al. 1997, Williams et al. 1999, Matsuura 1998, Matsuura 2000, Matsuura et al. 2005, Matsuura et al. 2008, Matsuura et al. 2013 and Nakatsugawa et al. 2015). According to many of the above-mentioned studies, the Japanese early warning criteria i.e. Soil-water index (SWI) and Effective rainfall index etc. need to be revised for the prediction of slope failures in seasonally cold regions. These criteria do not consider the soil water content supplied from the snowmelt. Compared to the hourly rate of rainfall precipitations, the hourly rate of snowmelt water is relatively very small. Instead, the snowmelt process is continuous during thawing season resulting in a continuous supply of water to the soil surface. As the cumulative amount of snowmelt water is large and its effects on soil instabilities are higher, the above-mentioned criteria fail to predict the oncoming soil slope failures and debris flows due to the larger pre-determined rainfall threshold values (Ishida et al. 2000). For these reasons, a method to quantify the hourly rate of snowmelt is necessary so that it can be incorporated in these early warning criteria. Based on this background, a criterion which

can be used for the early warning of soil slope failures and debris flow disasters is proposed in this study. Two case studies of soil slope failures occurred in Hokkaido are studied. The applicability of the existing early warning systems is studied by applying those criteria to the case studies. An empirical method to estimate the hourly snowmelt rate is presented. A new early warning criterion to predict the snowmelt induced soil slope failures in seasonal cold regions is introduced. The applicability and validity of the new criterion is examined through detailed parametric numerical simulation studies.

5.3 Applicability of early warning systems to the case examples

60-minute cumulative rainfall and Soil Water Index relationships (SWI) for the soil slope failure occurred on April 2013 along National Highway Route 230 is calculated and shown in Figure 5.3. Calculated 60-minute cumulative rainfall and SWI are based on the method given by Okada (2005). The CL for each region in Japan is determined based on the occurrences and non-occurrences of sediment disasters corresponding to a value of 60-minute rainfall and Soil Water Index (Osanai et al. 2010). Critical Line (CL) designated for Hokkaido is referred from Nakatsugawa et al. (2015).

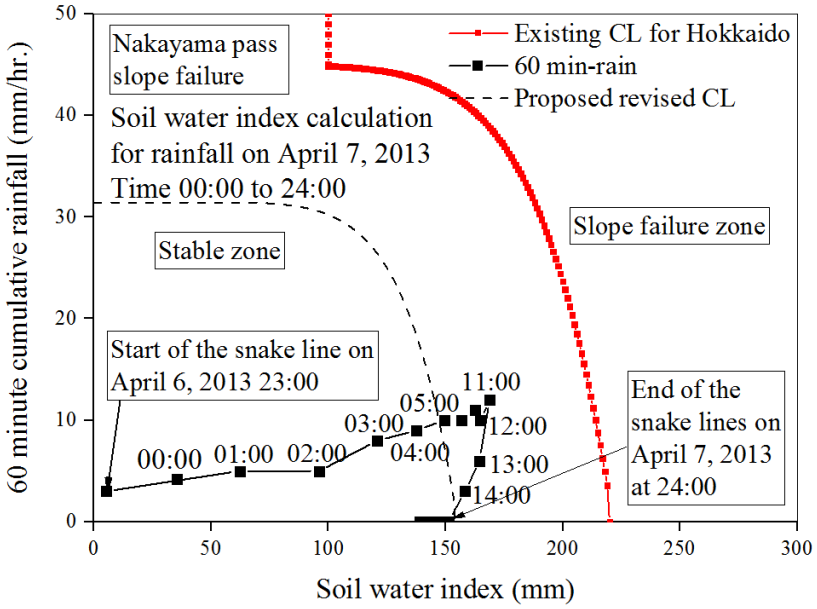

Figure 5.3 60-minute cumulative rainfall and Soil Water Index relationships (SWI) for Slope failure on April 2013 along National Highway Route 230

As the CL is determined only based on the occurrence of disasters induced by rainfall, it could not consider the long-term snowmelt water infiltration and cannot be used to predict the

snowmelt induced slope failures. Iwakura et al. (2010) attempted to define a new CL by reducing the threshold values of 60-minute rainfall and Soil Water Index. Further, there is no slope failure predicted as shown in Figure 6. Snake lines are much below than the CL. The reasons could be due to the negligence of snowmelt water and the threshold level is much higher. It is very clear that a new CL for SWI would be necessary. On the other hand, 60-minute cumulative rainfall and Soil Water Index relationships (SWI) for the climate data collected from Nissho pass, Karikachi pass and Nozuka telemetries are calculated as shown in Figure 5.4. The timeframe is set as April 1, 2016 up to August 31, 2016 to visualise at what occasions the CL is exceeded and to validate it against the actual slope failure data.

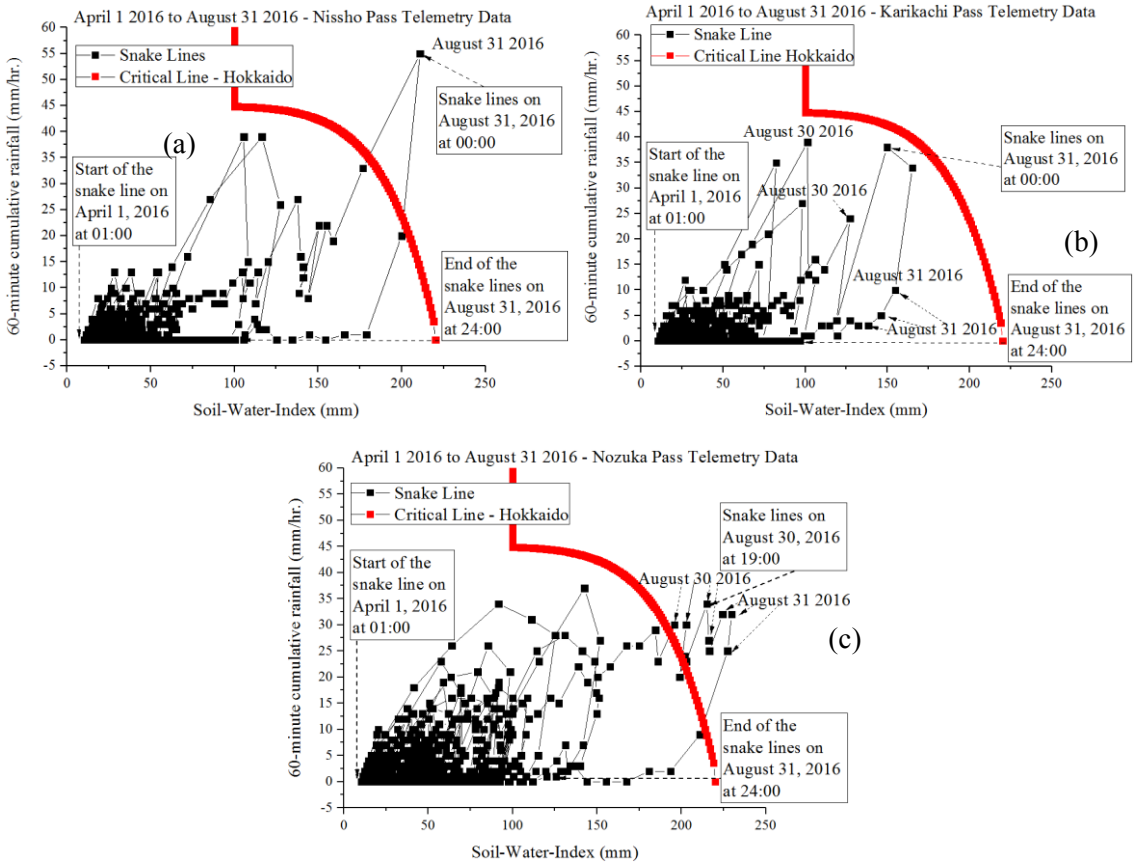

Figure 5.4 60-minute cumulative rainfall and Soil Water Index relationships (SWI) for data collected from (a) Nissho pass, (b) Karikachi pass and (c) Nozuka pass telemetries

For the sediment disasters induced by the Typhoon during August 2016, the occurrences are predicted and the snake lines exceeds the CL for location Nissho pass and Nozuka pass telemetries. Whereas for the Karikachi pass, the CL is not exceeded. Similar cases in which the threshold for SWI is higher were met during the 2016 typhoon on prefectures like Nara and

Wakayama. JMA proposed lowering the threshold values up to 50 % to 80 % for these places (JMA, 2016). On an average, the threshold level could be considered applicable to predict such large amount of rainfall disasters in Hokkaido. From this observation, it is very clear that the 60-minute cumulative rainfall and Soil-Water-Index relationships are applicable for the prediction of large sediments disasters induced by heavy rainfall and may not predict the slope failures induced by snowmelt water. The existing threshold level designated for Hokkaido is not applicable and not realistic for the prediction of snowmelt induced soil slope failures.

The ER index is applied to the Nakayama pass slope failure as shown in Figure 5.5. The slope failure is not predicted as the snake lines are just below the CL. The reason could be the non-consideration of snowmelt water. Even if the half-life of the ER is changed to either 6 hours or 24 hours instead the 72 hours, the slope failure is still not predicted.

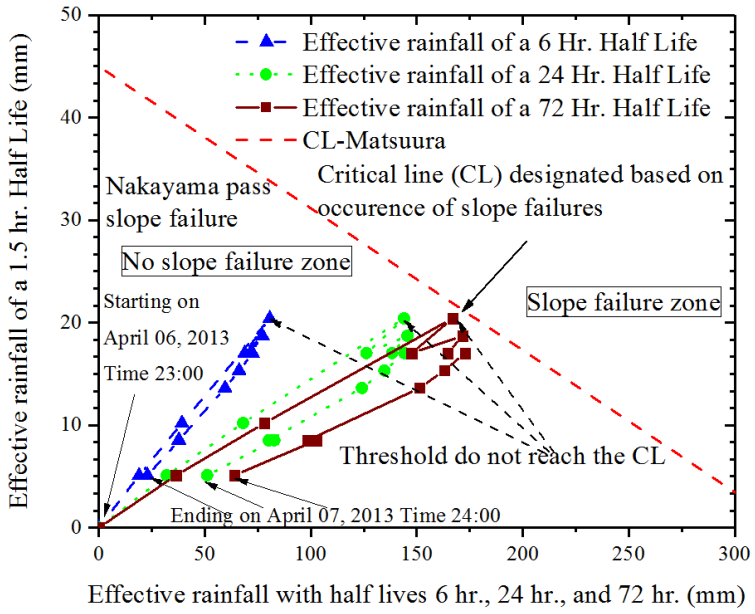

Figure 5.5 Plot of Effective rainfall index with half-life 1.5 hours (y axis) and half-lives 6 Hours, 24 Hours and 72 hours in (x axis) for the case of Nakayama pass slope failure.

The ER based on 1.5 hours and 72 hours half-lives are calculated for the climate data obtained from Nissho, Karikachi and Nozuka pass telemetries and as shown in Figure 5.6 (a), (b) and (c). It could be seen from Figure 5.6 that for all the cases of climate data sets recorded for the typhoon rainfall, the criteria are applicable and many occurrences of sediments disasters are predicted. For the case of Nissho pass telemetry and Nozuka pass telemetry data, the CL is exceeded on August 23, 2016 and July 28, 2016 respectively, though there are no slope failures

recorded at that time. Since the CL threshold set by Matsuura et al. (2013) is small compared with the CL set for rainfall induced slope failures i.e. Yano (1990), Senoo et al. (2001) and Tereda and Nakaya (2001), the line can be exceeded with considerable amount of rainfall. At any case the CL set by Matsuura et al. (2013) is also on the safer side. In this aspect, it may be necessary to establish a different CL for rainfall induced slope failures in cold regions. Tereda and Nakaya (2001) have established some guidelines to set CL for rainfall induced slope failures using 1.5 hr. and 72 hr. half-lives. In their research, they superimpose the Y axis with 1.5 hr. half-life of ER instead 1 hr. half-life and keep the X axis 72 hr. half-life and validated the CL threshold against actual slope failure cases. Following the guideline by Tereda and Nakaya (2001), in this study four different CLs proposed by Yano (1990), i.e. CL1, CL2, CL3 and CL4 shown in Figure 5.6 have been used. Of those 4 CLs, Yano (1990) recommends the use of CL3 for the Nikko area in Tochigi prefecture. To check the appropriateness of the CLs proposed by Yano (1990), in this study all the 4 CLs are used for the cases of rainfall induced slope failures. It could be seen that the CLs lines set by Yano (1990) delineates the slope failure for the Typhoon 10 more clearly. According to the research by Senoo et al. (2001), the standard CL for effective rainfall index for rainfall induced disasters varies significantly based on the area. Senoo et al. (2001) have analysed the difference in CL among areas i.e. Fukushima, Sado and Kochi. In this aspect, the CLs proposed by Yano (1990) for Nikko area in Tochigi prefecture should be validated for its use in Hokkaido prefecture.

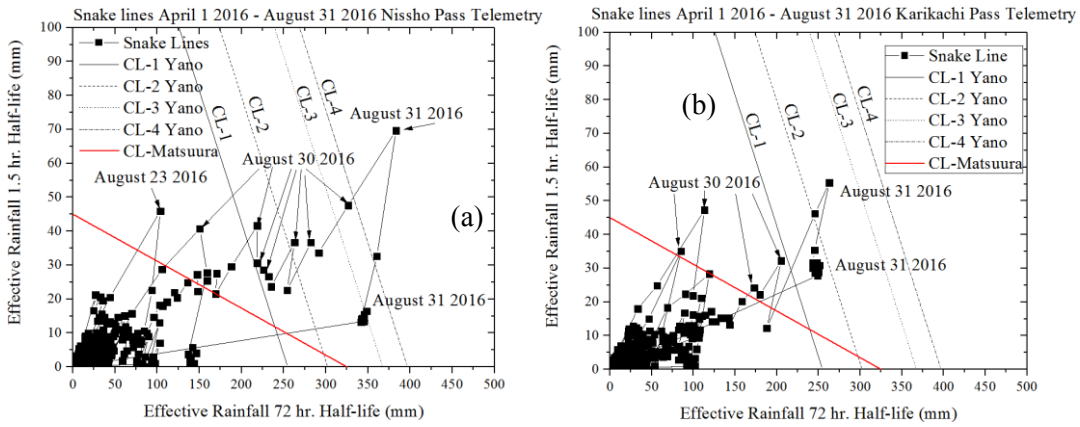

(c)

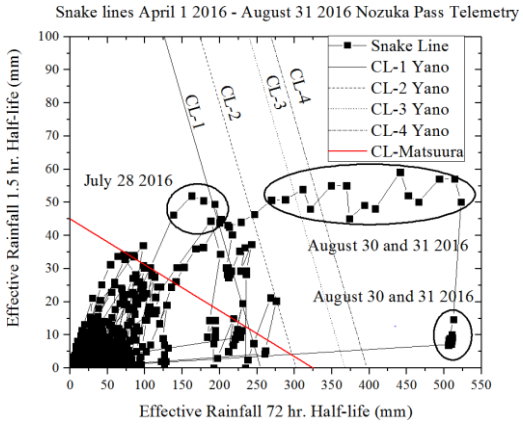

Figure 5.6 Snake lines plotted for the data recorded from (a) Nissho Pass, (b) Karikachi Pass and (c) Nozuka Pass Telemetries

From these observations, it is very clear that different CLs are required for both SWI and ER to predict the snowmelt induced slope failures. In general, rather than the threshold level for the SWI, the threshold level designated for the ER seems to be applicable for both rainfall and snowmelt induced soil slope failures since there are different CLs available for both the cases. For the case study of Nakayama pass slope failure, the disaster is not predicted from both the criteria SWI and ER. The major reason could be due to the negligence of snowmelt water. It is very clear that a proper estimation of snowmelt water is required for the precise prediction of snowmelt induced soil slope failures in seasonal cold regions.

5.4 Snowmelt simulation

The estimation of hourly rate of snowmelt is necessary for early warnings. Use of many energy balance methods are common in practice (Berris and Harr, 1987; Kondo and Yamazaki, 1990). In this study a simple yet reliable estimation method of the snowmelt water is introduced which considers almost all the physical processes included in the melting process of snow (Riley et al. 1969). The method could be termed as an analytical method. The key influencing climatic factors are considered i.e. air temperature, snow surface temperature, melt factor etc. Climate data obtained from the Automatic Meteorological Data Acquisition System (AMeDAS) (JMA) is used for the estimations. For the estimation of snowmelt water from the meteorological data, a method is employed considering the physical process of snowmelt (Riley et al. 1969, Motoyama, 1990) as given below,

$$SM = 0.4 \times SD \times RI \times (T_a - T_{st}) \times (1\text{-}Al) + \left[(T_a - T_{st}) \times \frac{P}{144} \right] \quad \textbf{(5.9)}$$

where *SM* = Snowmelt (mm/hr.), T_a = air temperature (°C), T_{st} = snow freezing temperature (°C). The snowmelt is determined based on the air temperature as (Riley et al. 1969), *SD* = Snow Depth (mm), *RI* = Radiation Index (%), *Al* = Albedo (%), *P* = Precipitation (mm/hr.).

The model adopted for the estimation of snowmelt water is calculated using Equation 5.9 and the concept is shown in Figure 5.7. As shown in the figure the model considers the snow density, melt factor and liquid water holding capacity of snowpack etc. explicitly. The snowmelt model is used to estimate the amount of snowmelt water for the case of Nakayama pass slope failure. The results are shown in Figure 5.8 (b) and (c). A total of 31 mm snowmelt water is estimated on April 07, 2013 using the model. Hokkaido regional development bureau (mentioned as MLIT in Figure 2.8) estimated the cumulative snowmelt water on April 07, 2013 to be 31 mm. The total cumulative snowmelt water estimated using the model matches with the estimation of MLIT. On the other hand, to validate the snowmelt model, a comparison of the estimated snow depth to the measured snow depth data for the Nakayama pass slope failure starting from 01-11-2012 to 07-04-2013 is made as shown in Figure 5.8 (b). The estimated results from the snowmelt model also match well with the measured results. From these observations, the snowmelt model may be reliable to estimate the hourly snowmelt water.

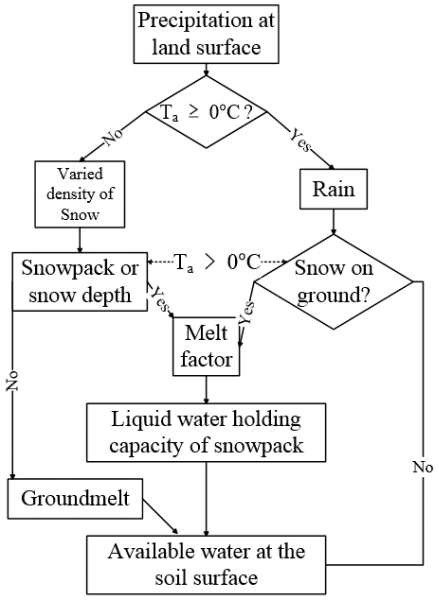

Figure 5.7 Model to estimate the hourly snowmelt water

In this study the snow surface albedo is considered as a function of air temperature (Tooming, 1996). Snow surface albedo (α) cannot be neglected in the estimation of net radiation over a

snowpack (Petzold, 1974) and thus it is a parameter necessary for the successful calculation of the surface heat exchange and melt rates of a snowpack (Price, 1977; Taylor-Alt, 1975). Petzold (1974) has also shown that a snow surface can exhibit a high day to day variability in which is a sharp contrast to that of a naturally vegetated surface. So, the hourly variation of snow surface albedo should be considered for proper prediction of hourly snowmelt. Further for simplification purpose, the changes in surface albedo and air temperature have been studied using the relationship given by global energy balance models (Warren and Schneider 1979).

$$Q(1-\alpha) = I_R + O_R T_a \tag{5.10}$$

Q = radiant energy flux over snow surface (W/m^2), a = snow surface albedo, I_R = incoming solar radiation (W/m^2), O_R = outgoing solar radiation (W/m^2 •°C). T_a = temperature of air (°C). The radiant energy flux over the snow surface is now a function of albedo. Albedo is expressed as a function of air temperature as,

$$\alpha = 0.80 \because T_a \le 0°C \tag{5.11}$$

$$\alpha = 0.40 + 0.40\left(\frac{10 - T_a}{40}\right) \because T_a \le 0 - 10°C \tag{5.12}$$

The solar radiation index of snow is a function of snow surface albedo. Here the snow surface albedo is a function of air temperature. The radiation index RI, is defined as the ratio of incoming and outgoing radiant energy fluxes from the snow surface. Riley et al. (1969) suggest a value of 1.09 (60/55) for the ratio between incoming and outgoing radiant energy fluxes from the snow surface during snowmelt seasons March, April and May. Here, the RI is calculated as a function of snow surface albedo as follows Petzold (1974).

$$RI = \frac{I_R}{O_R} \times \alpha \tag{5.13}$$

By this way the Albedo and RI are calculated as a function of air temperature in this study. These calculations may have some limitations over the percentage of preciseness. Anyhow, for a purpose of accounting the contribution of radiation energy in the melt process the above-mentioned way is deemed acceptable.

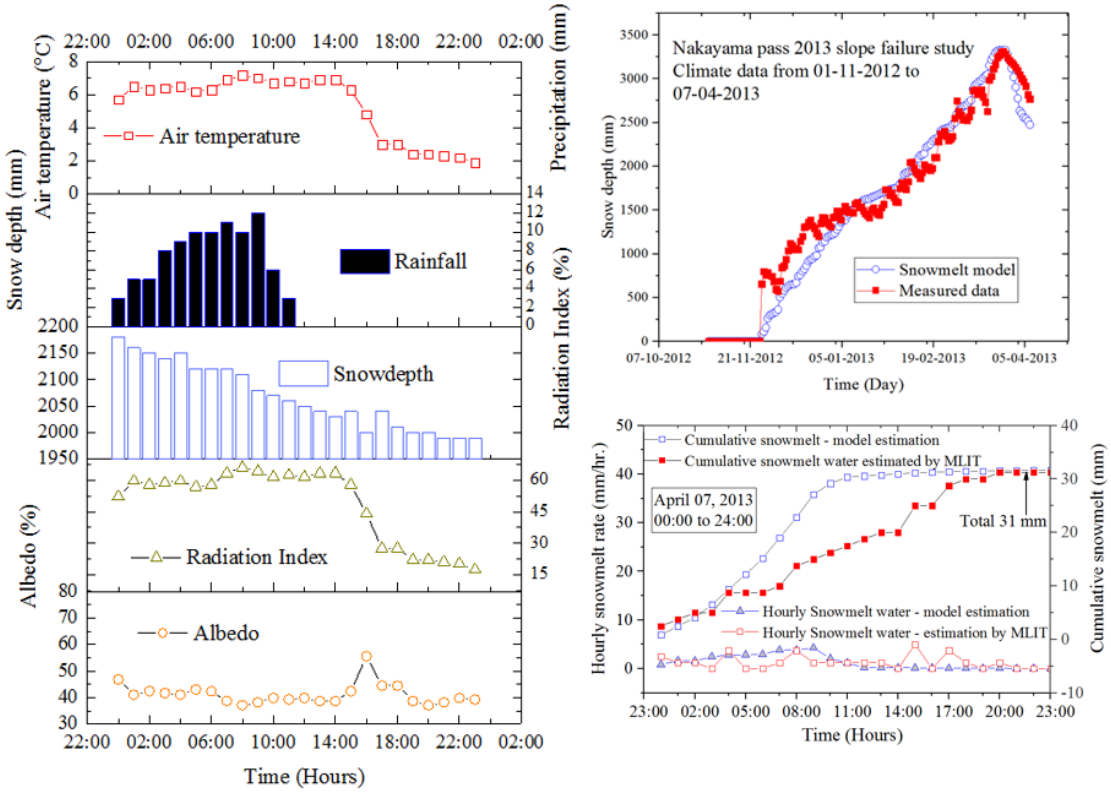

Figure 5.8 Estimation of snowmelt water using snowmelt model (a) climate data for Nakayama pass slope failure on 07-04-2013, (b) comparison of estimated and measured change in snow depth and (c) comparison of estimated snowmelt water on April 07, 2013.

5.5 Parametric studies of soil slope failures under different magnitudes of rainfall and snowmelt water

For the revisions/proposal of early warning criteria, many numbers of soil slope failures should be examined to check the appropriateness and applicability. On the other hand, it is time consuming and cumbersome to collect data and study in detail many slope failure case examples. In consideration to these aspects, many conceptual soil slope failures are studied using numerical simulations based on a recommended slope stability assessment approach. The applicability and validity of the numerical simulation method is detailly examined by Siva Subramanian et al. (2017) and in Chapter 4. In this study, an embankment slope model made up of a volcanic soil is chosen for the parametric studies due to the fact that volcanic soils are spread all over Japan and especially in Hokkaido 40 % of the surface is occupied by various types of volcanic soils. The soil material properties considered are same as the previous study. In the previous study (Chapter 4), the simulation was performed for a duration of 373 days

starting from November 9, 2012 to October 17, 2013. Further details about the embankment slope and its numerical simulations can be found from Matsumura (2014), Kawamura et al. (2016) and Siva Subramanian et al. (2015). In this study, the numerical analyses were done with different initial water content distributions chosen from different time. Those cases are as listed in Table 2. The slope geometry and boundary conditions are shown in Figure 5.9.

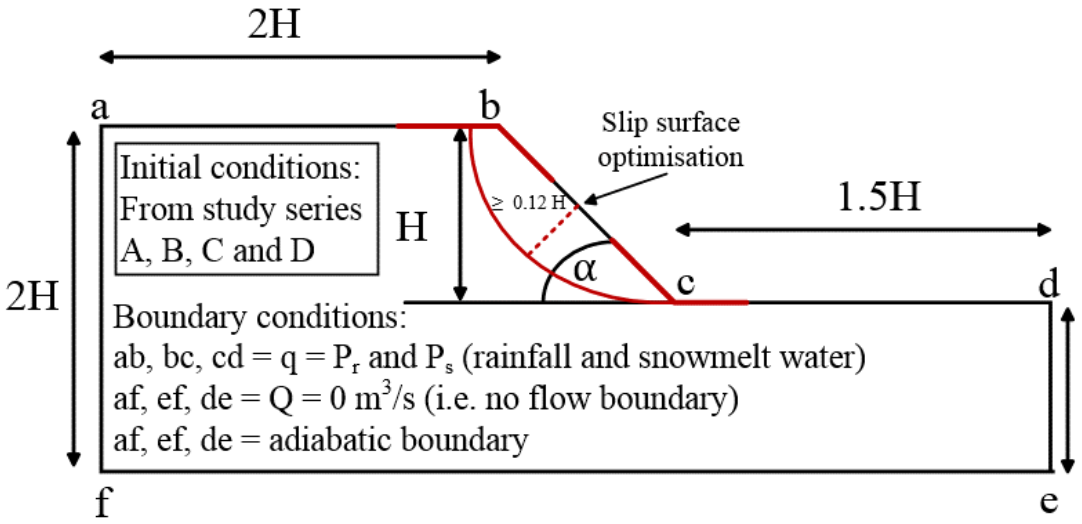

Figure 5.9 Slope geometry and boundary conditions for homogeneous soil slope used in parametric studies

Initial volumetric water content distributions and temperature distributions for the parametric studies are shown in Figure 5.10 and Figure 5.11 respectively.

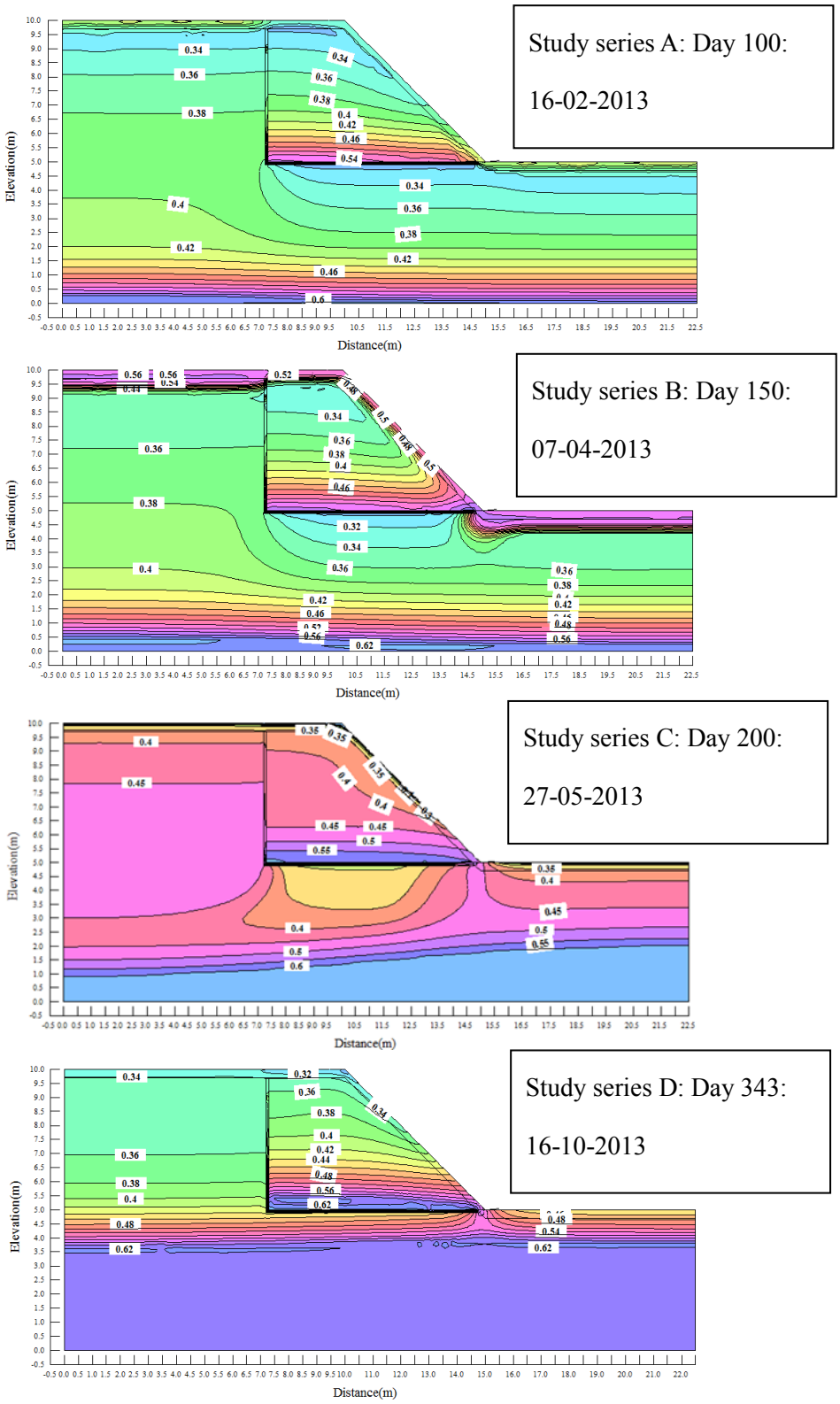

Figure 5.10 Initial volumetric water content (m^3/m^3) distributions during four different seasons

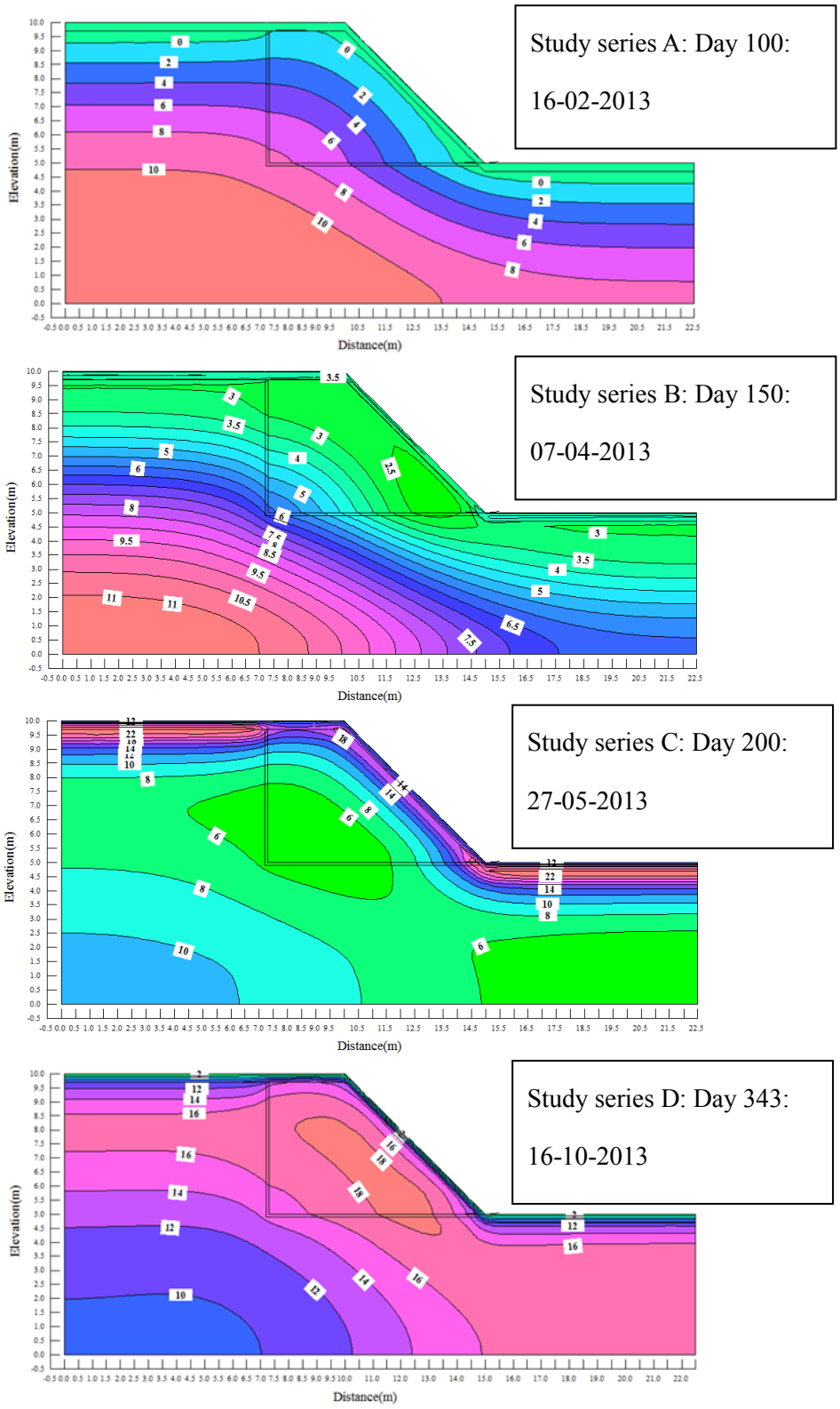

Figure 5.11 Initial temperature (°C) distributions during four different seasons

The primary variables considered in the parametric study are the initial water content distribution chosen from day 100, 150, 200 and 343 and termed as Series A, B, C and D respectively. The slope height (H), the slope angle (α), different rainfall (P_r) and snowmelt rates (P_s) considered are summarised in Table 5.1 and Table 5.2. Different combinations of rainfall and snowmelt water are applied as given below.

- Long-term rainfall with low 60-minute rainfall amount with and without snowmelt water
- Short-term rainfall with high 60-minute rainfall amount with and without snowmelt water
- Long-term and short-term rainfall with slow snowmelt rate and rapid snowmelt rate

The following conditions are adopted as shown in Table 5.2.

- For long term rainfall, the duration is considered as 24 hours. The amount of rainfall is considered as 10 mm/hr.
- For short term rainfall, the duration is considered as 6 hours. The rainfall amount is considered as 30 mm/hr.
- Two different snowmelt rates are considered 4 mm/hr. (slow snowmelt rate) and 15 mm/hr. (rapid snowmelt rate) in consideration to some extensive field studies (Matsuura, 1998).
- The duration of the snowmelt is considered as 24 hours in which the snowmelt is assumed to be a sinusoidal function. At 12:00 noon the snowmelt rate is at the maximum.

Table 5.1 Analytical conditions and summary of combination of factors and independent variables used in parametric studies

Study Series	Slope angle α (°)	Slope heights H (m)	Rainfall rate P (mm/hr.) and duration	Snowmelt rate P (mm/hr.)
A, B, C and D	30, 35, 40 and 45	5, 10, 15 and 20	(a) 10 (24 hours) (b) 30 (00:00 ~ 06:00) (c) 30 (06:00 ~ 12:00) (d) 30 (12:00 ~ 18:00) (e) 30 (18:00 ~ 24:00)	(i) 0, (ii) 0~4 and (iii) 0~15

4 Initial water content distributions, 4 slope angles, 4 slope heights, 5 rainfall rates and 3 snowmelt water rates = 4×4×4×5×3 = 960 numerical simulations

Table 5.2 Different combinations of rainfall (P_r) and snowmelt rates (P_s) considered.

S. No	Rainfall amount (mm/hr.)	Duration	Type
1	10	24 hours	Continuous
2	30	6 hours	Continuous
S. No	**Snowmelt rate (mm/hr.)**	**Duration**	**Type**
1	0 ~ 4	24 hours	Sinusoidal (Max. at 12:00)
2	0 ~ 15	24 hours	Sinusoidal (Max. at 12:00)

As found from the previous studies (Ishikawa et al. 2015 and Nakatsugawa et al. 2015) the macro factor that influence the soil slope stability in snowy cold regions are the amount of rainfall and snowmelt water. Various magnitudes of rainfall and snowmelt water are considered under different influential conditions and the stability scenarios are studied. Different slope angles were considered, 30˚, 35˚, 40˚ and 45˚ with different slope heights 5 m, 10 m, 15 m and 20 m as shown in Table 5.2. Table 5.2 also shows the summary of analytical conditions of selected slope models with different slope angles. The different infiltration boundary conditions are shown in Table 4. The series are named as A, B, C and D based on the initial conditions. The rainfall boundary conditions are named as a, b, c, d and e with the snowmelt rates as (i), (ii) and (iii) respectively. The stability is evaluated using limit equilibrium method as explained in Chapter 3. For these numerical simulations, the search of the slip surface has been limited to circular shape with a range of slip surface depth ≥ 0.12 H (H = slope height) per shallow to deep seated slope failures (see Figure 5.9). Surface erosion type failures are not considered. In order to filter the factor of safety values with minimum slip surfaces 0.12 H, a limit has been specified in the slip surface search routine. Only the slip surfaces with a factor of safety less than 1 and a slip depth of minimum 0.6 m are considered as valid slope failures. All the failure cases found are subjected to this condition. A total number of 960 numerical simulations were performed, of those 512 numbers of slope failures and 448 numbers of stable scenarios were obtained. These stable and failure scenarios are used for the revision and proposal of early warning criteria as discussed in section 5.6. The results of all the 960 numerical slope failure cases for each series are summarised in Tables 5.3, 5.4, 5.5 and 5.6 for series A, B, C and D respectively.

Table 5.3 Results of numerical simulations showing stable and failure cases for series A.

Series	Slope height (m)	Slope angle (°)	Boundary conditions														
			a(i)	a(ii)	a(iii)	b(i)	b(ii)	b(iii)	c(i)	c(ii)	c(iii)	d(i)	d(ii)	d(iii)	e(i)	e(ii)	e(iii)
A	5	30	×	×	×	×	×	×	×	×	×	×	×	×	×	×	×
A	5	35	×	×	×	×	×	×	×	×	×	×	×	×	×	×	×
A	5	40	×	×	×	×	×	×	×	×	×	×	×	×	×	×	×
A	5	45	×	×	×	×	×	×	×	×	×	×	×	×	×	×	×
A	10	30	×	×	×	×	×	×	×	×	×	×	×	×	×	×	×
A	10	35	×	×	×	×	×	×	×	×	×	×	×	×	×	×	×
A	10	40	×	×	×	×	×	×	×	×	×	×	×	×	×	×	×
A	10	45	×	×	×	×	×	×	×	×	×	×	×	×	×	×	×
A	15	30	×	×	×	×	×	×	×	×	×	×	×	×	×	×	×
A	15	35	×	×	×	×	×	×	×	×	×	×	×	×	×	×	×
A	15	40	×	×	×	×	×	×	×	×	×	×	×	×	×	×	×
A	15	45	×	×	×	×	×	×	×	×	×	×	×	×	×	×	×
A	20	30	×	×	×	×	×	×	×	×	×	×	×	×	×	×	×
A	20	35	×	×	×	×	×	×	×	×	×	×	×	×	×	×	×
A	20	40	×	×	×	×	×	×	×	×	×	×	×	×	×	×	×
A	20	45	×	×	×	×	×	×	×	×	×	×	×	×	×	×	×

× - no slope failure; O – slope failure; Number of slope failures = 0

Table 5.4. Results of numerical simulations showing stable and failure cases for series B.

Series	Slope height (m)	Slope angle (°)	Boundary conditions														
			a(i)	a(ii)	a(iii)	b(i)	b(ii)	b(iii)	c(i)	c(ii)	c(iii)	d(i)	d(ii)	d(iii)	e(i)	e(ii)	e(iii)
B	5	30	×	O	O	O	O	O	O	O	O	O	O	O	O	O	O
B	5	35	×	O	O	O	O	O	O	O	O	O	O	O	O	O	O
B	5	40	×	O	O	O	O	O	O	O	O	O	O	O	O	O	O
B	5	45	×	O	O	O	O	O	O	O	O	O	O	O	O	O	O
B	10	30	×	O	O	O	O	O	O	O	O	O	O	O	O	O	O
B	10	35	×	O	O	O	O	O	O	O	O	O	O	O	O	O	O
B	10	40	×	O	O	O	O	O	O	O	O	O	O	O	O	O	O
B	10	45	×	O	O	O	O	O	O	O	O	O	O	O	O	O	O
B	15	30	×	O	O	O	O	O	O	O	O	O	O	O	O	O	O
B	15	35	×	O	O	O	O	O	O	O	O	O	O	O	O	O	O
B	15	40	×	O	O	O	O	O	O	O	O	O	O	O	O	O	O
B	15	45	×	O	O	O	O	O	O	O	O	O	O	O	O	O	O
B	20	30	×	O	O	O	O	O	O	O	O	O	O	O	O	O	O
B	20	35	×	O	O	O	O	O	O	O	O	O	O	O	O	O	O
B	20	40	×	O	O	O	O	O	O	O	O	O	O	O	O	O	O
B	20	45	×	O	O	O	O	O	O	O	O	O	O	O	O	O	O

× - no slope failure; O – slope failure; Number of slope failures = 224; Number of stable cases = 16

Table 5.5. Results of numerical simulations showing stable and failure cases for series C.

Series	Slope height (m)	Slope angle (°)	Boundary conditions														
			a(i)	a(ii)	a(iii)	b(i)	b(ii)	b(iii)	c(i)	c(ii)	c(iii)	d(i)	d(ii)	d(iii)	e(i)	e(ii)	e(iii)
C	5	30	×	O	O	O	O	O	O	O	O	O	O	O	O	O	O
C	5	35	×	O	O	O	O	O	O	O	O	O	O	O	O	O	O
C	5	40	×	O	O	O	O	O	O	O	O	O	O	O	O	O	O
C	5	45	×	O	O	O	O	O	O	O	O	O	O	O	O	O	O
C	10	30	×	O	O	O	O	O	O	O	O	O	O	O	O	O	O
C	10	35	×	O	O	O	O	O	O	O	O	O	O	O	O	O	O
C	10	40	×	O	O	O	O	O	O	O	O	O	O	O	O	O	O
C	10	45	×	O	O	O	O	O	O	O	O	O	O	O	O	O	O
C	15	30	×	O	O	O	O	O	O	O	O	O	O	O	O	O	O
C	15	35	×	O	O	O	O	O	O	O	O	O	O	O	O	O	O
C	15	40	×	O	O	O	O	O	O	O	O	O	O	O	O	O	O
C	15	45	×	O	O	O	O	O	O	O	O	O	O	O	O	O	O
C	20	30	×	O	O	O	O	O	O	O	O	O	O	O	O	O	O
C	20	35	×	O	O	O	O	O	O	O	O	O	O	O	O	O	O
C	20	40	×	O	O	O	O	O	O	O	O	O	O	O	O	O	O
C	20	45	×	O	O	O	O	O	O	O	O	O	O	O	O	O	O

× - no slope failure; O – slope failure; Number of slope failures = 224; Number of stable cases = 16

Table 5.6. Results of numerical simulations showing stable and failure cases for series D.

Series	Slope height (m)	Slope angle (°)	Boundary conditions														
			a(i)	a(ii)	a(iii)	b(i)	b(ii)	b(iii)	c(i)	c(ii)	c(iii)	d(i)	d(ii)	d(iii)	e(i)	e(ii)	e(iii)
D	5	30	×	×	×	×	×	O	×	×	O	×	×	O	×	×	O
D	5	35	×	×	×	×	×	O	×	×	O	×	×	O	×	×	O
D	5	40	×	×	×	×	×	O	×	×	O	×	×	O	×	×	O
D	5	45	×	×	×	×	×	O	×	×	O	×	×	O	×	×	O
D	10	30	×	×	×	×	×	O	×	×	O	×	×	O	×	×	O
D	10	35	×	×	×	×	×	O	×	×	O	×	×	O	×	×	O
D	10	40	×	×	×	×	×	O	×	×	O	×	×	O	×	×	O
D	10	45	×	×	×	×	×	O	×	×	O	×	×	O	×	×	O
D	15	30	×	×	×	×	×	O	×	×	O	×	×	O	×	×	O
D	15	35	×	×	×	×	×	O	×	×	O	×	×	O	×	×	O
D	15	40	×	×	×	×	×	O	×	×	O	×	×	O	×	×	O
D	15	45	×	×	×	×	×	O	×	×	O	×	×	O	×	×	O
D	20	30	×	×	×	×	×	O	×	×	O	×	×	O	×	×	O
D	20	35	×	×	×	×	×	O	×	×	O	×	×	O	×	×	O
D	20	40	×	×	×	×	×	O	×	×	O	×	×	O	×	×	O
D	20	45	×	×	×	×	×	O	×	×	O	×	×	O	×	×	O

× - no slope failure; O – slope failure; Number of slope failures = 64; Number of stable cases = 176

5.6 Revisions/proposal of new early warning criteria

Possible revisions of the early warning criteria are studied by incorporating the amount of snowmelt water along with rainfall in both the SWI and ER indices. Revisions of the effective rainfall index, 60-minute rainfall and SWI relationships are studied through;

1. Including snowmelt water in ER/SWI calculation
2. Determining/revising the threshold – Critical Line (CL)

The revisions of the early warning are done for the slope failure scenarios observed from the conceptual numerical slope failure cases. From those simulations performed as explained in section 5.5, the failure as well as stable scenarios are classified based on the factor of safety value (FOS). The FOS values lower than 1 are considered as slope failures.

5.7 Proposal of new criteria Effective Precipitation (EP) index

For all the failure and stable scenarios obtained from the simulations, the Effective Precipitation index and Soil Water Index were calculated. The method to calculate the EP index is explained as follows. The slope disasters occur in seasonal cold regions are influenced by the short-term and long-term soil surface infiltration caused by the rainfall and continuous snowmelt process respectively. In this study, a new criterion to predict the snowmelt induced soil slope failures, considering the short-term and long-term soil surface infiltration is proposed. The new criterion Effective Precipitation index (EP) considers the rainfall and snowmelt water by adopting two half-lives namely 1.5-hour half-life and 72-hours half-life and can be calculated as,

$$EP = P_t + \sum \left[P_{t\text{-}n} \times 0.5^{n/T_h} \right] \tag{5.14}$$

where, EP = Effective Precipitation (mm), P_t = the 1-hour precipitation (rainfall and snowmelt water) at the present time (mm/hr.), $P_{t\text{-}n}$ = the precipitation recorded n hours beforehand (mm/hr.) and T_h = the half-life time (hours). The precipitation P_t includes the hourly rainfall as well as the hourly snowmelt water. The proposed criteria EP index is similar to the MR proposed by Matsuura et. al. (2013). Matsuura et al. (2013) considered the snowmelt water in their calculation by setting up monitoring stations in Busuno, Japan. On the other hand, it is never possible to set up monitoring stations all over the targeted area (i.e. Hokkaido). To overcome such intricacy, in this study the hourly snowmelt water is estimated from the

snowmelt estimation method given in section 5.4. If an early warning criteria should be adopted for Hokkaido region, many case examples of slope failures should be studied considering different snowmelt and rainfall rates. Further, Matsuura et al. (2013) have shown only one case of slope failure during snowmelt season and two cases of slope failures during rainy seasons from which it will be difficult to adapt the concept of MR all over Hokkaido. Considering all these aspects in this study a criteria EP index is proposed and validated against many cases of slope failures.

Effective precipitation index 1.5 hours and 72 hours considering snowmelt water is shown in Figure 5.12 for the Nakayama pass slope failure. It could be seen that the criteria successfully predict the slope failure as the snake line exceeding the Critical Line (CL) proposed by Matsuura et al. (2013).

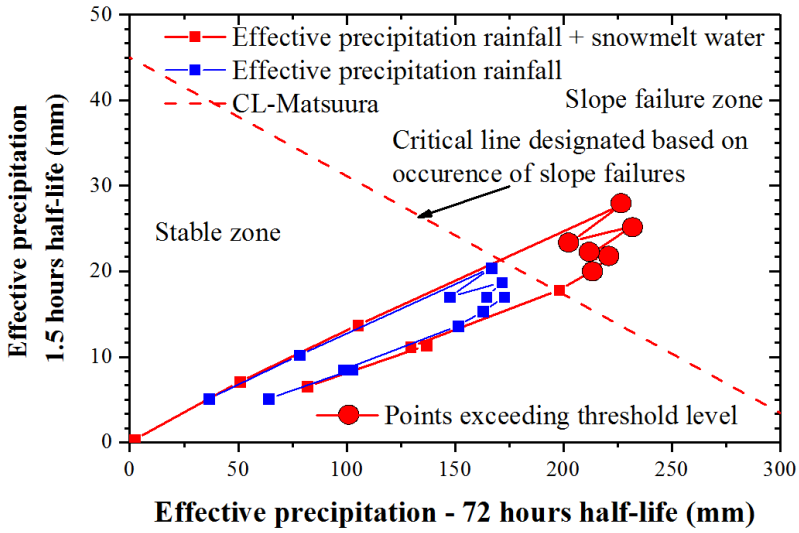

Figure 5.12 Possible revisions of the Effective rainfall index with snowmelt water/ Effective precipitation index

Additionally, the effective precipitations are studied for the numerical parametric studies as shown in Figure 5.13 and Figure 5.14. These two figures are arranged like, in the left the factor of safety (FOS) obtained from the simulations, in the centre EP index and in the right SWI for the corresponding cases. The stability of the slope is inferred from FOS values in the left figures. Then, the middle and right figures are checked whether the criteria predict the slope failure or not. In Figure 17, there are two cases in which slope failure occur. The slope failures occur at times 19:00 for case a(ii) and at 12:00 for case a(iii). For both the cases the EP predicts the slope

failure as the CL is exceeded. In this way, the applicability of the EP and SWI are checked and validated. In other words, it could be described that, once the CL is exceeded there is a danger of slope failure and since the EP value continue to increase with time a failure is observed.

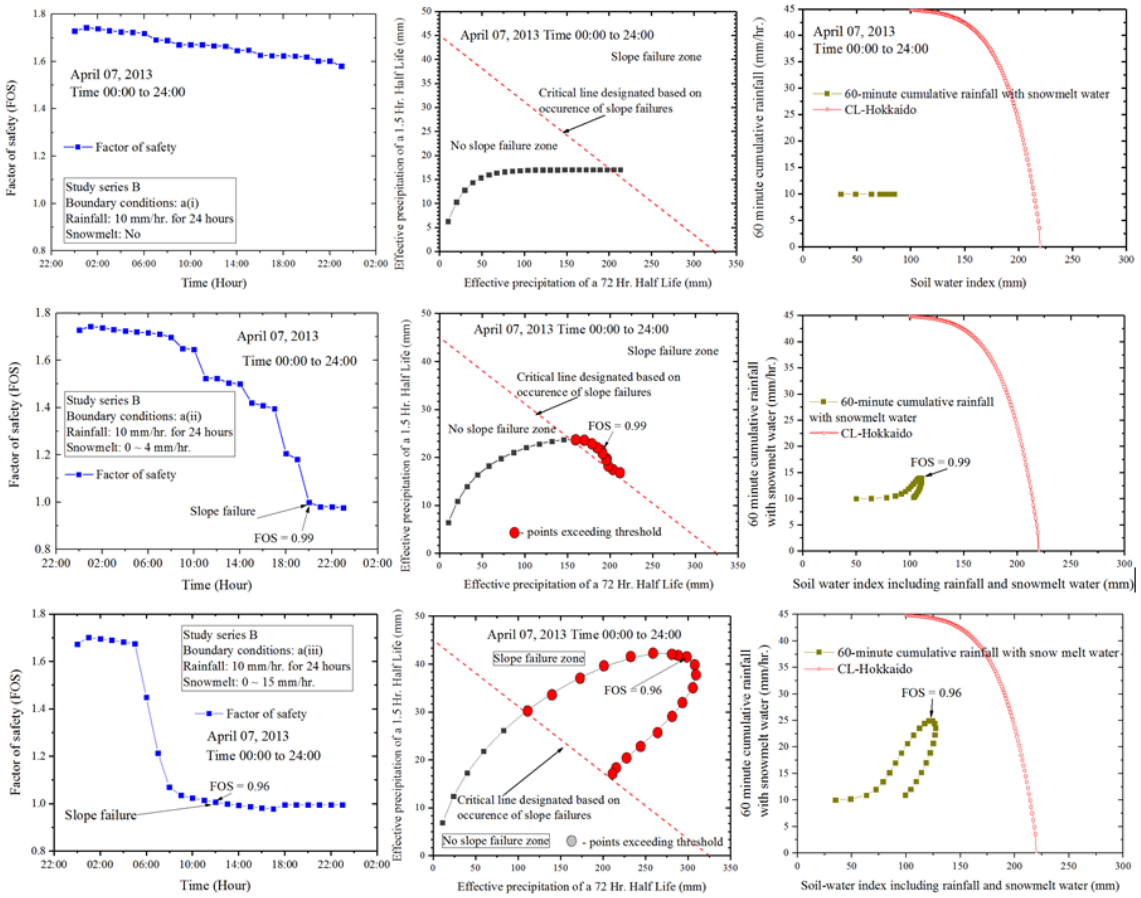

Figure 5.13 Factor of safety, Effective Precipitation index and Soil Water Index for study series B with 45° slope angle, 5 m slope height, 10 mm/hr. rainfall with two different snowmelt rates

The soil slope failures usually will get triggered after some considerable duration of rainfall. Owing to these conditions, the prediction by the EP index would also be considered appropriate. It could be seen that for most of the cases of failures and stable scenarios the criteria perform well for the cases in Figure 5.13 and Figure 5.14. The Effective Precipitation index for half-lives 6 hours and 24 hours were also plotted in Figure 5.15 and Figure 5.16 to compare it with 72 hours effective precipitation. For the case of slope failures in Figure 5.15, the Effective Precipitation with half-lives 6 hours and 24 hours do not predict the slope failure. Table 5.7 shows the number of slope failures and stable cases for each series and the rate of predictions by EP using three different half-lives. The number of slope failures observed in each series A, B, C

and D are 0, 224, 224 and 64 respectively (total 512). It could be seen that for all the slope failures during thawing and after thawing seasons (series B and C), the EP with 72 hours half-life gives 100 % prediction whereas the EP with half-lives 6 hours and 24 hours give 86.66 % of successful predictions.

Table 5.7 Rates of successful predictions (proper identification of the slope failure) using EP index (CL – Matsuura) with different half-lives.

S. No.	Study Series	Slope failures	Stable cases	% of prediction EP (1.5 hr. and 72 hr.)		% of prediction EP (1.5 hr. and 24 hr.)		% of prediction EP (1.5 hr. and 6 hr.)	
				Success	Unsuccessful	Success	Unsuccessful	Success	Unsuccessful
1	A	0	240	-	-	-	-	-	-
2	B	224	16	100 %	0 %	86.66 %	13.33 %	86.66 %	13.33 %
3	C	224	16	100 %	0 %	86.66 %	13.33 %	86.66 %	13.33 %
4	D	64	176	100 %	0 %	100 %	0 %	100 %	0 %

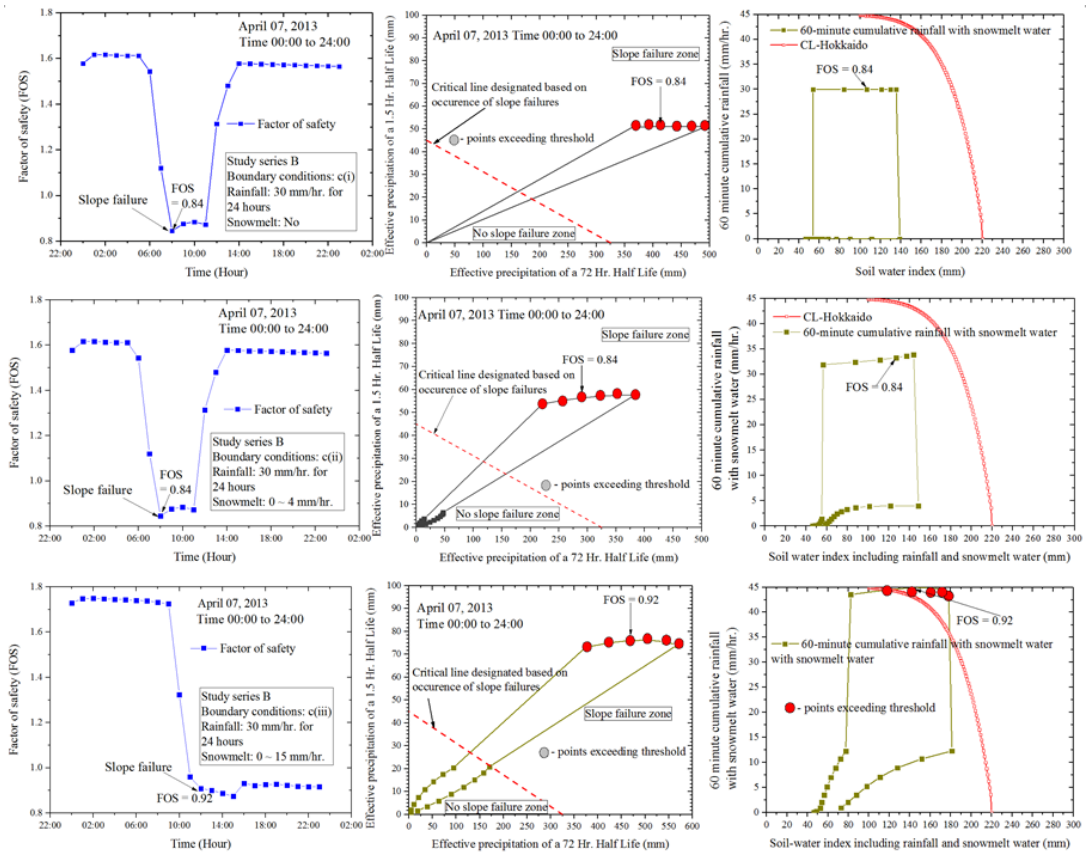

Figure 5.14 Factor of safety, Effective Precipitation index and Soil Water Index with 45° slope angle, 5 m slope height, 30 mm/hr. rainfall with two different snowmelt rates

Only for the case of failures induced by high amount of rainfall and snowmelt water, the slope failure is predicted by 6 hours and 24 hours half-lives as shown in Figure 5.16. In all these situations, the applicability of 72 hours half-life Effective Precipitation was found to be appropriate. From this observation, it could be said that for the prediction and early warning of snowmelt induced soil slope failures, the proposed new criteria with half-lives of 1.5 hours and 72 hours will be helpful. On the other hand, it is noteworthy to discuss the trend of false predictions (stable cases predicted as failures) by the EP index so that the limitations of the criteria can be understood. As shown in Table 5.8, the rate of false predictions is calculated for series A, B, C and D using CL defined by Matsuura et al. (2013) and CL3 defined by Yano (1990). All the slopes were stable in series A (during freezing) and 176 numbers of stable cases were observed in series D (before freezing).

Table 5.8 Rates of false predictions (stable cases identified as slope failures) using EP index reference to CL – Matsuura and CL3 - Yano.

S. No.	Study Series	Slope failures	Stable cases	% of false predictions EP (1.5 hr. and 72 hr.) CL – Matsuura	% of false predictions EP (1.5 hr. and 72 hr.) CL3 - Yano
1	A	0	240	100 %	0 %
2	B	224	16	0 %	0 %
3	C	224	16	0 %	0 %
4	D	64	176	100 %	0 %

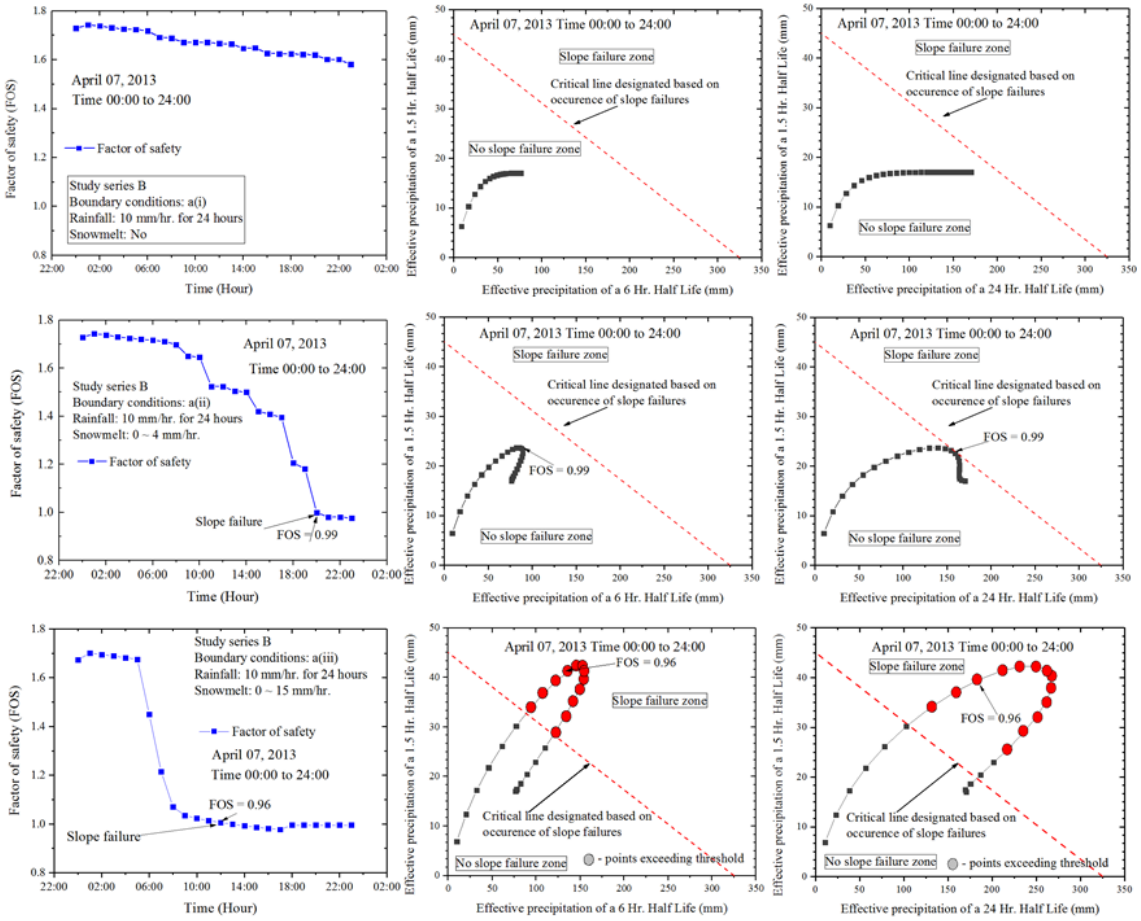

Figure 5.15 Comparison of Factor of safety, Effective Precipitation index 6 hours half-life and 24 hours half-life for study series B with 45° slope angle, 5 m slope height, 10 mm/hr. rainfall with two different snowmelt rates

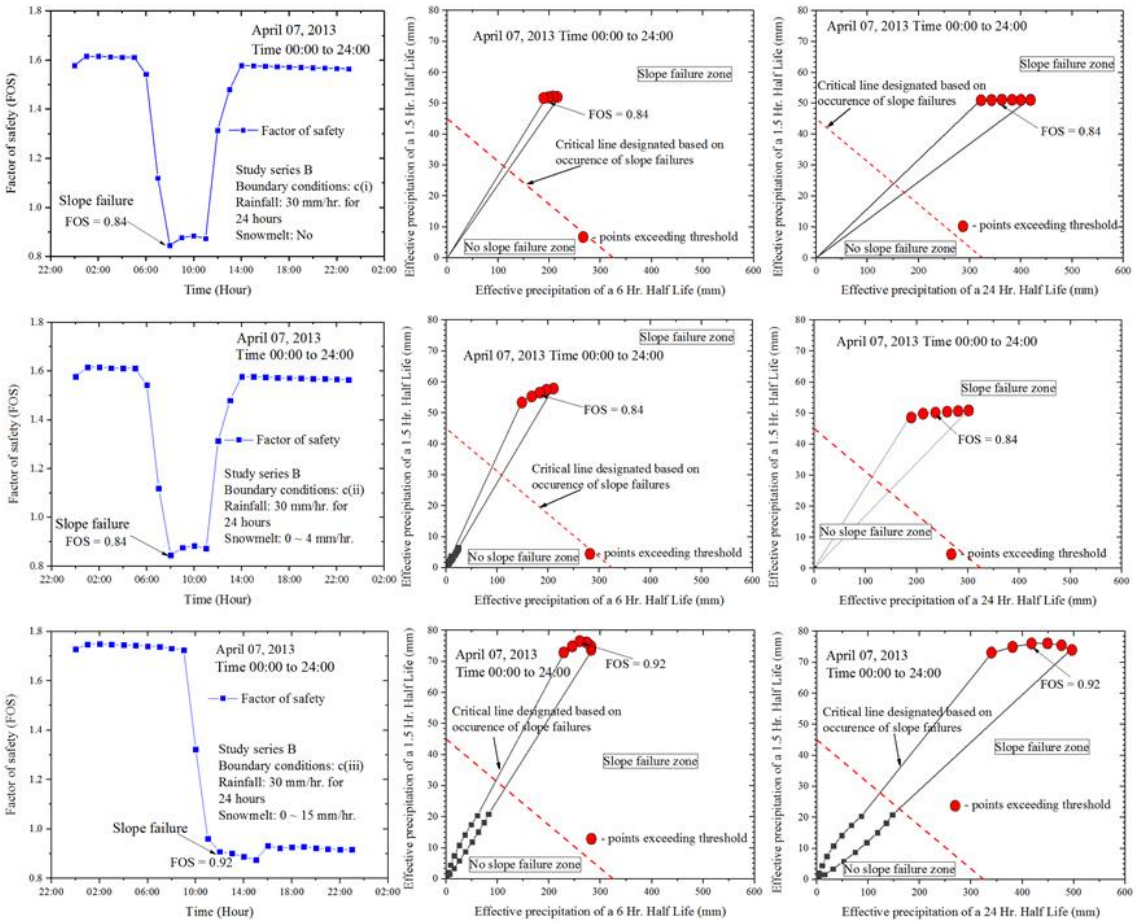

Figure 5.16 Comparison of Factor of safety, Effective Precipitation index 6 hours half-life and 24 hours half-life for study series B with 45° slope angle, 5 m slope height, 30 mm/hr. rainfall with two different snowmelt rates

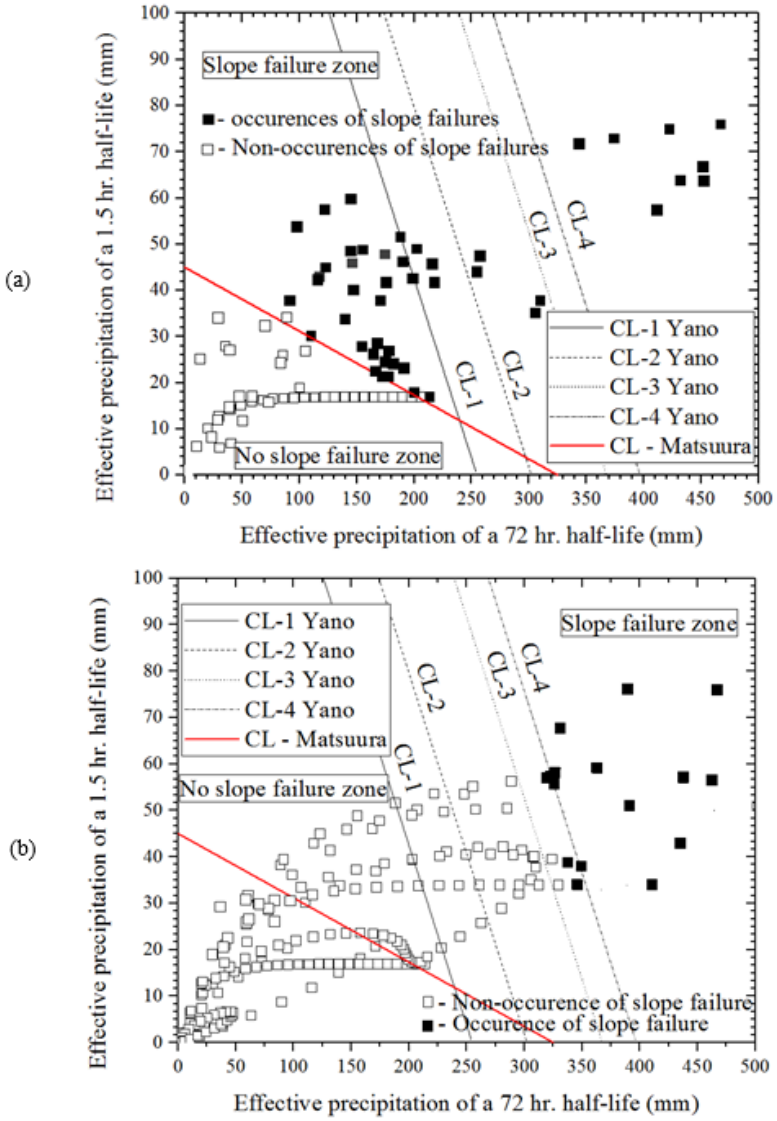

Figure 5.17 Plots of all slope failures and stable cases using Effective Precipitation index with half-lives 1.5 hours and 72 hours (a) series B and C, (b) series A and D.

Since the threshold value (CL proposed by Matsuura et al. 2013) of the EP index is low for all these stable cases, the CL will be exceeded and a false warning may be made. Whereas if the CL3 proposed by Yano (1990) is used, the false warnings can be avoided as shown in Table 6. Similar trend was also observed for the cases of Typhoon disaster in Hokkaido using the ER index discussed in section 5.1.2. Different critical lines (CL) are necessary during rainfall season and snow melting and thawing season. For the cases of series B and C (thawing and after thawing seasons), there are no false warnings observed. All the slope failures are predicted as failures and all the stable cases were also identified properly. It could be said that the CL

proposed by Matsuura et al. (2013) designated using the EP index is especially applicable for soil slope failure in snow melting and thawing season and after thawing season. Whereas for the case of rainfall induced slope failures the CL proposed by Yano, (1990) is found applicable. Figure 5.17(a) and (b) show the Effective Precipitation index for all the numerical case examples for series B and C and series A and D respectively. These Figures are plotted in the following way. Unlike the continuous snake lines plotted for EP in Figure 5.13 and Figure 5.14, in Figure 5.17(a), the black square boxes show the EP for slope failures at which the FOS value reduces less than 1 and the white square boxes show the EP for stable slope cases (FOS equal to or greater than 1) for the series B and C. Similarly, in Figure 5.17(b), snake lines are plotted with the black square boxes showing the EP for slope failures at which the FOS value reduces less than 1 and the white square boxes show the EP for all stable slope cases (FOS equal to or greater than 1) for the series A and D. This will give an idea about the location of slope failures along the snake lines in a two-dimensional plot. It could be seen that using the designated CL proposed by Matsuura et al. (2013), the failures and stable scenarios during snow melting and thawing seasons are explicitly delineated. The rainfall slope failures are clearly distinguished by the CL proposed by Yano (1990). In comparison to other CLs, the CL3 predicts the slope failure and stable cases more clearly. Unlike SWI, the EP index does not require a revision in the CL for slope failures occur during snow melting and thawing season. The EP index show the fact that the CL proposed by Matsuura et al. (2013) can be applied to the slope failures in Hokkaido because the original model can consider the effects of snowmelt water on slope failures. Therefore, it is reasonable to apply the CL to slope failures in Hokkaido. On the other hand, the CL for SWI proposed by Nakatsugawa et al. (2015) does not consider the effects of snowmelt water.

5.8 Revisions of the 60-minute rainfall and SWI relationships

Revisions for the 60-min rainfall and SWI relationships are done by considering the snowmelt water as an input in the calculation of SWI. The criteria are then applied to the slope failure cases as shown in Figure 5.18. It could be seen that even after incorporation of the snowmelt water in the calculation, the index does not predict the slope failure. A revision for the threshold line is designated for Hokkaido. In addition, from Figure 5.13 and 5.14, it could be seen that the SWI fail to predict the slope failures as the threshold value (CL) is much larger. Similar behaviour has been observed for the Nakayama pass slope failure case (Figure 5.3) and have

been reported by Iwakura et al., (2010) and Nakatsugawa et al., (2015) as well. The basic concept of the currently operating Japanese early-warning system (Osanai et al., 2010) explains that the CL for a particular region can be revised if it is necessary. As many researchers, have found that the CL designated is not appropriate for the snowy Hokkaido region, in this study the revisions are studied. The critical line designated for Hokkaido is revised based on the slope failure data using the conceptually derived RBFN (Radial Basis Finite Network) lines as shown in Figure 5.18. The RBFN is a cluster of slope failure as well as stable data through which JMA delineates the CL. At JMA, the RBFN lines are derived from years and years of occurrences and non-occurrences of slope failures within the preferred area. Of those RBFN lines, the one which could delineate the margin between the failure and stable scenarios is selected as a CL. For all the 448 numbers of slope failures from series B and C and 64 numbers of slope failures from series D, the corresponding SWI were plotted in two-dimensional plane along with many CL as shown in Figure 5.19(a) and (b) respectively. The failures are identified by checking the FOS is lesser than 1. The stable and failure cases from the series B and C are plotted in Figure 5.19(a) and from series A and D are plotted in Figure 5.19(b). These figures are plotted in the same way as the EP index shown in Figure 5.17(a) and (b). It could be seen that the designated CL does not predict the failures and stable scenarios clearly in Figure 5.19(a). A clear demarcation between the failures and stable cases are identified at line connecting 30 mm/hr. rainfall and 150 mm SWI. Similar to the procedure followed by JMA (Osanai et al. 2010), a CL line can be delineated between the occurrence and non-occurrences of failures as shown in Figure 5.19(a). From the possible revisions studied the line with a minimum of 30 mm 60-minute cumulative rainfall and 150 mm SWI is found to be appropriate for the prediction of snowmelt induced soil slope failures. The improvement effect of the prediction by SWI is studied and shown in Table 5.9.

Table 5.9 Rates of successful predictions (proper identification of the slope failure) using SWI before and after revising CL.

S. No.	Study Series	Slope failures	Stable cases	% of prediction by SWI before revising CL		% of prediction by SWI after revising CL	
				Success	Unsuccessful	Success	Unsuccessful
1	A	0	240	-	-	-	-
2	B	224	16	0 %	100 %	92.85 %	7.15 %
3	C	224	16	0 %	100 %	92.85 %	7.15 %
4	D	64	176	100 %	0 %	100 %	0 %

It could be seen from Table 5.10 that before revising the CL, the rate of successful prediction of slope failures is 0 % for series B and C (thawing and after thawing seasons). After revising the CL, the rate of successful prediction of slope failures is improved to 92.85 % with an unsuccessful prediction rate of 7.15 % for series B and C. Analysing the rate of false predictions (stable cases noted as failures), as shown in Table 5.6., the rate is 0 % for all the series A, B, C and D before revising the CL.

Table 5.10 Rates of false predictions (stable cases identified as slope failures) using SWI before and after revising CL.

S. No.	Study Series	Slope failures	Stable cases	% of false prediction by SWI before revising CL	% of false predictions by SWI after revising CL
1	A	0	240	0 %	100 %
2	B	224	16	0 %	0 %
3	C	224	16	0 %	0 %
4	D	64	176	0 %	100 %

Since there is no prediction made, the possibility of making a false prediction is always zero. Whereas, after revising the CL the false prediction rates increase to 100 % for series A and D and remain 0 % for series B and C. In Figure 5.19(b) the slope failures and stable cases from series A and D are plotted considering the CL designated for Hokkaido. It could be seen that most of the slope failures are predicted when considering the existing CL. From this observation, it could be said that the revised CL for SWI is applicable only for the slope failures induced by snowmelt water during thawing and after thawing seasons.

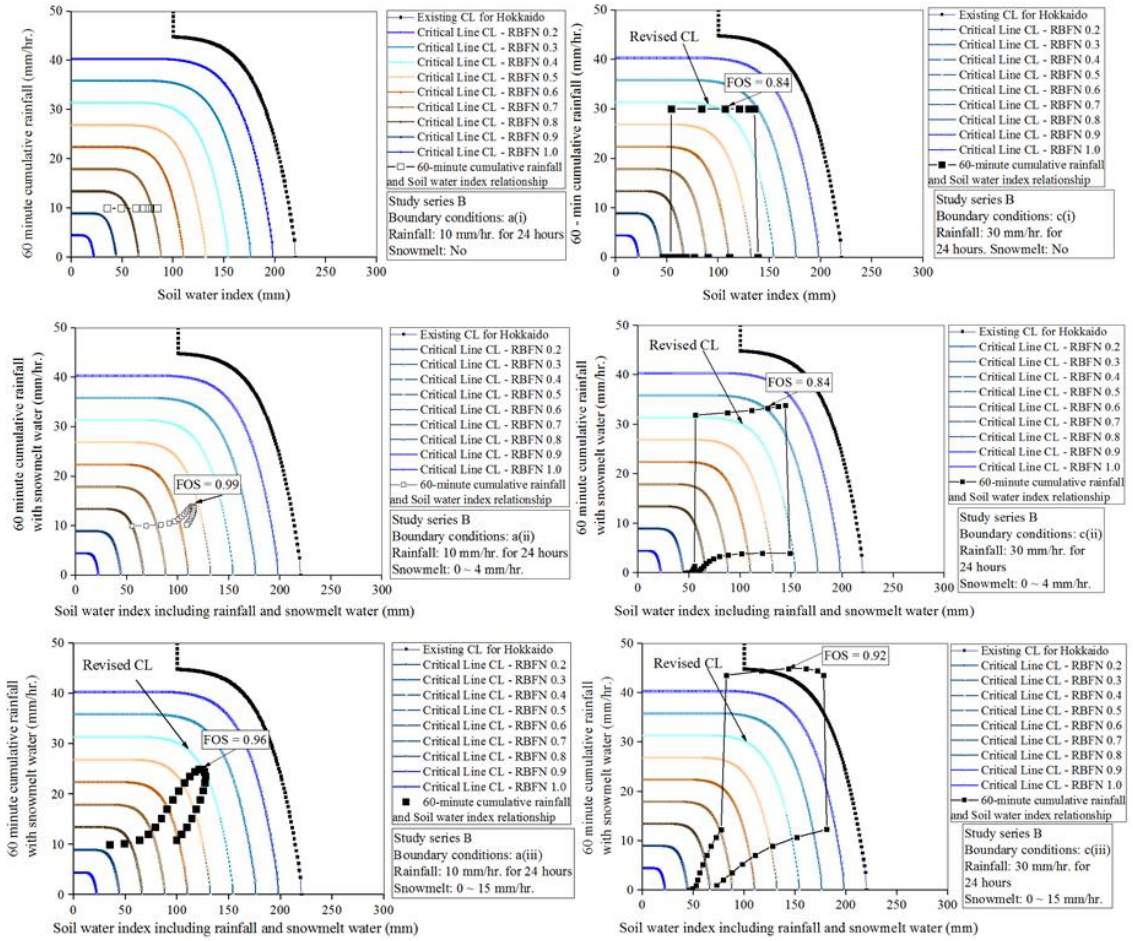

Figure 5.18 Revision of CL for SWI based on occurrence and non-occurrence of slope failures using data from study series B with 45° slope angle, 5 m slope height, 10 mm/hr. and 30 mm/hr. rainfall with two different snowmelt rates

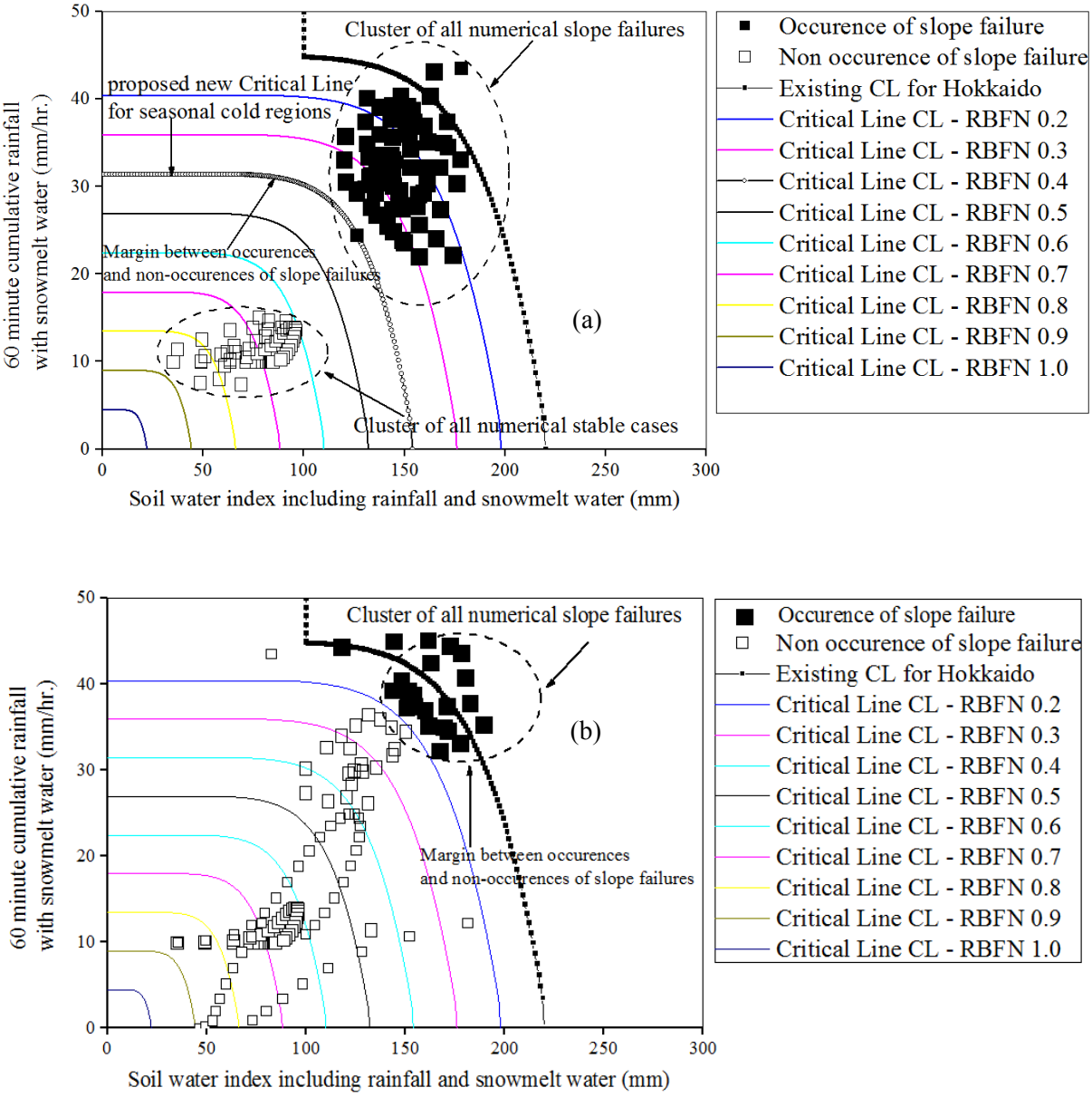

Figure 5.19 Possible revisions of the Critical Line designated for Hokkaido. Revision threshold lines are conceptual/equivalent RBFN lines (a) series B and C, (b) series A and D.

5.9 Discussion on merits and shortcomings of the proposed method

The merits and demerits of the early warning criteria studied in this paper are summarized here. The Effective Precipitation (EP) index will be useful to predict the slope failures induced by slow soil surface infiltration derived from the snowmelt water. For this purpose, the Effective Precipitation with a 72 hours half-life was found to be appropriate. On the other hand, as seen from the case examples on Typhoon induced sediment disasters in Hokkaido, the CL proposed

by Matsuura et al. (2013) for the Effective Precipitation index was found to be exceeding to a large value at all stages as observed from Figure 5.4. Further, it is found from the numerical simulations that the EP criteria with the CL proposed by Matsuura et al. (2013) considerably over estimates the slope failures for cases in series A and D with a false prediction rate of 100 %. Whereas the CL proposed by Yano (1990) predicts the slope failure and stable cases for the series A and D without a false prediction rate. However, for the cases of slope failures in series B and C (thawing and after thawing seasons), the EP index with the CL proposed by Matsuura et al. (2013) shows 100 % successful prediction rate. Due to this fact, it could be said that the threshold CL for Effective Precipitation index should be changed considering the season. The CL proposed by Matsuura et al. (2013) should be used during snowmelt season and the CL proposed by Yano (1990) should be used during rainy seasons.

The SWI calculated for the case of Nakayama pass slope failure shown in Figure 16 does not predict the slope failure even if the snowmelt water is taken into consideration. The increase in SWI is very small as compared with the increase in Effective Precipitation index when considering the snowmelt water (Figure 5.13 and Figure 5.14). Even if the hourly snowmelt water is considered, the SWI does not increase to reach the CL designated for Hokkaido. Whereas, by using the revised CL, the slope failures for most of the cases in series B and C are predicted with a success rate of 92.85 %. The Nakayama pass slope failure could also be predicted if the revised CL is considered (Figure 5.3). The 7.15 % of unsuccessful rate comes due to the SWI fail to predict the slope failure in case the amount of rainfall is very low. Whereas, a 100 % success rate is achieved by the EP index predicting all the numerical slope failures and case examples during the snowmelt season precisely. On the other hand, the revised CL for SWI considerably over estimates the slope failures for cases in series A and D with a false prediction rate of 100 %. With the currently available CL for Hokkaido, the slope failures and stable cases are delineated with more accuracy as shown in Figure 5.19(b).

It could be suggested that, for the prediction of snowmelt induced soil slope failures, the Effective Precipitation index would be appropriate rather than the Soil Water Index. Whereas, the Soil Water Index would be appropriate to predict the failures induced by heavy rainfall i.e. Typhoon etc. Since the objective of this study is to find some criteria for the prediction of snowmelt induced soil slope failures in cold regions, the use of Effective Precipitation (EP) index is recommended. On the other hand, from these detailed studies of early warning criteria,

it is also significant to note the advantages of performing numerical simulations to revise the CLs for EP and SWI. Based on the studies performed, it has been found that numerical simulations can be reasonably used to set the CL for both snowmelt and rainfall induced slope failures since the results of stable and slope failure cases agree well with the existing CLs.

CHAPTER 6

6 RECOMMENDATIONS AND CONCLUSIONS

The conclusions and recommendations of this study are summarised in two parts. The first part is from Chapter 4 explaining the main conclusions of the numerical simulations performed using the stability assessment approach for case examples. The second part is from Chapter 5 detailly explaining the main finding of the study on prediction and early warning of snowmelt induced soil slope failures in snowy cold regions.

6.1 Conclusions and recommendations from Chapter 4 – Stability assessment approach

A slope stability assessment approach applicable to analyse the long-term stability of soil slopes i.e. embankment slopes, and natural cut slopes along highways in seasonal cold regions is recommended in this study. The validity of the proposed approach has been studied by applying the method for two soil slope failure case examples that occurred in a seasonal cold region in Hokkaido, Japan. Based on the detailed studies performed, it has been found that the adopted slope stability assessment approach can be used for the design of slope structures along highways through performing pre-assessment of stability against anticipated climatic influences. Through the various parametric studies performed, the following conclusions can be drawn.

- The freeze-thaw action has a considerable effect on soil water content distribution which in turn influences the stability of soil slope. It is important to consider the freeze-thaw action in estimating the soil water content distribution for the proper pre-judgement of slope stability.
- The soil water content distribution inside the soil slope is seriously affected by the snowmelt water infiltration. Ignoring the amount of water derived from the snowmelt may not predict the soil water content distribution of the slope precisely.
- The weight of snow accumulated above the soil ground may reduce the slope stability considerably. The consideration of snow weight in the estimation of the factor of safety is essential if the snow during accumulation is not removed manually.
- The frozen shear strength of the soil should be properly considered to analyse the stability during freezing seasons if it is expected that the soil ground will freeze for a considerable depth.

— The freeze-thaw action and snowmelt water infiltration have a substantial impact on soil slope stability regardless of the slope angle considered.

In geotechnical engineering practice, the factors such as freeze-thaw action, snowmelt water infiltration are generally not considered for the design and analysis of slope structures, especially for cold regions like Hokkaido. It is evident that these factors seriously affect the soil slope stability. The stability assessment approach adopted in this study is found to be very useful in analysing the slope stability against anticipated climatic factors i.e. freeze-thaw action and snowmelt water infiltration. Based on the studies performed, it is strongly recommended that an assessment of the long-term stability of soil slopes considering the climatic effects will be helpful for the prevention and mitigation of such disasters.

6.2 Conclusions and recommendations from Chapter 5 – Prediction and early warning of soil slope failures in snowy cold regions

Prediction of snowmelt induced soil slope failure in cold regions of Japan have always been highly multifaceted. To find a suitable criterion for the prediction of soil slope failures in seasonal cold regions, the applicability of the early warning criteria Soil water index (SWI) and Effective Rainfall index (ER) are studied for the snowmelt induced soil slope failures in Hokkaido, Japan. It is found that these criteria are not appropriate for the predictions. Evidently, the criteria like SWI and ER index need revisions. Modifications of the early warning criteria are studied by incorporating the snowmelt water into the calculation and through performing conceptual soil slope failures using numerical simulations. Following findings can be outlined from this study.

— Consideration of snowmelt water improves the prediction using SWI, provided a revision of Critical Line for Hokkaido is made. The revisions for the criteria are studied and an hourly threshold rainfall + snowmelt value 30 mm/hr. is proposed and for SWI a value of 150 mm is recommended. The suggested revised CL for the SWI is applicable only for the slope failures occur during snow melting and thawing and after thawing seasons. For the slope failure occurring during rainy seasons the existing CL for Hokkaido is found appropriate.

— The proposed Effective Precipitation (EP) index performs well if snowmelt water is included in the calculation. As compared with other half-lives (6 hours and 24

hours), the 72-hour half-life provides a reasonable estimation of the soil moisture. The EP with 1.5 hours half-life and 72 hours half-life considers both the effect of high rainfall amount for short duration and small rainfall amount for long duration through which the short-term and long-term infiltration effects of soil moisture can be considered as seen from the comparative studies. The snowmelt water can also be precisely considered in these criteria.

— As compared with the SWI using revised CL, the proposed Effective Precipitation (EP) index predicts the snowmelt as well as rainfall induced soil slope failures with higher accuracy provided different CLs are used in accordance with the respective types of slopes failure. The different critical lines presented for snowmelt as well as rainfall induced slope failures predicts the failures and stable scenarios more accurately than the SWI.

— The results of numerical simulations (stable cases and slope failures) performed in this study agree well with the existing CL of EP and SWI. Numerical simulations can be practically used to set the CL for both snowmelt and rainfall induced soil slope failures.

An Effective Precipitation index for the prediction of snowmelt and rainfall induced soil slope failures in cold regions is recommended in this study. The proposed early warning criteria uses the estimation of hourly snowmelt and rainfall from the meteorological data in a straight forward way to calculate the threshold levels. The validation of the proposed criteria using slope failure case examples and numerical simulations have been done stating that the criteria will be useful for the prediction of oncoming slope/sediment disasters in snowy cold regions. Further evaluation of these methods using many slope failure case examples considering different soil types, and analysing various slope failures case studies may be necessary to standardise the proposed threshold values due to the fact that the revisions of the criteria in this study are performed based on numerical simulations considering a single type of volcanic soil.

6.3 General design guidelines for manmade embankments/natural slopes in seasonal cold regions

Some specific design guidelines for soil slopes in seasonal cold regions are outlined here. Note the guidelines provided here are drafted from the conclusions of the study and not relevant to any geotechnical society specific design standards or criteria.

- The maximum anticipated depth of the freezing front during winter periods need to be known before starting the slope construction.
- If it is expected that the soil ground will freeze for a considerable depth i.e. more or less 1 m deep for a 5 m tall slope, the shear strength of frozen soil need to measured explicitly through a laboratory experimental program and these values have be used in the stability calculation.
- For the above mentioned purpose a slope height to freezing depth ratio can be established as a guideline.
- The maximum anticipated depth of snow accumulation need to be predetermined to decide whether manual removal of snow is necessary or not. If manual removal is not necessary, calculation of anticipated snowmelt water is essential.
- If it is found that there will be excess amount of snowmelt water, methods to drain the melt water should be constructed beforehand.
- The factor of safety of the designed slope should be predicted against the extreme rainfall and snowmelt event over a period of past ten years.

6.4 Recommendations for further studies

This dissertation proposes a slope stability assessment approach and an early warning criteria for soil slope instabilities in seasonal cold regions. The studies have been performed through analysing three different case examples of soil slope failures in Hokkaido, Japan. The robustness and applicability of the proposed methods has been validated through performing detailed case to case studies of all the three slope failures and further parametric studies. Some further recommendations and guidelines for future studies are outlined here.

- Examination of the slope stability assessment method based on numerical simulations for many soil slope failures in seasonal cold regions using climate data/forecast is advisable.
- Examination of the early warning criteria for soil slope failures in seasonal cold regions using climate data/forecast is strongly advised.
- Detailed studies on small, regional to large scale slope failure using numerical simulations and early warning predictions.
- Performing reliability analysis for the numerical slope simulation studies and studying the validity of all FOS values in 960 numerical simulations.

LIST OF REFERENCES

Andersland, Orlando B Ladanyi, Branko Andersland, Orlando B. Introduction to frozen ground engineering (2004). Frozen ground engineering (2nd ed). Wiley ; [Reston, Va.] : ASCE, Hoboken, NJ

Arenson, L.U., Springman, S.M., 2005. Mathematical descriptions for the behaviour of ice-rich frozen soils at temperatures close to 0 °C. Can. Geotech. J. 42, 431–442. doi:10.1139/t04-109

Berris, S. N. and Harr, R. D. 1987. Comparative snow accumulation and melt during rainfall in forested and clear-cut plots in the western Cascades of Oregon. Water Resources Research, 23(1), 135-142.

Black, P.B., Tice, A.R., 1989. Comparison of soil freezing curve and soil water curve data for Windsor sandy loam. Water Resour. Res. 25, 2205–2210. doi:10.1029/WR025i010p02205

Bras, R.L., 1990. Hydrology: An introduction to hydrologic science. Addisson Wesley. Inc.

Burgess, M.M., 1993. Snow depth and density measurements Norman Wells Pipeline study sites Mackenzie Valley 1985 to 1991. Geological Survey of Canada, Open File 2626.

Chen, X., Liu, J., Feng, Y., Li, X., Tian, Y., Fang, J., 2013. A pseudo-coupled numerical approach for stability analysis of frozen soil slopes based on finite element limit analysis method. Sci. Cold Arid Reg. 5, 478–487.

Childs, E.C., Collis-George, N., 1950. The Permeability of Porous Materials. Proc. R. Soc. Lond. A. Math. Phys. Sci. 201, 392–405.

Coussy, O., 2005. Poromechanics of freezing materials. J. Mech. Phys. Solids 53, 1689–1718. doi:10.1016/j.jmps.2005.04.001

Deschamps, R., Yankey, G., 2006. Limitations in the Back-Analysis of Strength from Failures. J. Geotech. Geoenvironmental Eng. 132, 532–536. doi:10.1061/(ASCE)1090-0241(2006)132:4(532)

Duncan, J.M., Stark, T.D., 1992. Soil Strengths from Back-Analysis of Slope Failures. Proceedings of Specialty Conference STABILITY AND PERFORMANCE OF SLOPES AND EMBANKMENTS-II, ASCE, Berkeley, CA, Geotechnical Special Publication. 31, 890-904.

Duncan, J.M., Wright, S.G., 2005. Soil Strength and Slope Stability, John Wiley and Sons Inc.

Edlefsen, N., Anderson, A., 1943. Thermodynamics of soil moisture. Hilgardia 15, 31-298. doi:10.3733/hilg.v15n02p031

Flerchinger, G.N., Saxton, K.E., 1989. Simultaneous Heat and Water Model of a Freezing Snow-Residue-Soil System I. Theory and Development. doi:10.13031/2013.31040

Fredlund, M.D., Wilson, G.W., Fredlund, D.G., 2002. Use of the grain-size distribution for estimation of the soil-water characteristic curve. Can. Geotech. J. 39, 1103–1117. doi:10.1139/t02-049

Gens, A., 2010. Soil–environment interactions in geotechnical engineering. Géotechnique 60, 3–74. doi:10.1680/geot.9.P.109

Gitirana Jr., de F.N.G., 2005. Weather-related geo-hazard assessment for railway embankment stability. Ph.D. Thesis. University of Saskatchewan, Saskatoon. SK. Canada.

Goodrich, L.E., 1982. The influence of snow cover on the ground thermal regime. Can. Geotech. J. 19, 421–432. doi:10.1139/t82-047

Harlan, R.L., Nixon, J.F., 1978. Ground Thermal Regime, in: Andersland, O.B., Anderson, D.M. (Eds), Geotechnical Engineering for Cold Regions. McGraw-Hill Inc.

Hooke, R., Dahlin, B., & Kauper, M. (1972). Creep of Ice Containing Dispersed Fine Sand. Journal of Glaciology, 11(63), 327-336. doi:10.1017/S0022143000022309

Hoek, E., Brown, E.T., 1997. Practical estimates of rock mass strength. Int. J. Rock Mech. Min. Sci. 34, 1165–1186. doi:http://dx.doi.org/10.1016/S1365-1609(97)80069-X

Hokkaido Regional Development Bureau., 2013. Report on slope disaster, recovery and survey design. Route No 230 Sapporo general national highway. Sapporo Development and Construction Department, Sapporo (In Japanese).

Hokkaido Regional Development Bureau., 2016. Report on slope disaster, recovery and survey design. Route No 274 Sapporo general national highway. Sapporo Development and Construction Department, Sapporo (In Japanese).

Ishida, K., Minami., N. Yamada, T., Ishida, T., Kato, N. and Yoshikawa, M. 2000. A Study for Determining the Warning and Evacuation Criteria of Snowmelt - induced Debris Flow. Journal of the Japan Society of Erosion Control Engineering. 52 (5), 46-51. (in Japanese with English abstract).

Ishikawa, T., Kijiya, I., Tokoro, T., Sato, M., 2016. Application of coupled thermo-hydro-mechanical analysis to frost-heave behavior of earth structures. Japanese Geotech. Soc. Spec. Publ. 2, 531–536. doi:10.3208/jgssp.JPN-047

Ishikawa, T., Tokoro, T., Seiichi, M., 2015. Geohazard at volcanic soil slope in cold regions and its influencing factors. Japanese Geotech. Soc. Spec. Publ. 1, 1–20. doi:10.3208/jgssp.KEY-1

Iwakura, T., Takayoshi, K., Otani, H., Tanimoto, K., Tokioka, S. and Watanabe, T. 2010. Study of warning and evacuation standard-setting approach to the sediment-related disasters that occur in the

snowmelt season. 59th Annual Meeting of the Society of Erosion Control Research. Paper 229. (In Japanese).

Jame, Y.W., 1977. Heat and mass transfer in freezing soil. PhD Thesis, University of Saskatchewan, Saskatoon, Saskatchewan, Canada.

Japan Meteorological Agency (JMA) 2012. Soil Water Index, http://www.jma.go.jp/jma/kishou/know/bosai/dojoshisu.html (in Japanese), Date accessed: August 20th, 2012.

Japan Meteorological Agency (JMA) 2016. Talas Soil Water Index, http://www.jma.go.jp/jma/en/News/Talas_soil_water_index.html. Date accessed: December 15th, 2016.

Joshi, B., Barbour, S.L., Krause, A.E., Wilson, G.W., 1993. A finite element model for the coupled flow of heat and moisture in soils under atmospheric forcing. Finite Elem. Anal. Des. 15, 57–68. doi:http://dx.doi.org/10.1016/0168-874X(93)90070-7

Kawamura, S., Miura, S., Matsumura, S., 2016. Stability evaluation of full-scale embankment constructed by volcanic soil in cold regions. Japanese Geotech. Soc. Spec. Publ. 2, 971–976. doi:10.3208/jgssp.JPN-063

Kawamura, S., Miura, S., 2013. Rainfall-induced failures of volcanic slopes subjected to freezing and thawing. Soils Found. 53, 443–461. doi:http://dx.doi.org/10.1016/j.sandf.2013.04.006

Kawamura, S., Miura, S., Yokohama, S., Kudo, A., Kaiya, N., 2013. Field Monitoring of Embankment Constructed by Volcanic Soil and Its Evaluation, in: Geo-Congress 2013. American Society of Civil Engineers, pp. 373–382. doi:doi:10.1061/9780784412787.037

Kersten, Miles S., 1949. Thermal Properties of Soils. University of Minnesota. Retrieved from the University of Minnesota Digital Conservancy. http://hdl.handle.net/11299/124271 (accessed 15.02.2015)

Kolditz, O., Bauer, S., Bilke, L., Böttcher, N., Delfs, J.O., Fischer, T., Görke, U.J., Kalbacher, T., Kosakowski, G., McDermott, C.I., Park, C.H., Radu, F., Rink, K., Shao, H., Shao, H.B., Sun, F., Sun, Y.Y., Singh, A.K., Taron, J., Walther, M., Wang, W., Watanabe, N., Wu, Y., Xie, M., Xu, W., Zehner, B., 2012. OpenGeoSys: An open-source initiative for numerical simulation of thermo-hydro-mechanical/chemical (THM/C) processes in porous media. Environ. Earth Sci. 67, 589–599. doi:10.1007/s12665-012-1546-x

Kondo J., and Yamazaki T. 1990. A Prediction Model for Snowmelt, Snow Surface Temperature and Freezing Depth using a Heat Balance Method, J. Appl. Meteor., 29, 375–384.

Koniorczyk, M., Gawin, D., Schrefler, B.A., 2015. Modeling evolution of frost damage in fully saturated porous materials exposed to variable hygro-thermal conditions. Comput. Methods Appl. Mech. Eng. 297, 38–61. doi:10.1016/j.cma.2015.08.015

Krahn, J., 2012a. Vadose Zone Modeling with VADOSE/W - An Engineering Methodology. GEO-SLOPE/W International Ltd., Alberta, Canada.

Krahn, J., 2012b. Stability modelling with SLOPE/W - An Engineering Methodology. GEO-SLOPE/W International Ltd., Alberta, Canada.

Lai, Y., Pei, W., Zhang, M., Zhou, J., 2014. Study on theory model of hydro-thermal-mechanical interaction process in saturated freezing silty soil. Int. J. Heat Mass Transf. 78, 805–819. doi:10.1016/j.ijheatmasstransfer.2014.07.035

Liang, X., Lettenmaier, D. P., Wood, E. F., Burges, S. J., 1994. A simple hydrologically based model of land surface water and energy fluxes for GSMs. J. Geophys. Res., 99, 415-428. doi:10.1029/94JD00483

Li, N., Chen, B., Chen, F., Xu, X., 2000. The coupled heat-moisture-mechanic model of the frozen soil. Cold Reg. Sci. Technol. 31, 199–205. doi:http://dx.doi.org/10.1016/S0165-232X(00)00013-6

Li, N., Chen, F., Su, B., Cheng, G., 2002. Theoretical frame of the saturated freezing soil. Cold Reg. Sci. Technol. 35, 73–80. doi:http://dx.doi.org/10.1016/S0165-232X(02)00029-0

Li, N., Chen, F., Xu, B., Swoboda, G., 2008. Theoretical modeling framework for an unsaturated freezing soil. Cold Reg. Sci. Technol. 54, 19–35. doi:http://dx.doi.org/10.1016/j.coldregions.2007.12.001

Liu, Z., Yu, X., 2011. Coupled thermo-hydro-mechanical model for porous materials under frost action: Theory and implementation. Acta Geotech. 6, 51–65. doi:10.1007/s11440-011-0135-6

Luo, B., Ishikawa, T., Tokoro, T., Lai, H., 2017. Coupled Thermo-Hydro-Mechanical Analysis of Freeze–Thaw Behavior of Pavement Structure over a Box Culvert. Transp. Res. Rec. J. Transp. Res. Board 2656, 12–22. doi:10.3141/2656-02

Mackay, J.R., 1981. Active layer slope movement in a continuous permafrost environment, Garry Island, Northwest Territories, Canada. Can. J. Earth Sci. 18, 1666–1680. doi:10.1139/e81-154

Matsumura, S., 2014. Laboratory and in-situ studies on mechanical properties of volcanic soil embankment in cold region. PhD Thesis, Graduate School of Engineering, Hokkaido University, Japan. http://hdl.handle.net/2115/55535 (accessed 01.02.2015)

Matsumura, S., Miura, S., Yokohama, S., Kawamura, S., 2015. Cyclic deformation-strength evaluation of compacted volcanic soil subjected to freeze–thaw sequence. Soils Found. 55, 86–98. doi:http://dx.doi.org/10.1016/j.sandf.2014.12.007

Matsuura, S., 1998. Difficulties in Predicting Snow-induced Landslides. Journal of Japan Landslide Society 34 (4), 39-46. (In Japanese with English abstract)

Matsuura, S., 2000. Fluctuations of pore-water pressure in a landslide in a heavy snow district. Journal of Japan Landslide Society 37 (2), 10-19.

Matsuura, S., Matsuyama, K., Asano, S., Okamoto, T. and Takeuchi, Y., 2005. Fluctuation of the seasonal snowpack in a mountainous area of the heavy-snow district in the warm-temperate zone of Japan. J. Glaciol. 51, 547–554. doi:10.3189/172756505781829052

Matsuura, S., Asano, S. and Okamoto, T., 2008. Relationship between rain and/or meltwater, pore-water pressure and displacement of a reactivated landslide. Eng. Geol. 101, 49–59. doi:10.1016/j.enggeo.2008.03.007

Matsuura, S., Okamoto, T., Asano, S. and Matsuyama, K., 2013. Characteristics of meltwater and/or rainfall regime in a snowy region and its effect on sediment-related disasters. Bull. Eng. Geol. Environ. 72, 119–129. doi:10.1007/s10064-012-0456-1

McRoberts, E.C., Morgenstern, N.R., 1974a. The Stability of Thawing Slopes. Can. Geotech. J. 11, 447–469. doi:10.1139/t74-052

McRoberts, E.C., Morgenstern, N.R., 1974b. Stability of Slopes in Frozen Soil, Mackenzie Valley, N.W.T. Can. Geotech. J. 11, 554–573. doi:10.1139/t74-058

Michalowski, R.L., Zhu, M., 2006. Frost heave modelling using porosity rate function. Int. J. Numer. Anal. Methods Geomech. 30, 703–722. doi:10.1002/nag.497

Morgenstern, N.R., Price, V.E., 1965. The Analysis of the Stability of General Slip Surfaces. Géotechnique 15, 79–93. doi:10.1680/geot.1965.15.1.79

Motoyama, H., 1990. Simulation of seasonal snow cover based on air temperature and precipitation. J. Appl. Meteorol. 29. 1104-1110.

Nakatsugawa, M., Usutani, T., Miyazaki, T., 2015. Risk assessment of sediment disaster based on watershed-wide hydrologic processes. E-proceeding of the 36th IAHR World Congress.

Neaupane, K.M., Yamabe, T., 2001. A fully coupled thermo-hydro-mechanical nonlinear model for a frozen medium. Comput. Geotech. 28, 613–637. doi:10.1016/S0266-352X(01)00015-5

Nishimura, S., Gens, A., Olivella, S., Jardine, R.J., 2009. THM-coupled finite element analysis of frozen soil: formulation and application. Géotechnique 59, 159–171. doi:10.1680/geot.2009.59.3.159

Niu, F., Cheng, G., Ni, W., Jin, D., 2005. Engineering-related slope failure in permafrost regions of the Qinghai-Tibet Plateau. Cold Reg. Sci. Technol. 42, 215–225. doi:http://dx.doi.org/10.1016/j.coldregions.2005.02.002

Okada K (2005) Soil water index. Sokkoujihou No.69, 5(5):67-100 (in Japanese)

Okimura, T. and Ichikawa, R., 1985. A prediction method for surface failures by movements of infiltrated water in a surface soil layer. Nat. disaster Sci. 7, 41–51.

Okui, Y., Tokunaga, A., Shinji, M., Mori, S., 1997. New back analysis method of slope stability by using field measurements. Int. J. Rock Mech. Min. Sci. 34, 234.e1-234.e16. doi:http://dx.doi.org/10.1016/S1365-1609(97)00170-6

Osanai, N., Shimizu, T., Kuramoto, K., Kojima, S., and Noro, T., 2010. Japanese early-warning for debris flows and slope failures using rainfall indices with Radial Basis Function Network. Landslides. 7, 325–338. doi:10.1007/s10346-010-0229-5

Petzold, D.E., 1974: "Solar and Net Radiation over Snow", Climatological Research Series, No.9, McGill University, 77 pp.

Price, A.G., 1977: Snowmelt Run Off Processes in the Subarctic Area, Climatological Research Series, No 10, McGill University.

Richards, L.A., 1931. Capillary Conduction of Liquids through Porous Mediums. J. Appl. Phys. 1. doi:http://dx.doi.org/10.1063/1.1745010

Riley, J.P., Chadwick, D.G. and Eggleston, K.O., 1969. Snowmelt Simulation. Reports. Paper 122. http://digitalcommons.usu.edu/water_rep/122.

Selvadurai, A.P.S., Hu, J., Konuk, I., 1999. Computational modelling of frost heave induced soil–pipeline interaction: I. Modelling of frost heave. Cold Reg. Sci. Technol. 29, 215–228. doi:http://dx.doi.org/10.1016/S0165-232X(99)00028-2

Senoo, K., Haraguchi, K., Kikui, T. and Yoshida, S., 2001. On the theme and improvement of standard rainfall for warning and evacuation from sediment disasters. Journal of the Japan Society of Erosion Control Engineering, Vol. 53, No. 6, p. 37-44. (in Japanese with English abstract)

Siva Subramanian, S., Ishikawa, T., Yokohama, S., Tokoro, T., 2015. Numerical simulation of volcanic soil slope failure under coupled freeze-thaw and rainfall infiltration effects. Japanese Geotech. Soc. Spec. Publ. 1, 5–10. doi:10.3208/jgssp.JPN-23

Siva Subramanian, S., Ishikawa, T. and Tokoro, T., 2017. Stability assessment approach for soil slopes in seasonal cold regions. Engineering Geology. doi: 10.1016/j.enggeo.2017.03.008

Singh, P., Spitzbart, G., Hubl, H. and Weinmeister, H. W., 1997. Hydrological response of snowpack under rain-on-snow events: a field study, Journal of Hydrology, 202(1-4), 1-20.

Tang, W.H., Stark, T.D., Angulo, M., 1999. Reliability in back analysis of slope failures. Soils Found. 39, 73–80. doi:10.3208/sandf.39.5_73

Taylor-A1t, B., 1975: "The Energy Balance Climate of Meighen Ice Cap, N.W.T.", Dept. of Energy, Mines and Resources, Polar Continental Shelf Project, Ottawa, 168 pp.

Tereda, H. and Nakaya, H., 2001. Operating methods of critical rainfall for warning and evacuation from sediment-related disasters. Technical Note of National Institute for Land and Infrastructure Management. No. 5. Ministry of Land, Infrastructure and Transport, Japan (in Japanese).

Thomas, H.R., Cleall, P., Li, Y.-C., Harris, C., Kern-Luetschg, M., 2009. Modelling of cryogenic processes in permafrost and seasonally frozen soils. Géotechnique 59, 173–184. doi:10.1680/geot.2009.59.3.173

van Genuchten, M.T., 1980. A Closed-form Equation for Predicting the Hydraulic Conductivity of Unsaturated Soils1. Soil Sci. Soc. Am. J. 44, 892–898. doi:10.2136/sssaj1980.03615995004400050002x

Vanapalli, S.K., Fredlund, D.G., Pufahl, D.E., Clifton, A.W., 1996. Model for the prediction of shear strength with respect to soil suction. Can. Geotech. J. 33, 379–392. doi:10.1139/t96-060

Warren, S.G. and S.T. Schneider, (1979). J. Atmos. Sci. 36,1377-91.

Wang, S., Liu, F., 2015. A Hypoplasticity-Based Method for Estimating Thaw Consolidation of Frozen Sand. Geotech. Geol. Eng. 33, 1307–1320. doi:10.1007/s10706-015-9902-8

Wang, J., Nishimura, S., Tokoro, T., 2017. Laboratory study and interpretation of mechanical behavior of frozen clay through state concept. Soils Found. 57, 194–210. doi:https://doi.org/10.1016/j.sandf.2017.03.003

Wilson, G.W., Fredlund, D.G., Barbour, S.L., 1994. Coupled soil-atmosphere modelling for soil evaporation. Can. Geotech. J. 31, 151–161. doi:10.1139/t94-021

Williams, M.W., Cline, D., Hartman, M. and Bardsley, T., 1999. Data for snowmelt model development, calibration, and verification at an alpine site, Colorado Front Range, Water Resources Research, 35-10, 3205-3209

Yano, K., 1990. Study of the method for setting standard rainfall of debris flow by the reform of antecedent rain. Japan Society of Erosion Control Engineering 43(4), 3-13 (in Japanese with English abstract).

Yasuda, S., Fujioka, K., 2012. Study on the Method for the Seismic Design of Expressway Embankments, in: Sakr, M.A., Ansal, A. (Eds.), Special Topics in Earthquake Geotechnical Engineering. Springer Netherlands, Dordrecht, pp. 241–272. doi:10.1007/978-94-007-2060-2_9

Zhang, H., Zhang, J., Zhang, Z., Chen, J., You, Y., 2016. A consolidation model for estimating the settlement of warm permafrost. Comput. Geotech. 76, 43–50. doi:10.1016/j.compgeo.2016.02.013

Zhang, K., Cao, P., Bao, R., 2013. Rigorous back analysis of shear strength parameters of landslide slip. Trans. Nonferrous Met. Soc. China 23, 1459–1464. doi:http://dx.doi.org/10.1016/S1003-6326(13)62617-5

Zhang, Y., Michalowski, R., 2015. Thermal-Hydro-Mechanical Analysis of Frost Heave and Thaw Settlement. J. Geotech. Geoenvironmental Eng. 141, 4015027. doi:10.1061/(ASCE)GT.1943-5606.0001305